DESIGN OF A NON-ISOLATED SINGLE PHASE ONLINE UPS TOPOLOGY WITH PARALLEL BATTERY BANK FOR LOW POWER APPLICATIONS

MUHAMMAD AAMIR

FACULTY OF ENGINEERING
UNIVERSITY OF MALAYA
KUALA LUMPUR

2016

DESIGN OF A NON-ISOLATED SINGLE PHASE ONLINE UPS TOPOLOGY WITH PARALLEL BATTERY BANK FOR LOW POWER APPLICATIONS

MUHAMMAD AAMIR

THESIS SUBMITTED IN FULFILMENT OF THE REQUIREMENTS FOR THE DEGREE OF DOCTOR OF PHILOSOPHY IN ENGINEERING

FACULTY OF ENGINEERING
UNIVERSITY OF MALAYA
KUALA LUMPUR

2016

UNIVERSITY OF MALAYA

ORIGINAL LITERARY WORK DECLARATION

Name of Candidate: Muhammad Aamir

Matric No: KHA130074

Name of Degree: Doctor of Philosophy

Title of ~~Project Paper/Research Report/Dissertation/~~Thesis (“this Work”):

DESIGN OF A NON-ISOLATED SINGLE PHASE ONLINE UPS TOPOLOGY WITH PARALLEL BATTERY BANK FOR LOW POWER APPLICATIONS

Field of Study: Power Electronics

I do solemnly and sincerely declare that:

(1) I am the sole author/writer of this Work;
(2) This Work is original;
(3) Any use of any work in which copyright exists was done by way of fair dealing and for permitted purposes and any excerpt or extract from, or reference to or reproduction of any copyright work has been disclosed expressly and sufficiently and the title of the Work and its authorship have been acknowledged in this Work;
(4) I do not have any actual knowledge nor do I ought reasonably to know that the making of this work constitutes an infringement of any copyright work;
(5) I hereby assign all and every rights in the copyright to this Work to the University of Malaya (“UM”), who henceforth shall be owner of the copyright in this Work and that any reproduction or use in any form or by any means whatsoever is prohibited without the written consent of UM having been first had and obtained;
(6) I am fully aware that if in the course of making this Work I have infringed any copyright whether intentionally or otherwise, I may be subject to legal action or any other action as may be determined by UM.

Candidate’s Signature Date:

Subscribed and solemnly declared before,

Witness’s Signature Date:

Name:

Designation:

ABSTRACT

Uninterruptible Power Supplies (UPS) are widely used to provide reliable and high quality power to critical loads such as airlines computers, datacenters, communication systems, and medical support systems in hospitals in all grid conditions. Online UPS system is considered to be the most preferable UPS due to its highest level of power quality and proven reliability against all types of line disturbances and power outages. This research presents a new topology of the non-isolated online uninterruptible power supply system. The proposed system consists of bridgeless boost rectifier, battery charger/discharger, and an inverter. The rectifier performs power factor correction and provides regulated DC-link voltage. The rectifier operates with a minimum semiconductor device, reducing the conduction losses of the circuit significantly. A new battery charger/discharger has been implemented, which ensures the bidirectional power flow between the DC-link and the battery bank, reducing the battery bank voltage to only 24V, and regulates the DC-link voltage during battery mode. The bidirectional operation of the converter is achieved by employing only three active switches, a coupled inductor, and an additional voltage clamped circuit. Batteries are connected in parallel depending on the backup time requirement of the system. Operating batteries in parallel improve the battery performance and resolve the problems related to conventional battery banks that arrange batteries in series. The inverter provides a regulated output voltage to the load. A new cascaded slide mode and proportional-resonant control have been proposed. Slide mode control is recognized as the most robust control with high stability while the proportional-resonant control shapes the output waveform closely according to the reference sinusoidal signal. Keeping in view the characteristics of slide mode and proportional-resonant control, a cascaded controller is proposed for the bipolar single-phase UPS inverter. The outer voltage loop uses the proportional-resonant control while the inner loop uses the slide mode control.

The proposed control scheme regulates the output voltage for both linear and non-linear load and shows excellent performance during transients and step changes in load. The proposed controller shows significant improvement in terms of reducing the total harmonics distortion to 0.5% for linear load and 1.25% for non-linear load, strong robustness, and fast response time of only 0.3ms. Operation principle and experimental results of 1kVA prototype have been presented to verify the validity of the proposed UPS. The efficiency of the proposed system is 94% during battery mode and 92% during the normal mode of operation.

ABSTRAK

Bekalan Kuasa Tidak Terganggu (UPS) digunakan secara meluas untuk menyediakan kuasa berkualiti tinggi kepada beban kritikal dalam seperti syarikat penerbangan komputer, pusat data, sistem komunikasi, dan sistem sokongan perubatan di hospital-hospital semua keadaan grid. sistem UPS talian dianggap sebagai UPS paling lebih disebabkan tahap tertinggi kualiti kuasa dan kebolehpercayaan terbukti terhadap semua jenis gangguan talian dan gangguan bekalan kuasa. Kajian ini membentangkan talian bekalan kuasa tidak terganggu (UPS) untuk sistem bukan terpencil. Sistem yang dicadangkan terdiri daripada penerus tanpa jejambat, pengecas / pengdiscaj bateri dan *inverter*. Penerus ini menyediakan pautan voltan DC terkawal dengan pembetulan faktor kuasa. Penerus beroperasi dengan bilangan peranti semikonduktor yang minimum untuk mengurangkan kehilangan kuasa di dalam litar. Litar pengecas / pengdiscaj bateri baru telah dibina untuk memastikan aliran kuasa dwiarah antara pautan voltan DC dan bank bateri dengan mengurangkan voltan bateri bank kepada hanya 25V, dan mengawal voltan DC semasa mod kuasa bateri. Operasi dwiarah penukar dicapai dengan menggunakan hanya tiga suis aktif, induktor dan litar pengapit voltan. Bateri yang beroperasi secara selari dapat meningkatkan prestasi bateri dan mengelakkan masalah yang berkaitan dengan bank bateri konvensional yang disusun secara siri. Inverter ini menyediakan voltan keluaran terkawal untuk beban. Kawalan mod slaid baru dan kawalan berkadar-resonen (PR) telah dicadangkan. Kawalan mod slaid (SMC) diiktiraf sebagai kawalan yang paling jitu dengan kestabilan yang tinggi manakala kawalan berkadar-resonen (PR) menjana gelombang keluaran mengikut isyarat rujukan sinus. Berdasarkan ciri-ciri mod slaid dan kawalan salunan berkadar, kawalan berperingkat adalah dicadangkan untuk fasa tunggal bipolar bekalan kuasa tidak terganggu (UPS) inverter. Gelung voltan luar menggunakan kawalan PR manakala gelung dalaman menggunakan kawalan mod slaid. Skim kawalan yang dicadangkan dapat mengawal keluaran voltan untuk kedua-dua beban linear dan bukan linear dan menunjukkan prestasi yang baik semasa transien dan semasa perubahan beban. Pengawal yang dicadangkan menunjukkan peningkatan yang ketara dari segi mengurangkan jumlah herotan harmonik kepada 0.5% untuk beban linear dan 1.25% untuk beban bukan linear. Kajian juga menunjukkan masa tindak balas yang cepat iaitu 0.3ms. Prinsip operasi dan keputusan eksperimen prototaip 1kVA telah dibentangkan untuk mengesahkan kesahihan sistem yang dicadangkan. Kecekapan sistem UPS yang dicadangkan adalah 94% dalam mod bateri dan 92% dalam mod operasi biasa.

ACKNOWLEDGEMENTS

First, I am thankful to the Almighty Allah for enabling me to complete this challenging task.

I would first like to express my deep gratitude to my supervisor, Prof. Saad Mekhilef. His great help made my study in University of Malaya possible. His guidance, patience, encouragement, and financial support lead my study successfully overcoming all the difficulties in the long struggling way to Ph.D degree. It is my valued opportunity to learn the rigorous attitude towards study and research from him.

To my friends, I would like to thank my fellow members from PEARL Lab and friends, especially, Adeel Ahmed, Wajahat Tareen, Kafeel Ahmed, Mudasir, Imran Shafique, Habib Hassan, Abdul Ghafoor, Usman, Adil and Manoj Tripati for their assistance and support throughout my candidature.

My deepest gratitude belongs to my parents Mr. Abdul Wadud and Ms. Hussan Ara, my brothers Mr. Abdul Basit, Mr. Muhammad Zahid, and Mr. Muhammad Nasir, and my sisters Tahira, Ayesha, and Maria for their countless prayers, love, sacrifice, and unconditional supports for my study.

I also like to thank my wife Sobia Aamir for her love and emotional support provided during the course of my study. Thank you for your sacrifices. For my kid Mishkat, your love compelled me to complete my research on time.

TABLE OF CONTENTS

Abstract iii

Abstrak v

Acknowledgements 1

Table of Contents 2

List of Figures 6

List of Tables 10

List of Abbreviations 11

List of Symbols 12

CHAPTER 1: INTRODUCTION 13

1.1 Background 13

1.2 Problem Statement 16

1.3 Objectives of the study 16

1.4 Research Methodology 17

1.5 Thesis Outline 19

CHAPTER 2: LITERATURE REVIEW 21

2.1 Introduction 21

2.2 Classification of UPS 21

2.2.1 Offline UPS 21

2.2.2 Line Interactive UPS system 22

2.2.3 Online UPS System 23

2.2.4 Grid faults and UPS solutions 24

2.3 Topology based Classification of Uninterruptible Power Supplies (UPS) systems 25

2.3.1 Conventional Transformer-based UPS system..25

2.3.2 High-Frequency Transformer Isolation..28

2.3.3 Transformer-less UPS System...30

2.3.3.1 Batteries arrangement:...34

2.3.3.2 Bidirectional DC-DC Converter...36

2.3.4 Comparison of transformer based and transformerless UPS system........38

2.4 Control Techniques for Uninterruptible Power Supplies (UPS) 41

2.4.1 Single Loop Control 41

2.4.2 Multi-loop System..41

2.4.2.1 Deadbeat Control...42

2.4.2.2 Model Predictive Control (Cortes et al., 2009; S.-K. Kim, Park, Yoon, & Lee, 2015): 44

2.4.2.3 Repetitive control scheme 46

2.4.2.4 Iterative Learning Scheme...48

2.4.2.5 Comparison of Multi-loop control schemes...............................49

2.4.3 Non-linear Control Schemes 50

2.4.3.1 Adaptive Control 50

2.4.3.2 Multi-resonant control scheme..51

2.4.3.3 Slide Mode control 52

2.4.4 Application of Slide Mode Control 54

2.5 Summary...56

CHAPTER 3: PROPOSED TRANSFORMERLESS ONLINE UPS SYSTEM 57

3.1 Introduction..57

3.2 Proposed Transformerless UPS system 57

3.3 Modes of Operation 58

3.4 Bidirectional Converter 60

3.4.1 Battery Charging/Buck operation 61

3.4.2 Battery discharging/ Boost Operation 65

3.4.3 Coupled Inductor Design 70

3.5 Rectifier 74

3.5.1 Circuit Operation 75

3.5.2 Power factor correction ability 77

3.5.3 Input Inductor in CCM Mode 78

3.6 Single Phase H-bridge Inverter 79

3.6.1 Output Filter Design 81

3.7 Power loss calculation for the UPS system: 82

3.7.1 Slow Diodes 82

3.7.2 MOSFET 83

3.7.3 Fast Diode 83

3.7.4 Total power loss in the UPS system: 84

3.8 Summary 84

CHAPTER 4: PROPOSED CONTROL SCHEME 86

4.1 Introduction 86

4.2 Control scheme for the online UPS system 86

4.3 Inverter Control 87

4.1.1. State Space Equation 88

4.1.2. Slide Mode Control 89

4.1.3. Proportional Resonant Control 94

4.4 Rectifier Control 100

4.5 Battery Charger and Discharger Control 103

4.6 Summary 109

CHAPTER 5: RESULTS AND DISCUSSION 111

5.1 Introduction.. 111

5.2 System Specifications 111

5.3 Single Phase AC-DC Inverter 112

5.4 Bidirectional battery charger/discharger 121

5.5 Power Factor Correction (PFC) Rectifier 125

5.6 Transformerless UPS system 125

5.7 Summary 129

CHAPTER 6: CONCLUSION AND FUTURE WORK 130

6.1 Conclusion 130

6.2 Future Work 131

References 132

List of Publications and Papers Presented 143

LIST OF FIGURES

Figure 1.1: Sources of Power Quality Disturbances("Business Case for PQ Investment by Commercial Buildings," 2014) ... 14

Figure 1.2: Flow chart of research methodology ... 18

Figure 2.1: Block diagram of offline UPS system ... 22

Figure 2.2: Block diagram of line interactive UPS system ... 23

Figure 2.3: Block diagram of online UPS system ... 24

Figure 2.4: Types of power quality disturbance ... 24

Figure 2.5: Conventional UPS system (Holtz et al., 1988) ... 26

Figure 2.6: Circuit diagram of single phase UPS system with trapezoidal AC supply(Jain et al., 1998) ... 27

Figure 2.7: Three leg type converter proposed in (J.-H. Choi et al., 2005) ... 28

Figure 2.8: UPS system proposed in (Torrico-Bascope, Oliveira, Branco, & Antunes, 2008) ... 29

Figure 2.9: UPS system with BIFRED converter(Nasiri et al., 2008) ... 29

Figure 2.10: UPS system proposed in (Vazquez et al., 2002) ... 30

Figure 2.11: Circuit diagram of four leg type converter(J. K. Park et al., 2008) ... 31

Figure 2.12: Non-isolated UPS system (C. G. C. Branco et al., 2008) ... 32

Figure 2.13: Block diagram of online UPS system ... 35

Figure 2.14: Block diagram of Online UPS system with bidirectional DC-DC converter ... 36

Figure 2.15: Isolated bidirectional DC-DC converter(Han & Divan, 2008) ... 37

Figure 2.16: Multi-loop control scheme ... 42

Figure 2.17: Deadbeat control for UPS system ... 44

Figure 2.18: Model predictive control for UPS system ... 45

Figure 2.19: Repetitive control for the UPS system ... 47

Figure 2.20: Adaptive control for the UPS inverter 50

Figure 3.1: Block diagram of proposed online UPS system 57

Figure 3.2: Schematic of the proposed UPS system 58

Figure 3.3: Modes of operation of proposed UPS system 59

Figure 3.4: Proposed Bidirectional DC-DC Converter 60

Figure 3.5: Characteristic waveforms of the buck mode of operation 61

Figure 3.6: Operation in buck mode during interval 1 ($t_0 \sim t_1$) 62

Figure 3.7: Operation in buck mode during interval 2 ($t_1 \sim t_2$) 63

Figure 3.8: Operation in buck mode during interval 3 ($t_2 \sim t_3$) 63

Figure 3.9: Operation in buck mode during interval 4 (t3 ~ t4) 64

Figure 3.10: Operation in buck mode during interval 5 ($t_4 \sim t_5$) 65

Figure 3.11: Characteristic waveforms of the boost mode 66

Figure 3.12: Operation in boost mode during interval 1 ($t_0 \sim t_1$) 67

Figure 3.13: Operation in boost mode during interval 2 ($t_1 \sim t_2$) 67

Figure 3.14: Operation in boost mode during interval 3 ($t_2 \sim t_3$) 68

Figure 3.15: Operation in boost mode during interval 4 ($t_3 \sim t_4$) 68

Figure 3.16: Operation in buck mode during interval 5 ($t_4 \sim t_5$) 69

Figure 3.17: Operation in boost mode during interval 6 ($t_5 \sim t_6$) 70

Figure 3.18: Graph of voltage gain vs duty ratio 72

Figure 3.19: The operation of the rectifier during positive half cycle 75

Figure 3.20: The operation of the rectifier during negative half cycle 76

Figure 3.21: Waveform of boost inductor current in CCM mode 77

Figure 3.22: Single phase full bridge inverter 80

Figure 4.1: Control circuit of proposed UPS system 87

Figure 4.2: Inverter control block diagram 88

Figure 4.3: Block diagram of the Slide Mode Control with inverter and LC filter 92

Figure 4.4: Smooth Control Law for Boundary Surface (Slotine & Li, 1991) 93

Figure 4.5: Control Interpolation in Boundary Layer 93

Figure 4.6: Equivalent control diagram with SMC and PR control 95

Figure 4.7: Bode plot of voltage loop with PR controller 96

Figure 4.8: PR control with Lead-Lag compensator 96

Figure 4.9: Bode plot of voltage loop with lead-lag compensator 97

Figure 4.10: Close loop control of the rectifier 101

Figure 4.11: Bode response of the current loop gain of the rectifier 102

Figure 4.12: Bode response of the voltage loop gain of the rectifier 102

Figure 4.13: Circuit diagram and control of battery charger/discharger 104

Figure 4.14: Bode response of the current loop gain of the battery charger/discharger 107

Figure 4.15: Bode response of the voltage loop gain of battery charger/discharger..... 107

Figure 4.16: Thevenin battery model 108

Figure 5.1 Simulation waveform of output voltage and output current for linear and non-linear load 114

Figure 5.2: Simulation waveform of step response of the inverter 116

Figure 5.3: Output Voltage and Current for linear load 117

Figure 5.4: Output Voltage and Current for Non-linear Load, ... 118

Figure 5.5: Experimental waveform of Output voltage and Current for resistive load 118

Figure 5.6: Experimental waveform of output voltage and current for the non-linear load 118

Figure 5.7 Comparison of THD between SMC and SMC+PR 119

Figure 5.8 Experimental waveform of step change from 0% to 100% 120

Figure 5.9 Experimental waveform of step change from 100% to 0 120

Figure 5.10 Experimental waveform of step change from 100% to 60% 120

Figure 5.11: Experimental waveform of bidirectional converter during buck mode 123

Figure 5.12 Experimental waveform of bidirectional converter during boost mode 124

Figure 5.13 ZVS of the switch S_3 during buck mode 124

Figure 5.14 Experimental waveforms of input voltage and current 125

Figure 5.15 Transition from Normal to Battery Powered Mode. Input Voltage V_{in} and Current I_{in}, Output Voltage Vout and Current I_{out} 126

Figure 5.16 Transition from Battery power mode to Normal mode, Input Voltage V_{in} and Current I_{in}, Output Voltage V_{out} and Current I_{out} 126

Figure 5.17 Prototype image and experimental setup 127

Figure 5.18 Efficiency graph in normal and battery powered mode 128

LIST OF TABLES

Table 2.1: Grid faults and UPS classification ... 25

Table 2.2 Comparison of different UPS system configurations ... 33

Table 2.3 Comparison of Transformer-based and Transformerless UPS system ... 40

Table 3.1: Summary of buck operation mode ... 65

Table 3.2: Summary of the Boost mode of Operation ... 70

Table 3.3: Comparison of bidirectional converter ... 73

Table 3.4: Power loss by each component in UPS system ... 84

Table 4.1: Comparison of different control methods ... 100

Table 4.2: Specifications of the rectifier ... 103

Table 4.3 Battery Specifications ... 108

Table 4.4 Specification of the battery charger ... 109

Table 5.1 Specification of the proposed UPS system ... 112

Table 5.2 Specifications of the single-phase inverter ... 113

Table 5.3: Controller parameters of inverter ... 113

Table 5.4 Specification of the Battery Charger/Discharger ... 122

Table 5.5: Specifications of the Rectifier ... 125

Table 5.6 Comparison of Transformerless UPS ... 129

LIST OF ABBREVIATIONS

UPS	:	Uninterruptible Power Supply
THD	:	Total Harmonics Distortion
EMI	:	Electromagnetic Interference
MTBF	:	High Mean Time Before Failure
RMS	:	Root Mean Square
MC	:	Magnetic Contactor
EPRI	:	Electric Power Research Institute
PFC	:	Power Factor Correction
BMS	:	Battery Management System
SVM	:	Space Vector Modulation
MPC	:	Model Predictive Control
ILS	:	Iterative Learning Control
EMC	:	electromagnetic compatibility
SMC	:	Slide Mode Control
ZAD	:	Zero Average Dynamics
PR	:	Proportional Resonant
PI	:	Proportional Integral
ZVS	:	Zero Voltage Switching
CCM	:	Continuous Conduction Mode
DCM	:	Discontinuous Conduction Mode
PWM	:	Pulse Width Modulation
CC	:	Constant Current
CV	:	Constant Volume
SoC	:	State of Charge
HVS	:	High Voltage Side
LVS	:	Low Voltage Side

LIST OF SYMBOLS

g	:	Cost function
K_g	:	Control gain
D_1	:	Duty ratio of S_3
D_3	:	Duty ratio of S_4
L_m	:	Magnetizing Inductance
i_{LS}	:	Secondary winding current
i_{LP}	:	Primary winding current
V_{DC}	:	DC-link voltage
V_{Bat}	:	Battery voltage
G_{buck}	:	Buck gain
L_{11}, L_{12}	:	Boost Inductor
Re	:	Emulated Resistance
L_f	:	Filter inductor
C_f	:	Filter Capacitor
f_{sw}	:	Switching frequency
P_{Cond}	:	Conduction loss
P_{sw}	:	Switching loss
R_{DS}	:	Drain to source resistance
V_m	:	Magnitude of carrier wave of inverter
H(s)	:	Open loop gain
K_P	:	Proportional Gain
K_I	:	Integral gain
K_r	:	Resonant Gain
S(x)	:	Sliding Surface
C_d	:	DC-link capacitor
E_O	:	Ideal Battery voltage
V_{CP}		Polarization voltage
R_i		Internal resistance
i_{limit}		Current limiter for the battery bank
V_{in}		Input Voltage
V_{out}		Output Voltage
fr		Grid Frequency
fo		Output Frequency
N_b		Number of Batteries
f_{cut}		Cuttoff frequency for inverter

CHAPTER 1: INTRODUCTION

This chapter presents the background information, general features, and common characteristic of the Uninterruptible Power Supply (UPS) system. The problem statement has been defined, and the objectives of this research have been stated. Research methodology of the proposed work has been explained briefly followed by thesis outline.

1.1 Background

Modern economic activities are increasingly reliant on the digital technologies which are very sensitive to electrical disturbances. Any power disturbance such as power outage or voltage sag/swell results in malfunctioning of the sensitive equipment’s, loss in productivity and data, and in case of health care, loss of lives is also possible. Hence, power quality and power continuity is an important factor that needs to be ensured for critical applications.

The various sources of power quality disturbances are presented in Figure 1.1, which shows that a major percentage of the disturbance is caused due to the equipment used in business or a facility. As a result, many applications required backup power to protect against the risk of disturbance in the utility grid. An Uninterruptible Power Supply (UPS) system is used to provide protection and supplies backup power to sensitive equipments such as airline's computers, data centers, communication systems, and medical support systems in hospitals. Generally; the output of the UPS system is regulated, with low total harmonic distortion (THD), and irrespective of the changes in the input voltage or abrupt changes in the load connected to the system (Gurrero, De Vicuna, & Uceda, 2007).

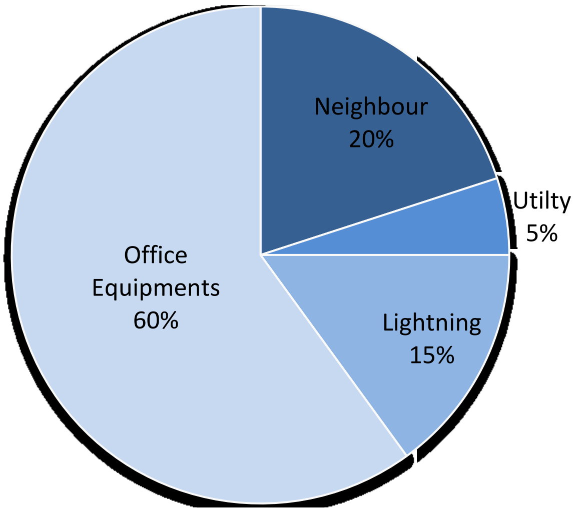

Figure 1.1: Sources of Power Quality Disturbances("Business Case for PQ Investment by Commercial Buildings," 2014)

UPS system is discovering widespread application scope along with ever accelerating informatization. Global UPS market sales for 2014 is estimated as USD 6.3 billion, and the figures in only China exceed USD 660 million. It is expected that the Chinese UPS market sales will exceed USD 820 million by 2017 ("China Uninterruptible Power System UPS Industry," 2014).

Currently, there are more than 3 million data centres all over the world, and the power capacity of these data centres is over 30,000 MW. During power blackouts caused by natural disasters, the failure of UPS system can bring about a huge loss. For example, the Fukushima nuclear power plant accident caused a 71 billion dollar loss. Data centre downtime of some famous Internet companies cause millions of dollars loss within several minutes. Hence, a high-surety and long backup time UPS system is thus the key to avoid these economic losses (Xu, Li, Zhu, Shi, & Hu, 2015).

Broadly the UPS can be classified as the Static UPS system and Rotary UPS system. The static UPS system uses power electronics converters and inverters to process, store, and deliver power during grid failure while Rotary UPS uses motors and generators for the same function. Sometimes the combination of both static and rotary UPS system is used usually called hybrid UPS System (King & Knight, 2003; Windhorn, 1992). A wide range of UPS systems is available in the market depending upon their ratings. The smaller units of only 300 VA are there to provide backup to a single computer, but the bigger unit of UPS may provide backup to an entire building of several megawatts.

Generally, the ideal UPS system should have the following features (Emadi, Nasiri, & Bekiarov, 2004)

1. Regulated sinusoidal output voltage with low total harmonic distortion (THD) independent of the changes in the input voltage or in the loading condition.
2. Zero switching time for transition from normal to backup mode and vice versa
3. Unity input power factor and low THD of the input voltage
4. High efficiency
5. High reliability
6. Low cost, weight, and size
7. Bypass as a redundant source of power in the case of internal failure
8. Low electromagnetic interference (EMI) losses and acoustic noise
9. Electric isolation of the battery, output, and input
10. High Mean Time Before Failure (MTBF)

With the advancements in power electronics during past few decades, different topologies of the UPS system have been developed. The researchers have been trying to improve the performance of the UPS system by implementing advanced control schemes, utilizing next-generation power switches, reducing the bulky magnetics, and expanding the application area of the UPS system.

The inverter of the UPS system must fulfil the following requirements in order to generate the output voltage (Heng Deng, Oruganti, & Srinivasan, 2005; Per Grandjean-Thomsen, 1992).

1. Constant steady state RMS voltage for 2% variation in any parameter like temperature, load current, or battery voltage.
2. Maximum of 10% transient peak voltage deviation is allowed during both loading and unloading of the UPS system.
3. The voltage drop of not more than 5% of the rated voltage cannot be tolerated for more than 2 AC cycles.
4. Inverter output voltage with total harmonic distortion (THD) of only 4% is allowed for all the loading conditions.

1.2 Problem Statement

Transformerless online UPS systems are famous due to its small volumetric size, light weight, and high efficiency of the system. However, the battery bank voltage in transformerless UPS systems is enormously high (C. G. C. Branco, Cruz, Torrico-Bascope, & Antunes, 2008; Marei, Abdallah, & Ashour, 2011; Schuch et al., 2006). Normally, the batteries are connected in series to achieve high battery bank voltage. However, the series battery arrangement leads to many problems of charging and discharging, decreasing the reliability of the system (H. S. Park, Kim, Park, Moon, & Lee, 2009). It also causes an increase in the volumetric size, weight, and cost of the system. Although a conventional bidirectional charger/discharger has been proposed to overcome the size of the battery bank, but still the battery bank voltage is very high, which is not a suitable design for low power UPS system (J. K. Park, Kwon, Kim, & Kwon, 2008). Hence, a flexible uninterruptible power supply needs to be developed depending upon the size, weight, protection, and battery bank considering the individual application, with additional requirements of efficiency and response time of the system.

1.3 Objectives of the study

The overall goal of this study is to develop a novel topology of non-isolated online UPS system, with the new robust control scheme for non-linear loading, mainly emphasizing on the volumetric size, efficiency, and battery bank voltage of the UPS system. The specific objectives of this work are as follows;

1. To propose a new non-isolated online UPS topology for low power applications.
2. To design a new robust control scheme for the proposed UPS system
3. To implement the proposed topology and control scheme of UPS system.
4. To analyze the performance of the UPS system for the parallel connected battery bank.
5. To perform stability analysis of different parts of the UPS system and their performance for different loading conditions.

1.4 Research Methodology

To fulfil the above mention objectives of this research study, a literature review of the research topic is performed to understand and analyze the state-of-art-works done on the transformerless UPS system. In order to develop the proposed UPS system, mathematical modeling and analysis is performed to find design parameters for the development of the proposed system. Each part of the proposed system is evaluated using simulation software Matlab/Simulink and PSIM. Similarly, the control schemes for the inverter, rectifier, and battery charger are realized mathematically and using simulations tools.

The developed topology of UPS system with optimum design parameters is implemented in hardware to get the final prototype of the proposed system. Different tests are performed to validate the performance of the UPS system and experimental results are presented. Furthermore, the comparison of the proposed system is performed with the other research done in the same transformerless UPS system. The flowchart of the research methodology is presented as follows;

Research Methodology

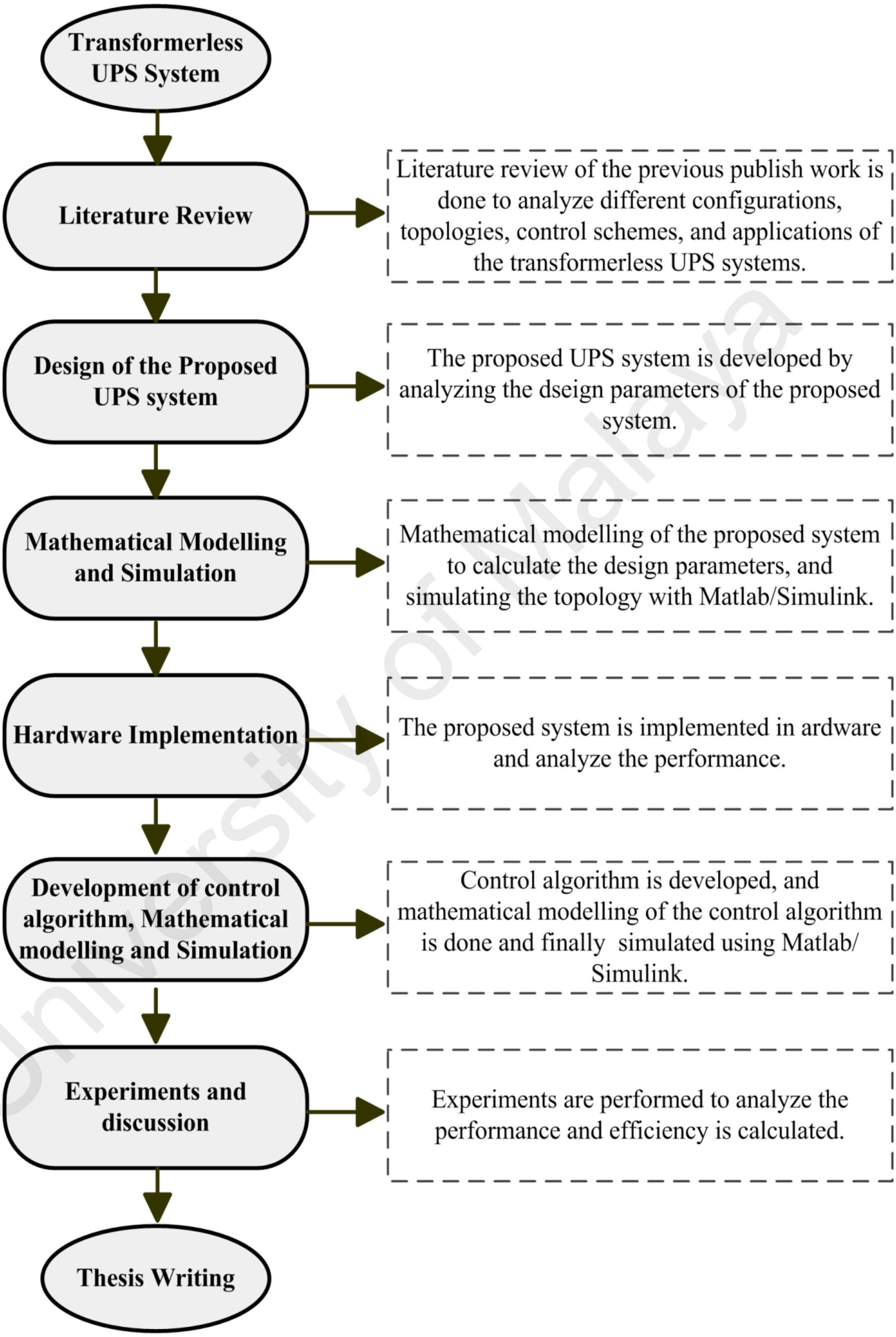

Figure 1.2: Flow chart of research methodology

1.5 Thesis Outline

This thesis introduces a new topology and control scheme of online transformerless UPS system, and presents its literature review, theoretical study, analysis, simulation and experimental analysis of UPS. The thesis is organized as follows;

Chapter 2 presents the detail literature review of the UPS system. The classifications of the UPS is explained based on configuration and circuit topology. Important features of the state-of-the-art work in both transformer-based and transformerless UPS system is presented. Besides, different control schemes for the UPS system is explained in detail, and comparison of their characteristics is performed.

In **Chapter 3**, different parts of the proposed topology of transformerless online UPS system is explained in detail. Modes of operation of the UPS are described, whereas mathematical modeling and design procedure of each power part is added to validate the feasibility of the implemented system.

Chapter 4 explains the proposed control scheme for the online transformerless UPS system. The control scheme comprises of the cascaded slide mode and proportional-resonant control for the inverter control, constant current/ constant voltage control for the battery charger/discharger, and the average current control scheme of the rectifier of the proposed UPS system. Mathematical modeling and design procedure of each control part has been explained comprehensively.

In **Chapter 5**, the simulation and experimental results of different parts of the UPS system is presented. The organization of this chapter is as such that; firstly, the simulation and experimental results of each part is explained separately. And then the experimental results of the combined UPS system are presented. These results depict the performance of the UPS system by displaying the input power factor, battery charging, zero voltage switching, and inverter output for different loading condition. Similarly, experimental results of the changing of operation modes of the UPS system is shown in this chapter. At the end, comparison of the proposed UPS system is performed with other state of the art works.

In **chapter 6**, conclusion of the research work is presented. The key contributions and their outcomes are illustrated. Finally, the future work of this study is highlighted.

CHAPTER 2: LITERATURE REVIEW

2.1 Introduction

This chapter presents the detail literature review of the UPS system. The classifications of the UPS is explained based on configuration and circuit topology. Important features of the state-of-the-art work in both transformer-based and transformerless UPS system is presented. Besides, different control schemes for the UPS system are explained in detail, and comparison of their characteristics is performed.

2.2 Classification of UPS

Depending on the topological configuration, the UPS systems are classified as Offline UPS, Line interactive UPS, and Online UPS system (Bekiarov & Emadi, 2002; Karve, 2000; Niroomand & Karshenas, 2010; Racine, Parham, & Rashid, 2005; Solter, 2002).

2.2.1 Offline UPS

The offline UPS consists of a battery charger, a static switch, and an inverter as shown in Figure. 2.1 (Marei et al., 2011; Martinez, Castro, Antoranz, & Aldana, 1989). A filter and a surge suppressor are sometimes used at the output of the UPS to avoid the line noise and disturbance before being provided at the output of the UPS. During normal mode operation, the battery charger will charge the battery bank, and at the same time the load is being provided by the power from main AC line. The inverter is rated at 100% of the load's demand. It is connected in parallel to the load and remains standby during the normal mode of operation. When there is a power failure, the static switch disconnects the load from the utility grid. Now the power is provided by the battery bank through the inverter to the load. The switching time of the static switch is normally less than 10ms, which does not affect the normal computer load (Martinez et al., 1989).

The advantages of the offline UPS are low cost, simple design, and smaller size of the system. However, the lack of real isolation from the load and the lack of voltage regulation are the main disadvantages of the offline UPS system. Furthermore, the performance of this system for non-linear load is very poor. Offline UPS system is commonly good for a small load with a rating of about 600 VA.

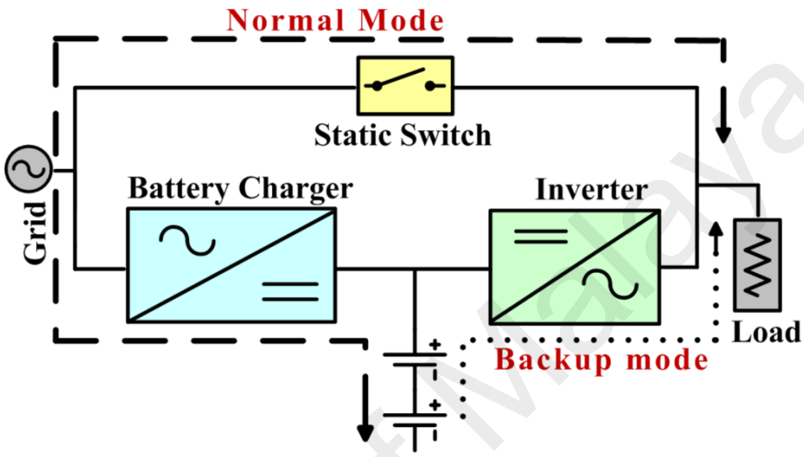

Figure 2.1: Block diagram of offline UPS system

2.2.2 Line Interactive UPS system

Line Interactive UPS consists of a static switch, bidirectional converter/inverter, and a battery bank as shown in Figure. 2.2 (Fu-Sheng & Shyh-Jier, 2006; Shen, Jou, & Wu, 2012). The bidirectional converter/inverter connects the battery bank to the load. During a normal mode of operation, the main AC line supplies the power to the load, and the bidirectional converter/inverter charges the battery. During the grid failure, the static switch disconnects the load from the main supply, and the bidirectional converter/inverter starts supplying power to the load. The line interactive UPS has the advantage of low cost, small size, and high efficiency. The only disadvantage is that it does not provide any voltage regulation during the normal mode of operation. Generally, the line interactive UPS system is rated between 0.5 kVA to 5 kVA and the efficiency of the system is normally greater than 97% provided the main AC line is clean from any transients and spikes.

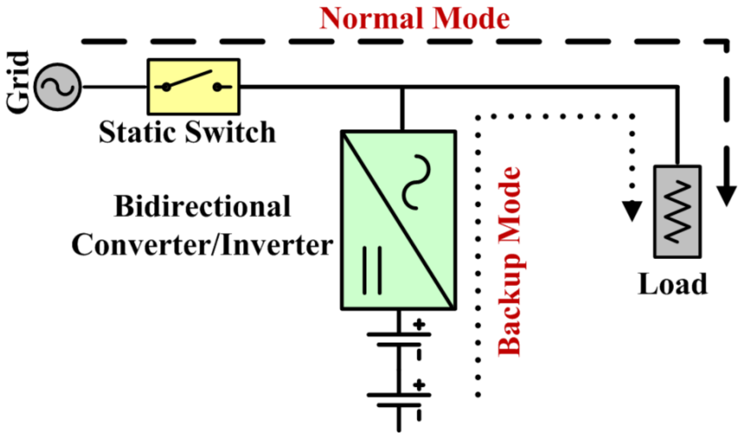

Figure 2.2: Block diagram of line interactive UPS system

2.2.3 Online UPS System

Online UPS consists of a rectifier, an inverter, and a static switch as shown in Figure 2.3(E. H. Kim, Kwon, Park, & Kwon, 2008; J. K. Park et al., 2008). During a normal mode of operation, the rectifier charges the batteries as well as maintains the constant DC-link voltage while the inverter converts the DC-link voltage to the required AC in order to feed the load. During a power failure, the Magnetic Contactor (MC) disconnects the AC line, but the inverter keeps supplying power to the load from the battery bank without any interruption. Thus, the inverter provides 100% load in both the mode operation. The inverter supplies clean and conditioned power to the load irrespective of the harmonics and variations in the grid voltage. The static switch provides redundancy of the power source in the case of UPS malfunction or overloading. The advantages of the online UPS include isolation of the load from the main line and almost negligible switching time. However, the major drawbacks of the online UPS include low efficiency, low power factor, and high total harmonic distortion (THD) (Gurrero et al., 2007). All the commercial units of 5 kVA and above are commonly online UPS system.

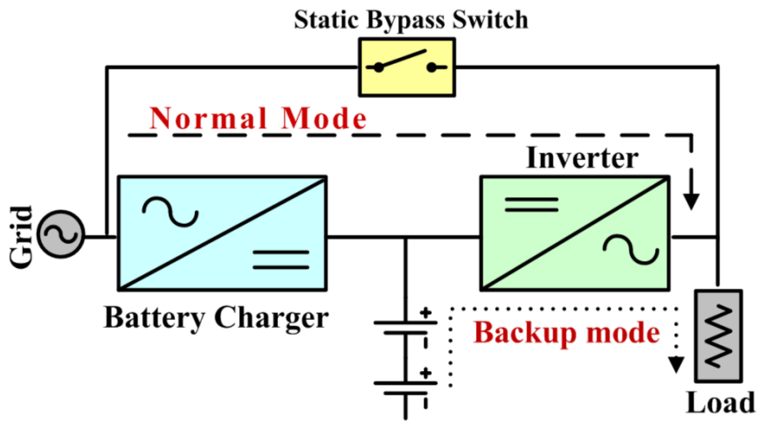

Figure 2.3: Block diagram of online UPS system

2.2.4 Grid faults and UPS solutions

The power supplied by the grid is not always very clean and continuous. There may be some major faults in the system which leads to long interruptions and completely black out of the grid. Besides, voltage swells and dropouts, voltage sag, harmonic distortion, etc. are other faults which are commonly encountered in the grid. Figure 2.4 shows the Electric Power Research Institute (EPRI) report of the year 1994 for different types of power quality disturbance in the state of Florida USA. Hence UPS system is important to protect the sensitive load from these disturbances. Different UPS system provides protection against the specific faults as shown in Table 2.1.

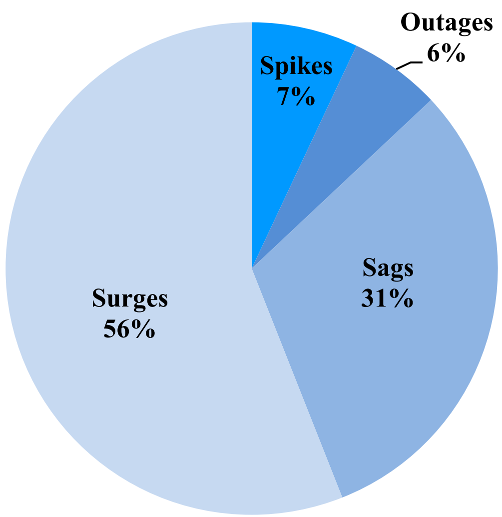

Figure 2.4: Types of power quality disturbance

Table 2.1: Grid faults and UPS classification

Sr. No	UPS System	Time	Common line Faults
1	Off-line UPS	>10ms	Line failure or long interruption, Voltage sags or dips, dynamic overvoltage
2	Line Interactive UPS	Continuous	Under voltage, Over voltage and voltage swell
3	Online UPS System	< 4ms, Continuous and periodic	Transients, Harmonic distortion, Noise, frequency variations, Impulses

2.3 Topology based Classification of Uninterruptible Power Supplies (UPS) systems

UPS system can be classified on the basis of the topologies and circuit configuration. The UPS system may be grid frequency transformer based, transformerless, or high-frequency transformer based system. These UPS systems are developed with different configurations keeping in view the features more suitable for the required application.

2.3.1 Conventional Transformer-based UPS system

Figure 2.5 shows the circuit diagram of conventional UPS system (Holtz, Lotzkat, & Werner, 1988; B. H. Kwon, Choi, & Kim, 2001). It consists of a rectifier, an inverter, grid frequency transformers, and a bypass circuit. The rectifier converts the grid voltage into a regulated DC-link voltage in order to charge the battery bank. The inverter converts the DC-link voltage into the regulated sinusoidal output voltage feed it to the connected load. Two grid frequency transformers are employed in the circuit. T_1 is used at the input side to step down the line voltage to low battery bank voltage while T_2 is employed at the output to step up the low battery bank voltage and also the operation of the bypass switch (Botteron & Pinheiro, 2007). Such system has an advantage of providing galvanic isolation from the transients and spikes generated inside the distribution grid. They are also more robust in operation and are designed for high power applications. However, both transformers are operated at grid frequency, so the size and weight of the system are enormously increased and so is the cost of the system. Additionally, most of the switches are connected to the low voltage battery bank. So high current is flowing through these switches; causing extra current stress in these switches. Hence, the efficiency of such systems is very low.

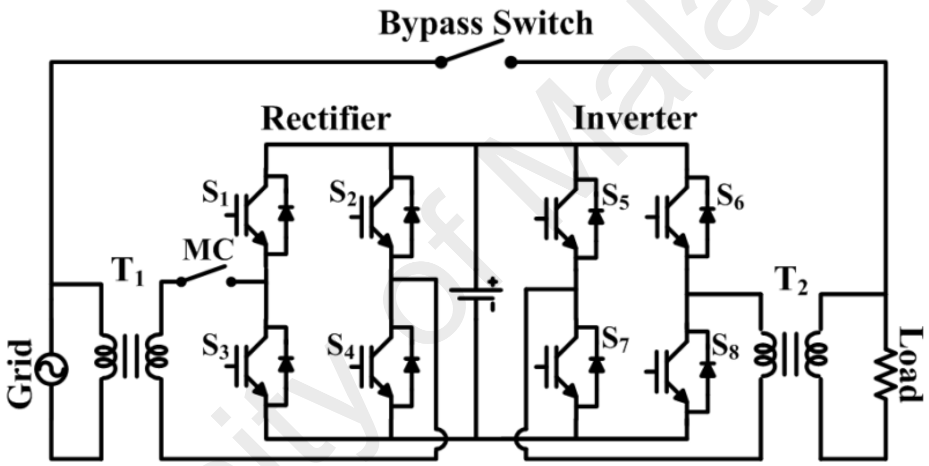

Figure 2.5: Conventional UPS system (Holtz et al., 1988)

Figure 2.6 shows a single stage UPS system which generates a trapezoidal shape output voltage and it is designed for the optical fiber/coax cable hybrid networks (Jain, Espinoza, & Jin, 1998). The circuit design of this UPS is almost similar to the conventional UPS system with the only difference of not using the power factor correction (PFC) circuit as smaller DC-link capacitor used in the circuit which helps to get the natural PFC. The trapezoidal shaped output voltage is synchronized with the input AC supply; hence, smaller DC-link capacitor is used to remove the current harmonics generated by the inverter. Since the transformer used in the system operates at low frequency, thus it is more costly and has large size and weight. Due to the absence of PFC circuit, the power factor of the system becomes low. Therefore, this UPS system is unsuitable for high power applications.

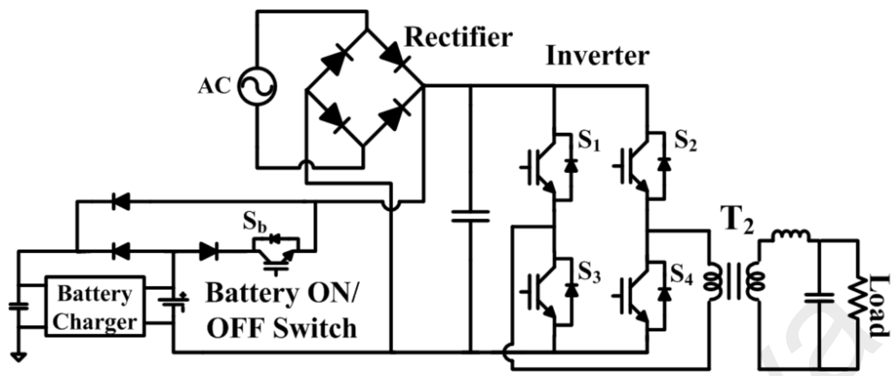

Figure 2.6: Circuit diagram of single phase UPS system with trapezoidal AC supply(Jain et al., 1998)

UPS systems using three leg type converter have been focused due to the reduced number of active switches (Chiang, Lee, & Chang, 2000; J.-H. Choi, Kwon, Jung, & Kwon, 2005; Jacobina, Oliveira, & da Silva, 2006). Figure 2.7 shows the circuit diagram of the UPS system proposed in (J.-H. Choi et al., 2005). In three leg type converter, the first leg and the common leg act as a rectifier which also charges the battery bank. The third leg and the common leg act as an inverter. The switches of the common leg are controlled at grid frequency. By using this common leg, the number of switches is reduced, which increases the overall efficiency of the system. Two leakage grid frequency transformers are used both at the input and output of the converter to reduce the cost of the system. Though the number of switches is reduced, but grid frequency transformers increase the size and weight of the system. Moreover, the batteries connected to the bus are high in number; charging and discharging at the same time. Thus, continuous overcharging may reduce the battery life.

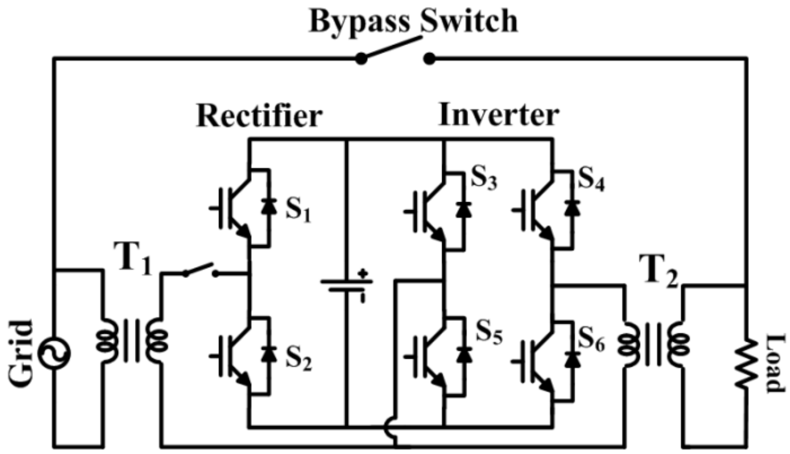

Figure 2.7: Three leg type converter proposed in (J.-H. Choi et al., 2005)

2.3.2 High-Frequency Transformer Isolation

With the development in the semiconductor industry, fast switches, and diodes are now available in the market with nearly ideal characteristics. Now the transformer can be used at high frequency with the advantages of reduced volume, an inherent property of galvanic isolation, and improved efficiency of the system. Several UPS topologies with high-frequency transformer have been introduced in (K Hirachi, Yoshitsugu, Nishimura, Chibani, & Nakaoka, 1997; Nasiri, Nie, Bekiarov, & Emadi, 2008; H. Pinheiro & Jain, 2002; Tao, Duarte, & Hendrix, 2008; R. Torrico-Bascopé, Oliveira, Branco, & Antunes, 2005; R. P. Torrico-Bascopé, Oliveira, Branco, Antunes, & Cruz, 2006; Vazquez et al., 2002; Yamada, Kuroki, Shinohara, & Kagotani, 1993). Such UPS system has smaller size and light weight as compare to the conventional UPS systems. However, an extra number of active switches are used to operate the transformer at high-frequency. It reduces the overall efficiency and increases the cost of the system.

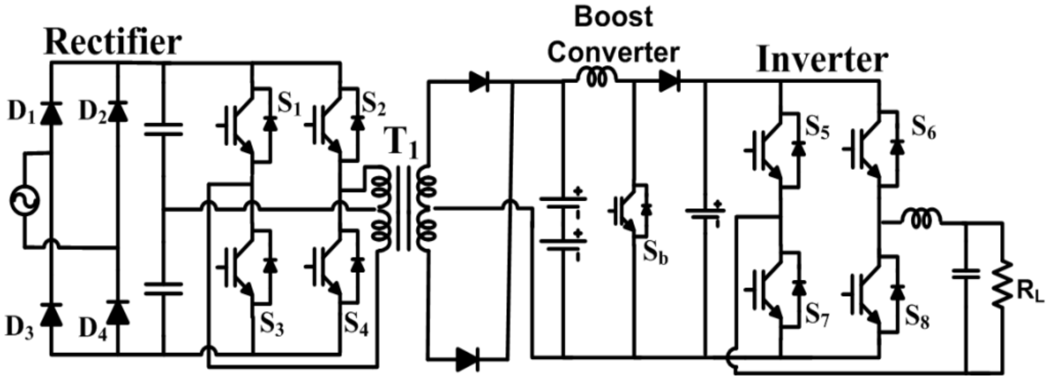

Figure 2.8: UPS system proposed in (Torrico-Bascope, Oliveira, Branco, & Antunes, 2008)

Figure 2.8 shows a flexible UPS topology which can operate over a wide range of input voltage (Torrico-Bascope et al., 2008). During a normal mode of operation, the chopper converts the grid voltage into DC and delivers high-frequency pulses to the primary of the high-frequency transformer. The transformer steps down the rectified voltage in order to charge the batteries. During the power failure mode, the battery bank voltage is stepped up using boost converter and is applied to the inverter which can supply regulated output voltage. Although this topology has the advantages of small size and light weight because of the high-frequency transformer and can also provide galvanic isolation. However, a high number of active switches and extra power processing stage decrease the efficiency of the system and add complexity to the circuit.

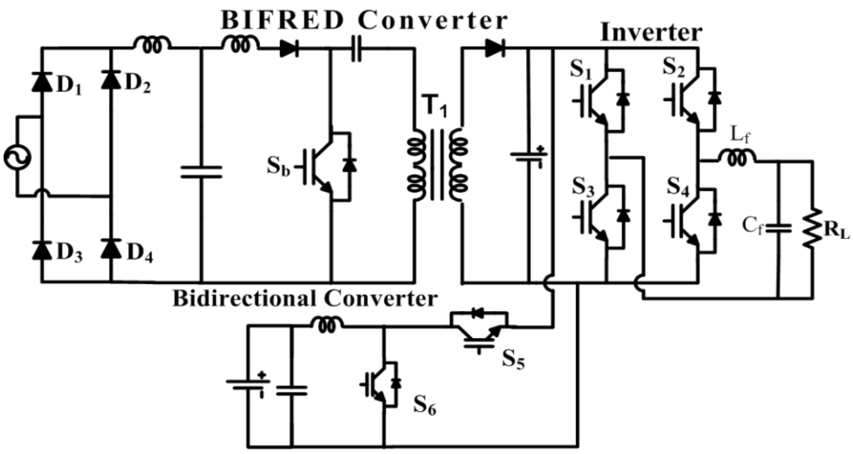

Figure 2.9: UPS system with BIFRED converter(Nasiri et al., 2008)

An improved UPS system is proposed in (Nasiri et al., 2008) as shown in Figure 2.9 which introduce boost integrated flyback rectifier/energy storage DC-DC converter (BIFRED) to maintains the constant DC-link and also charge the battery. But the battery bank voltage of the circuit will be increased significantly if the system is designed for 220V grid voltage.

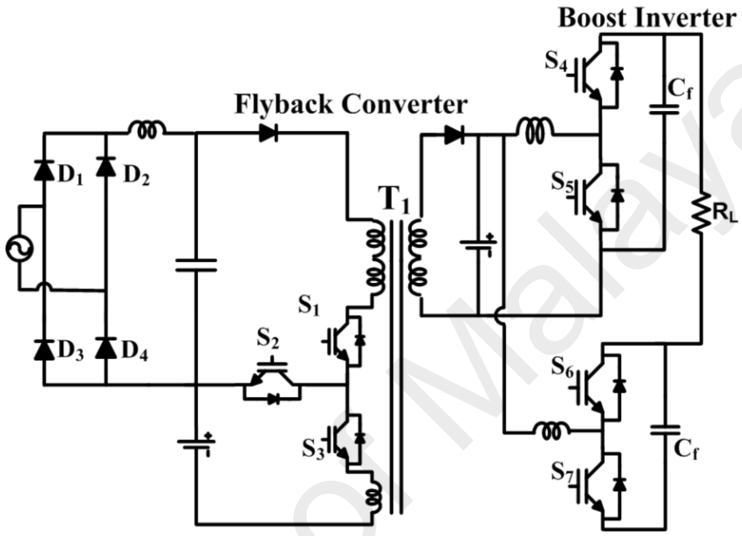

Figure 2.10: UPS system proposed in (Vazquez et al., 2002)

A two stage UPS as shown in the Figure 2.10 is proposed in (Vazquez et al., 2002). The first stage consists of single stage AC-DC converter utilizing flyback converter while the second stage consists of a boost inverter which supplies the regulated output voltage. Since the flyback converter may operate in discontinuous conduction mode, so the proposed topology is not suitable for high power applications.

2.3.3 Transformer-less UPS System

Nowadays, with the development of advanced microcontrollers and advancement in the power electronics, transformerless UPS is getting popularity in the market. These UPS are cheap, highly efficient, and most importantly smaller in size than the transformer-based UPS. However, the transformerless UPS has some major limitation, which needs to be addressed. This type of UPS is more likely to be affected by the transients and spikes caused by miscellaneous devices connected to the main utility grid (Koffler, 2003). The battery bank in transformerless UPS is very high. In order to achieve high DC-link voltage, many batteries are connected in series that increases the cost of battery bank and reduces the reliability of the system (Daud, Mohamed, & Hannan, 2013; J. K. Park et al., 2008).

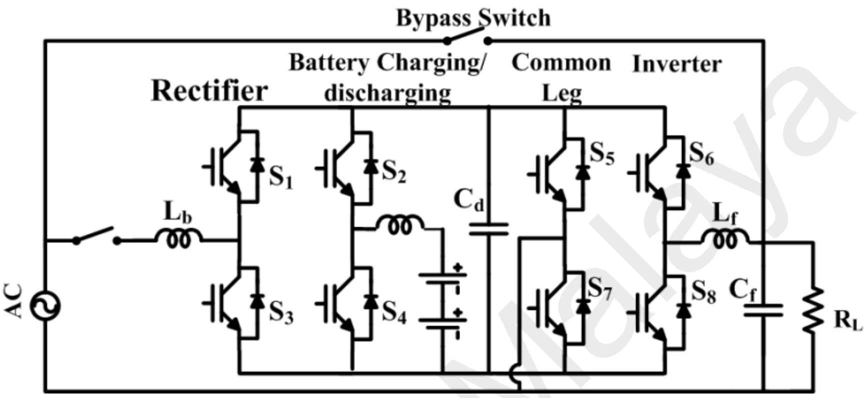

Figure 2.11: Circuit diagram of four leg type converter(J. K. Park et al., 2008)

Four leg type transformer-less online UPS system has been proposed in (J. K. Park et al., 2008). The four leg type converter act as a rectifier, battery charger/discharger, and an inverter as shown in the Figure 2.11. The common leg is switched at a grid frequency while the rectifier, the battery charger/discharger, and the inverter are switched at their respective PWM signals. Since a bidirectional converter has been used, it charges the battery during the normal mode and discharges the battery during the power failure mode. So the system has been operated without transformer, and the battery bank is reduced to 192V.

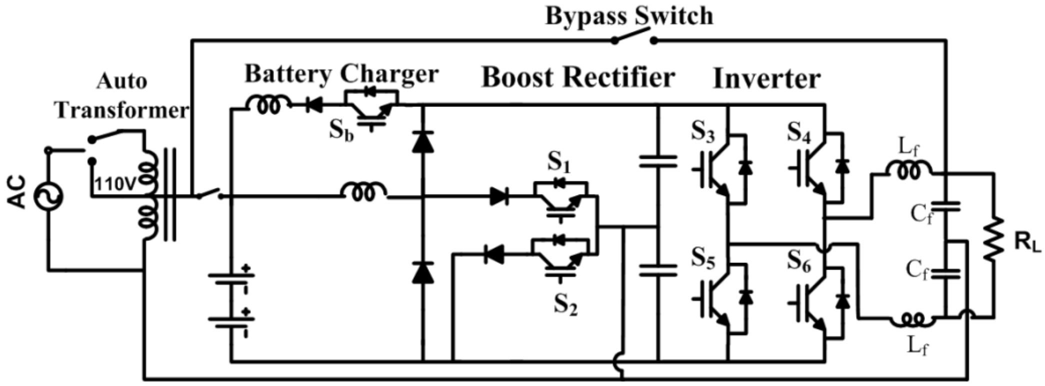

Figure 2.12: Non-isolated UPS system (C. G. C. Branco et al., 2008)

Another non-isolated online topology is proposed in (C. G. Branco, Cruz, Torrico-Bascopé, Antunes, & Barreto, 2006) as shown in the Figure 2.12. This UPS system can be operated at two different voltage levels and can also provide two output of 110V. The proposed UPS topology consists of a battery charger, three level boost rectifier, and a double half bridge inverter. The double half bridge inverter generates two independent 110V AC output voltages. An autotransformer is used at the input of the system to enable the operation at 110V. The DC-link voltage in this topology is about 108V and nine batteries connected in series, forming the battery bank, which is still quite high.

Table 2.2 shows the comparison of the different UPS configuration discussed in the literature. The size and weight of the system is related to number of the components used in the UPS system. More number of switches and diodes will leads to larges heat sink. Similarly the transformer, couples inductors, and capacitor also add to volumetric size and weight of the system. The volumetric size and weight of the transformer based UPS system are very high with low efficiency of the system. Similarly, the overall efficiency of the transformerless UPS system is high as compared to the transformer based UPS system.

Table 2.2 Comparison of different UPS system configurations

UPS topology \ Properties	Configuration	Efficiency	Power Ratings	Power Factor	System Specification	Battery bank	Size & Weight
Conventional Transformer Based UPS	Grid-Frequency Transformer	Less than 90%	75KVA	0.8 ~ 0.9	110V/220Vac	12V ~ 360V	Very High
Single Stage UPS system with trapezoidal AC supply (Jain et al., 1998)	Grid-Frequency Transformer	85%	1KVA	0.9	110Vac	80V	High
Three Leg Type Converter UPS system (J.-H. Choi et al., 2005)	Grid-Frequency Transformer	87%	3KVA	0.99	220Vac	192V	High
A UPS with 110/220-V Input Voltage and High-Frequency Transformer Isolation (R. P. Torrico-Bascopé et al., 2006)	High-Frequency Transformer	86%	2KV	0.7	110Vac as well as 220Vac	96V	Medium
An on-line UPS system with electric isolation using BIFRED converter (Nasiri et al., 2008)	High-Frequency Transformer	Less than 90%	<1KVA	high	110Vac	48V	Smaller
Two stage UPS with high power factor correction (Vazquez et al., 2002)	High-Frequency Transformer	84%	<500VA	0.99	110Vac	48V	Smaller
Transformer-less Online UPS System (J. K. Park et al., 2008)	Transformerless	96%	3KVA	0.99	220Vac	192V	Smaller
Non-isolated UPS with 110/220 V input –output voltage (C. G. Branco et al., 2006)	Transformerless	86%	2.6KVA	0.9	Both 110Vac & 220Vac	108V	Medium
Z-Source Inverter Based UPS System (Z. J. Zhou, Zhang, Xu, & Shen, 2008)	Transformerless	>90%	3KVA	-	220Vac	360V	Smaller

The battery bank is an important element in the design of the transformerless UPS system since it has a great impact on the cost, volume, and weight of the overall system. Therefore, special attention must be given to design the battery bank and its charger, to maximize battery life and reduce cost, weight, and volume of the battery bank (Schuch et al., 2006). The following possible solutions are proposed to this problem.

1. Connecting the batteries in series to achieve the required DC-link voltage
2. Introducing the bidirectional DC-DC converter between the DC-link and the battery bank can possibly reduce the battery bank voltage considerably.

2.3.3.1 Batteries arrangement:

The transformerless topology delivers better performance because of efficiency improvement, volume and weight reduction, decreasing the number of switches, and capital cost of the system. However, the size of the battery bank in all the proposed systems so far is enormously high as shown in Table 2.2. Normally, the batteries are connected in series to achieve the high battery bank voltage. Figure 2.13 shows the block diagram of the transformerless online UPS system. The efficiency of the series connected battery bank is high due to reduced conduction losses. However, in these topologies, the battery bank is subjected to a high voltage, reducing the reliability and increasing its cost, mainly for low-power UPS (Divan, 1989; Kazuyuki Hirachi, Sakane, Niwa, & Matsui, 1994) Moreover, the DC-bus voltage ripple will be absorbed by the battery bank, decreasing its lifetime (Kiehne, 2003).

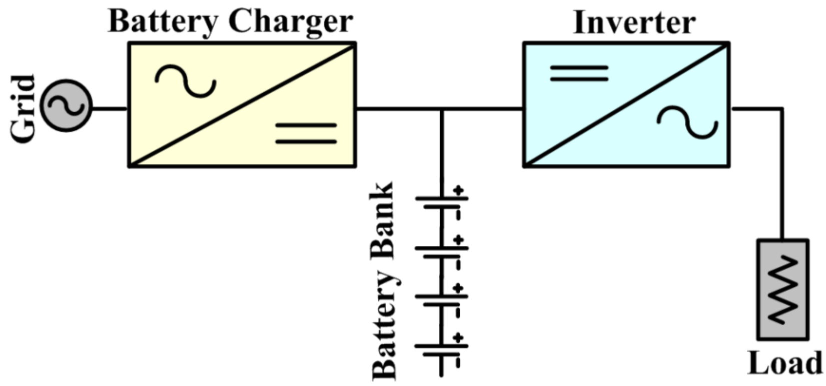

Figure 2.13: Block diagram of online UPS system

The series battery arrangement has major drawbacks and limitations in charging and discharging. A small imbalance in voltages occurs across the battery cells during charging and discharging since battery cells are not equal. Hence, these cannot provide the same performance during operation. Overcharging will cause severe overheating, low performance, and even destruction (H. S. Park et al., 2009). Similarly, deep discharge may cause the battery cell to be damaged permanently (Lee & Cheng, 2005). Battery Management System (BMS) needs to be installed for the protection of the series connected battery bank which adds to the capital cost and complexity of the system.

Due to this reason, small battery bank voltage with batteries operating in parallel improves the performance of the battery bank significantly. The batteries operating in parallel have following advantages;

1. The number of batteries is not restricted to the DC-link voltage. The volume, weight and backup time of the battery bank should be designed according to with specific desired application.
2. Cost reduction as no extra voltage balancing circuit is required.
3. Damaged batteries can be isolated or replaced from the battery bank, thus leaving the sensitive system operation uninterrupted. This is prime function of UPS system.

4. Since discharging currents of the batteries can be profiled individually. Hence, the stored energy in the batteries can be utilized more efficiently.

2.3.3.2 Bidirectional DC-DC Converter

Another possible solution for the problem of the high battery bank is to include a bidirectional converter for the DC-bus and battery bank interface, as depicted in Fig. 2.14. Thus, there is flexibility in the choice of the battery bank voltage, making it possible to minimize battery cost, volume, and weight. In addition, low frequency (100/120 Hz) DC-bus voltage ripple can be largely reduced in the battery bank charge process.

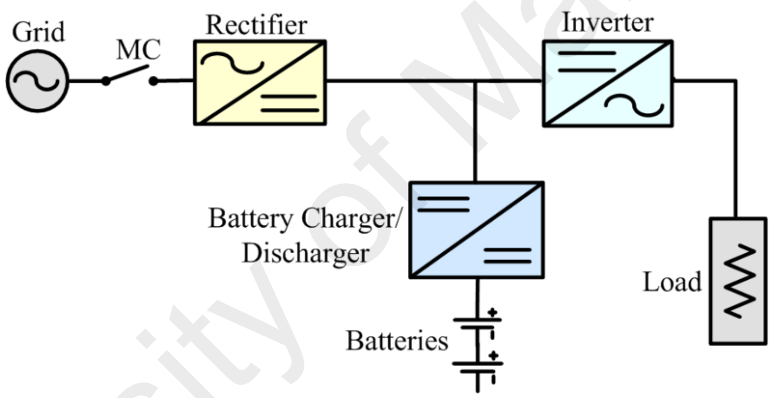

Figure 2.14: Block diagram of Online UPS system with bidirectional DC-DC converter

The bidirectional converter may be transformer isolated (Zhu, 2006) or non-isolated (Das, Laan, Mousavi, & Moschopoulos, 2009; Duan & Lee, 2012; I.-D. Kim, Paeng, Ahn, Nho, & Ko, 2007; M. Kwon, Oh, & Choi, 2014; Lin, Yang, & Wu, 2013; S.-H. Park, Park, Yu, Jung, & Won, 2010; Shiji, Harada, Ishihara, Todaka, & ALZAMORA, 2004; J. H. Zhang, Lai, Kim, & Yu, 2007). Isolated bridge-type bidirectional converters are probably the most popular topology in high power applications. Figure 2.15 shows an isolated bidirectional DC-DC converter. It consists of two full-bridge converters, two DC capacitors, an auxiliary inductor, and a high-frequency transformer. The high-frequency transformer provides the required galvanic isolation and voltage matching between two voltage levels. The auxiliary inductor serves as the instantaneous energy storage device. However, the major concerns of this topology are high switching losses; excessive voltage and current stress, and significant conduction losses because of the increased in the number of switches (Shiji et al., 2004). Hence, their practical implementation is quite complex.

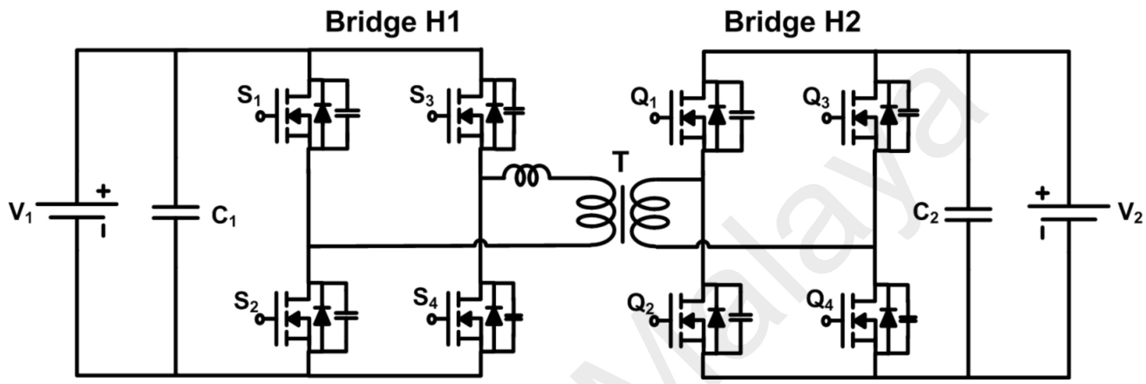

Figure 2.15: Isolated bidirectional DC-DC converter(Han & Divan, 2008)

Non-isolated converters have obvious merits of lower magnetics bulk, higher efficiency, and compactness (Han & Divan, 2008; Li & Bhat, 2010; Xuewei & Rathore, 2014). To improve the power density high-frequency operation of the DC-DC converter is necessary. However, at high device switching frequency, switching transition losses in semiconductor devices is very high; therefore, soft switching is desired.

Hard switching non-isolated converters have been reported in the literature (Hsieh, Chen, Yang, Wu, & Liu, 2014; Liang, Liang, Chen, Chen, & Yang, 2014; Wai, Duan, & Jheng, 2012) for microgrid application that offers high step up/ step down ratio. However, hard switching of the devices limits the device switching frequency.

With the incorporation of coupled inductor and zero voltage switching (ZVS), non-isolated bidirectional converters have attracted special interest due to the high conversion ratio, reduced switching losses, and simplicity in design. These types of topologies are cost-effective and acceptable due to high-efficiency improvement, and a considerable reduction in the weight and volume of the system. Several topologies of the non-isolated converters have been proposed so far (Das et al., 2009; I.-D. Kim et al., 2007; Shiji et al., 2004; J. H. Zhang et al., 2007). A ZVS bidirectional converter with single auxiliary switch has been proposed in (Das et al., 2009). Although the main switches operate under ZVS, which increases the efficiency of the system, but the auxiliary switch still performs hard switching, and the converter offers very limited voltage diversity (S.-H. Park et al., 2010).

Another approach is used in the quasi-resonant converter (Lee & Cheng, 2006). The main problem associated with such converter is high voltage stress on the power switches which makes difficult to control and implement it. Zero-voltage-transition (ZVT) bidirectional converter proposed in (Schuch et al., 2006) utilizes auxiliary circuit in order to operate the power switches under soft switching condition. However, the complexity of the circuit still remains.

Other high voltage gain bidirectional converters have been proposed in (Duan & Lee, 2012; Hsieh et al., 2014; M. Kwon et al., 2014; Lin et al., 2013). These converters provide high voltage gain in both the boost and buck mode of operation, but at the cost of a high number of active switches and extra auxiliary circuit components used in the circuit. This adds more complexity in the control circuitry, with high size and cost.

Hence, a high voltage gain bidirectional DC-DC converter allows the UPS system to operate at low battery bank voltage. In addition, the fewer semiconductor devices, high efficiency, and small volumetric size are the important characteristics need to be considered in the design of the bidirectional converter.

2.3.4 Comparison of transformer based and transformerless UPS system

Nowadays, the transformer-based UPS system is subjugated by the transformerless UPS system because of its small size, light weight, and high efficiency. This UPS system offers highly compact and cost effective design for low power applications without using any bulky power transformer**.** On the other hand, transformer based UPS system provides galvanic isolation, with high reliability, and robust operation of the system.

With so many choices to select the Uninterruptible Power Supply (UPS), which one is the most suitable UPS system according to the required circumstances? In selecting a UPS system, there is always a trade-off between certain features depending upon the specific application. Transformer-based UPS system isolates the load from the faults generated in the main supply. Hence, the applications where the UPS has to operate in high risk mission critical sectors such as telecoms and military environments, transformer-base UPS systems are the best choice. In fact, the transformer itself acts as a physical barrier and averts all the transients and spikes propagating to the DC-bus from the main supply and vice versa. Furthermore, because transformer-based UPSs inherently contain galvanic isolation, the power supply fed into the load is invariably superior to the mains supply itself. This attribute alone can be a major consideration for a number of crucial applications and installations. In fact, the latest electrical standards for medical installations (BS-EN 60601 and 61558-2) require that critical devices be connected through a Galvanic Isolation transformer, rather than directly to the raw mains.

The transformer based UPS is more reliable and robust in operation with high "Mean Time Before Failure" (MTBF). In contrast, the transformerless UPS system uses the electronic circuits to accomplish the online operation. Hence, they are more susceptible to faults from the transients, spikes and interference in the grid. However, the transformer-based UPS systems are significantly larger in size and heavier than transformerless UPS system. The efficiency of the transformerless UPS is about 10%

greater than the transformer based UPS system of the same specification due to the absence of the power frequency transformer. Besides, the transformer based UPS system makes continuous noise (hum sound) which makes it unsuitable for the offices. The transformerless UPS systems are quieter in operation and run considerable cooler as compare to its transformer base system.

Though the transformerless UPS system has a complex design, most of the components are semiconductors, which are cheaper than transformer-based variety. Hence, transformerless UPS is cheaper than transformer based UPS system. Without input and output transformer, the cost of the transformerless UPS system can be reduced to 30% or even more. Moreover, the size and weight can be reduced to 50% in transformerless UPS system. Table 2.3 shows the summary of comparison between transformerless and transformer based system.

Table 2.3 Comparison of Transformer-based and Transformerless UPS system

Sr. No	Properties	Transformerless UPS system	Transformer based UPS system
1	Volumetric Size	Small	Large
2	Weight	Light	Heavy
3	Efficiency	High	Low
4	Capital cost	Low	High
5	Meat Time Before Failure (MTBF)	Less	More
6	Reliability	Medium	High
7	Performance against transients and spike	Low	High
8	Performance in polluted grid environment	Low	High
9	Complexity of design	High	Less
10	Noise	Low	High

2.4 Control Techniques for Uninterruptible Power Supplies (UPS)

The control strategy is the most important part of all UPS systems. Parameters like total harmonics distortion, dynamic response to the transients and spikes, power factor correction, voltage and current regulation. are all dependent on the control strategy implemented in the UPS system. Nowadays many modern control techniques have been proposed in literature which shows better performance in all the circumstances. Broadly the control techniques can be classified as single loop and multi-loop control schemes.

2.4.1 Single Loop Control

In single loop control scheme, specific parameter (variable) is control using suitable compensation method. For example in voltage control scheme, the voltage feedback loop is used to provide the well-regulated output voltage with low THD (Karshenas & Niroomand, 2005). In this scheme, the peak voltage is detected and compared with the reference signal to generate an error that controls the reference to the modulator. Though this system is simple to design and quite inexpensive but its performance is poor in a complex system.

2.4.2 Multi-loop System

Multi-loop control schemes are more suitable in order to get better performance. They are more robust and flexible in control, even in non-linear and unbalanced system (Abdel-Rahim & Quaicoe, 1996; Jung & Ying-Yu Tzou, 1997). A conventional multi-loop control scheme has been shown in the Figure 2.16. In this control scheme, different parameters are used as a feedback to the controllers like filter inductor/capacitor current or output current and voltage. The outer loop uses output voltage as feedback signal; while the inner loop uses inductor or capacitor output filter current as the feedback signal. The feedback signal is compared with the reference signal to generate an error, which is compensated by the suitable compensator to achieve stable output. Similarly, the output of the voltage loop is the reference for the current loop. Hence both the voltage and current stability is achieved using multi-loop system. Different high performance controllers have been developed by employing multi-loop feedback control scheme which provide excellent performance (Cortes et al., 2009; H. Deng, Oruganti, & Srinivasan, 2007, 2008; Mattavelli, 2005; Xiao et al., 2002; K. Zhang, Kang, Xiong, & Chen, 2003) such as dead beat control(Buso, Fasolo, & Mattavelli, 2001; Mattavelli, 2005; Nasiri, 2007; Yongchang Zhang, Xie, & Zhang, 2014), model predictive control (Cortes et al., 2009; Rodriguez et al., 2013), iterative learning control (H. Deng et al., 2007) etc.

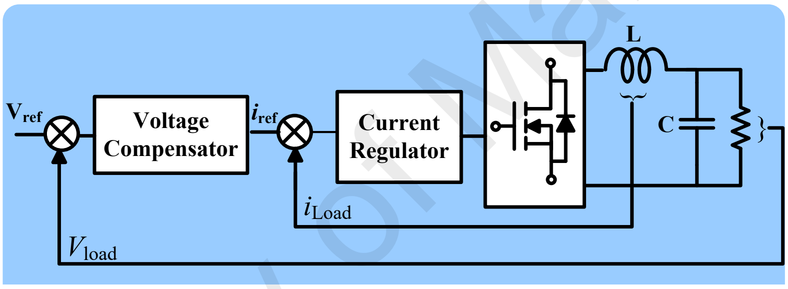

Figure 2.16: Multi-loop control scheme

2.4.2.1 Deadbeat Control

Deadbeat control is one of the most popular control schemes for UPS system (Mattavelli, 2005). In deadbeat control, the reference voltage is calculated during each sampling period using system model parameters, and is applied to follow the reference value in the next sampling instant. It offers fastest transient response because all the closed loop poles are placed near zero. This results in minimum settling time as few sampling steps are required. The deadbeat control together with space vector modulation (SVM) provides lowest distortion and current ripples(Le-Huy, Slimani, & Viarouge, 1994). However, the deadbeat control is very complex and is highly sensitive to parameter variations, loading uncertainties, and steady state error. The proportional integral compensator is connected in parallel to deadbeat control in order to overcome the issue of parameter sensitivity(Le-Huy et al., 1994). However the PI compensator works against unknown error dynamics which affect its performance. Introducing fuzzy logic tuned deadbeat control can remove the problem of parameter sensitivity with the cost of complex real time implementation of the algorithm(Tzou & Lin, 1998).

In order to improve the robustness of the deadbeat control, the uncertainties causing the voltage disturbance can be estimated and used in the feedforward control. Since the estimation is based on the inverse current dynamics, it results in noisier estimate. Therefore, a low-pass filter is adopted in the proposed estimators. The phase delay between the real voltage disturbance and the actual voltage disturbance degrades the compensation characteristics and limits the robustness range. In (Bode, Loh, Newman, & Holmes, 2005), new technique has been applied to improve the robustness of the deadbeat control against uncertainties by assuming the target current from the difference of the previous two current states in each cycle. However, the robustness and stability ranges are up to 53% mismatch in the load inductance. The robustness range has been extended but still unpredicted change in load inductance can cause instability.

The performance of the deadbeat control also reduces due to unpredicted sources of disturbance, such as dead-times, DC-link voltage fluctuations, and so on, since there is no inherent integral action in the control structure. Figure 2.17 shows a deadbeat control scheme for UPS system. A state observer is used to compute the delay while the load current is estimated using the disturbance observer. Any disturbance in the system is compensated by the state observer. This method gives better performance by reducing control sensitivity to model uncertainties, parameter mismatches, and noise in sensed variables.

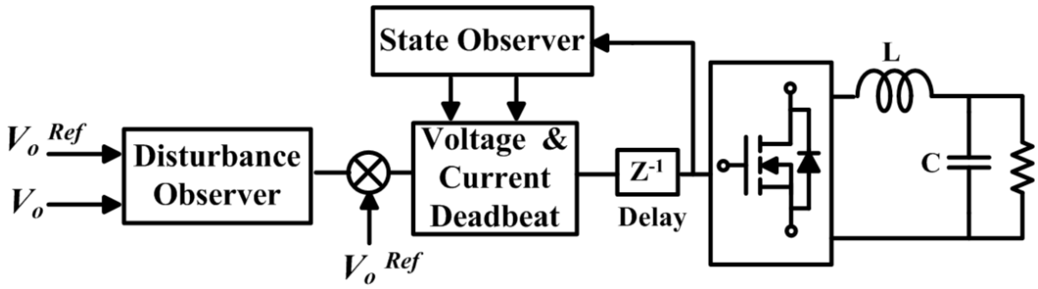

Figure 2.17: Deadbeat control for UPS system

2.4.2.2 Model Predictive Control (Cortes et al., 2009; S.-K. Kim, Park, Yoon, & Lee, 2015):

Model Predictive Control (MPC) is considered as one of the important advancement in the process control engineering. MPC provides high performance and stability in the control of UPS system. It is a flexible control scheme in which different system constrains e.g current and voltage limitation, switching states, and non-linearity can be included in the optimization of the controller. A cost function is usually formulated considering different variables and weighting factor. A switching state is selected in order to minimize the cost function and applied in the next switching state. Cost function can be formulated with many possible ways considering different rules and including several variables and weighting factors (Cortes, Kazmierkowski, Kennel, Quevedo, & Rodriguez, 2008). (Kley, Papafotiou, Papadopoulos, Bohren, & Morari, 2008) explains the use of different prediction horizons. Modulator can be used to apply optimal voltages, in order to ensure continuous inputs of the system (Veenstra & Rufer, 2005). The UPS inverter is modelled into finite number of switching states and only one time step horizon can be considered for the optimization (Rodriguez et al., 2007). Hence, online evaluation of all the switching states can be performed and the state which minimizes the cost function is selected.

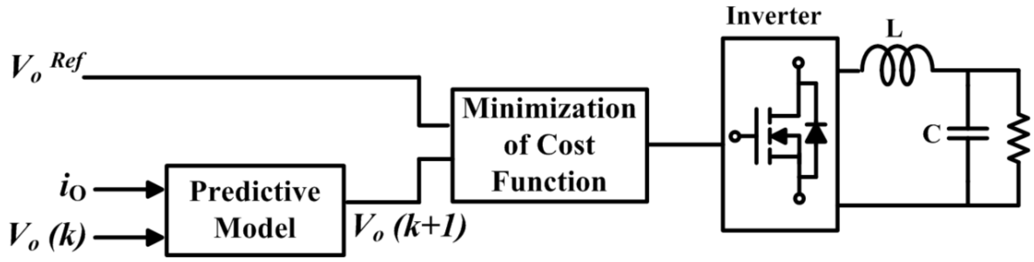

Figure 2.18: Model predictive control for UPS system

Figure 2.18 shows the common model predictive control for the inverter of UPS system. The load current measured at instant *K* is used as input to the predictive model which derives the value of the current for the next sampling time, for each switching state of the inverter. At each instant *K*, cost function over a finite horizon of length *N* is minimized and the horizon is shifted to next step, where another optimization has been performed.

Following are the summarized steps for implementation of Model Predictive control schemes for the inverter:

1. Measure the controlled variables
2. Apply the optimal switching state
3. For every switching state of the converter, predict (using the mathematical model) the behaviour of variable x in the next sampling interval x_p
4. Evaluate the cost function, for each prediction;

$$g = |x_{ref} - x_p| \qquad (2.1)$$

5. Select the optimum switching state that minimizes the cost function and store it in order to apply it to the converter in the next sampling period

2.4.2.3 Repetitive control scheme

Repetitive control scheme has widely been used for the rejection of periodic disturbance in a dynamic system (D. Chen, Zhang, & Qian, 2013; S. Chen, Lai, Tan, & Tse, 2008; K. Zhang et al., 2003). This scheme is based on the multiple feedback loops, with time delay unit which results in eliminating the periodic errors efficiently. But the limitations of this system include slow dynamic response, large memory requirements, and poor performance in non-periodic disturbance. Repetitive control has been introduced for the control of inverter with non-linear load. The steady state performance of the repetitive control is quite good but the dynamic response is not satisfactory because of long delay time between input and output. Therefore, repetitive control is normally incorporated with other feedback controller with fast dynamic response (K. L. Zhou & Wang, 2003; K. L. Zhou, Wang, Zhang, & Wang, 2009). The repetitive control scheme is combined with the dead beat control as presented in (Haneyoshi, Kawamura, & Hoft, 1988), and least square error state-feedback control (Tzou, Ou, Jung, & Chang, 1997), forming the inner loop of the control algorithm. Besides improving the response time of the inner loop, the dynamics of the inverter has also been improved. However, introducing instantaneous feedback control raises cost and complexity of the system.

Repetitive control combined with the SPWM control provides high quality output voltage of the inverter with reduced cost. Though the response time is not very fast, the performance of the system is very good. However the implementation of this control scheme is no easy due to bad dynamics of the inverter, especially at no load. In order to get the good dynamic response and precise compensation, the inverse transfer function need to derive considering all the parameters of the inverter (Nakajima, Sato, & Kawakami, 1990).

In repetitive controller, a periodic signal generator $(1/z^N - 1)$ has been added in the closed loop system for exact tracking a reference signal. The repetitive controller eliminates all the harmonics below the Nyquist frequency by introducing infinite gain at the harmonic frequency (K. L. Zhou et al., 2009).

A repetitive control system is shown in Figure 2.19. The feedback control and repetitive control are complementary. The transfer function of repetitive control is given as

$$G_g(z) = \frac{k_g Z^{-N_1}}{1-z^{-N}} G_f(Z) = \frac{k_g Z^{N_3}}{Z^N - 1} G_f(Z) \tag{2.2}$$

where $k_g$is the control gain and $G_f(Z)$ is a low-pass filter.

The conventional feedback controller offers fast response and robustness. However the feedback controller has no memory. Hence if there is any imperfection, it will keep repeating in all subsequent cycles. Similarly the repetitive controller stored pervious information in memory, and ensures steady-state zero error tracking by repetitive learning. But the zero error tracking took longer time. Hence the repetitive control scheme together with feedback controller ensures fast dynamic response of feedback controller and the high precision tracking ability of repetitive controller (K. L. Zhou & Wang, 2003).

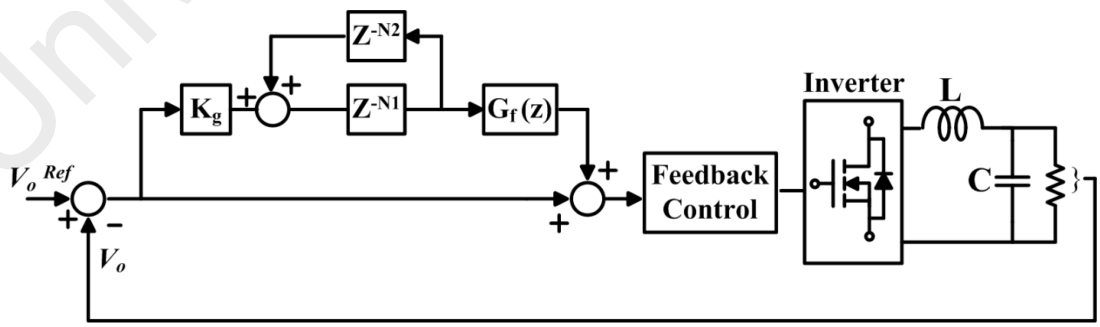

Figure 2.19: Repetitive control for the UPS system

2.4.2.4 Iterative Learning Scheme

In Iterative Learning Control (ILS), the control command is adjusted at each iteration thus converging to zero tracking error. The ILS aims to accomplish this result without the knowledge of the system. The system is examined at each cycle and is adjusted for the next repetition. But the design procedure of the ILS is very complex.

At stable DC input voltage of the UPS inverter, the ILC algorithm can be implemented with the single sensor. However, if the input voltage varies over a wide range, an additional sensor may be needed. ILC can achieve best dynamic response for the application where settling time of several fundamentals periods is acceptable. However for achieving fast dynamic response, other fast controllers are adopted in parallel to ILC.

ILS can be used to eliminate tracking error caused by the periodic disturbance. The updated rule for ILC is given by

$$u_{i+1}(z) = u_i(z) + k\emptyset(z)e_i(z) \tag{2.3}$$

Where $u_i(z)$ is the z-transform of the command that is given to the system at repetition 1, k is the learning gain and $\emptyset$ is the designed controller transfer function. While e_i is the z-transform of the racking error at repetition *i*.

$$e_{i+1}(z) = ((1 - k\emptyset(z)P(z))e_i(z) = T_f(z)e_i(z) \tag{2.4}$$

where T_f is the transfer function between the two consecutive repetitions. The error component at a particular frequency will decay over successive repetition if

$$\left|1 - k\emptyset\left(e^{jwT}\right)P\left(e^{jwT}\right)\right| < 1 \tag{2.5}$$

If equation 2-5 is satisfied for all ω, then monotonic decay of the tracking error to zero will take place over successive cycles, and stable operation will be achieved.

2.4.2.5 Comparison of Multi-loop control schemes

Table 2.3 shows the comparison between different multi-loop control schemes. The model predictive control is simple of all multi-loop control schemes with better performance. However, the MPC has the problem of computational burden, which slow down the response of the system. Nowadays with the development of the high speed controllers, the computational burden of the MPC can easily be reduced. The repetitive control and the iterative learning control shows excellent performance but are complex in implementation. Besides, the neural network control and the B-spline network give simple solution, with high performance for both linear and non-linear loads, and fast transient response for step change in the loading condition.

Table 2.3: Comparison of Different Control Schemes

Features / Control Scheme	Circuit Board	Response Time	Performance	Sensor	Complexity
Dead Beat Control (Mattavelli, 2005)	ADMC401	Slow, 0.5ms	Not good for Non-linear loads	Output Voltage, Inductive current	Complex
Model Predictive Control (Cortes et al., 2009)	TMS320C6713	Slow	Good	Output voltage, Filter current	Simple
Repetitive Control (K. Zhang et al., 2003)	TMS320FS40	Slow	Excellent	Output Voltage	Complex
Iterative Learning Controller (H. Deng et al., 2007)	TMS320F240/ MPC8240	Slow	Excellent	Output voltage	Complex
Neural Network Control (Xiao et al., 2002)	Analog Circuit	Fast, 7.55us	Good	Output Voltage	Complex
B-spline Network (BSN) Control (H. Deng et al., 2008)	DS1104	Fast, 7.78us	Excellent	Output Voltage	Simple

2.4.3 Non-linear Control Schemes

Non-linear controllers are more robust in operation and show better performance as compared to linear controllers. However the implementation of this system is very complex. The most common non-linear control system is slide mode control and adaptive control for the UPS inverter control.

2.4.3.1 Adaptive Control

Adaptive control is another robust control scheme which automatically adjusts to the structural and environmental uncertainties (Do, Leu, Choi, Choi, & Jung, 2013; Escobar, Mattavelli, Stankovic, Valdez, & Leyva-Ramos, 2007). It does not need a priori information about the uncertain parameters rather the system characteristics are obtained on-line, while the system is operating. The adaptive control provides high performance with excellent voltage regulation for both unbalance and non-linear loads. Also it provides fast transient behavior, small steady-state error, and low THD under sudden load change. However the computation complexity of adaptive control is very high.

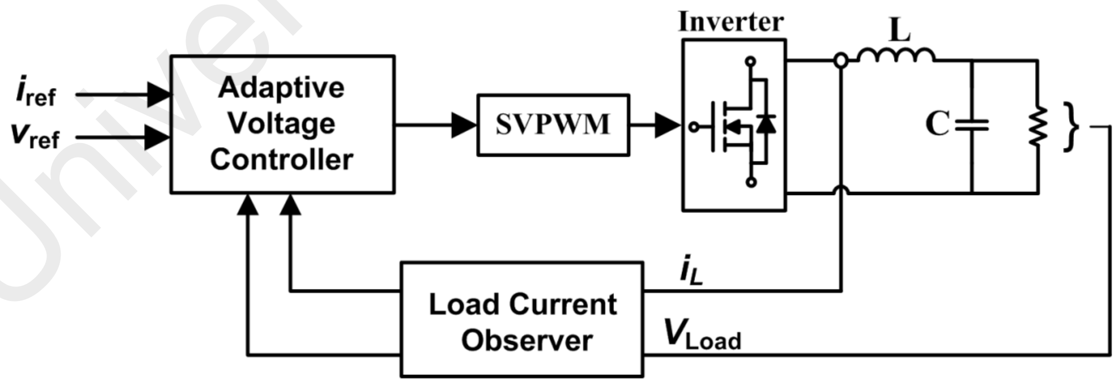

Figure 2.20: Adaptive control for the UPS inverter

Figure 2.20 shows the block diagram of adaptive control implemented in the inverter of the UPS system. A linear optimal load current observer is designed to accurately estimate load current. The load current observer is asymptotically stable in operation.

The load current information is forwarded to adaptive control law. For deriving the adaptive control law, the control input can be find using both the compensated control term and the feedback control term. Load current information can be acquired using the current sensors but its makes the system more expensive and less reliable. However, a linear optimal load current observer is designed to accurately estimate load current information that can heavily affect the controller performance.

2.4.3.2 Multi-resonant control scheme

The resonant control scheme has been adopted for the control of the UPS inverters (Fukuda & Imamura, 2005; Liserre, Teodorescu, & Blaabjerg, 2006). However for UPS systems, a resonant controller tuned in the fundamental frequency is not able to reject periodic disturbances in frequencies differing from its resonant frequency. For instance, a single resonant controller cannot cancel harmonic components resulting from a UPS system supplying energy to nonlinear loads. To overcome the problem of harmonic rejection, a set of resonant controllers are used by defining the resonant frequencies equal to the most relevant harmonic components (De & Ramanarayanan, 2010; Nian & Zeng, 2011). However, the tuning of such controllers is a difficult task due to the large number of parameters that have to be determined. Also there is lack of systematic procedure which can determine these parameters. Most of the time, the tuning of a multiple resonant controller is done on the trial and error procedure based on the phase margin adjustment.

Robust control scheme can be derived for UPS system by obtaining the output feedback from the optimization of Linear Matrix Inequality (LMI) constraints. In (Montagner & Peres, 2003), an LMI design procedure has been applied for designing a switched state feedback controller to a UPS system in order to guarantee a desired performance by means of a pole placement approach.

In (Pereira, Flores, Bonan, Coutinho, & da Silva, 2014), a multiple resonant control scheme has been proposed which provides very robust control framework to the UPS system. In this scheme, output feedback controller has been designed using Linear Matrix Inequality (LMI) constraints. The harmonic distortion generated by nonlinear loads is modeled as a periodic current disturbance. The attenuation of this disturbance (which leads to a minimization of the THD) is carried out by the minimization of an $H\infty$ criterion. Moreover, performance issues are explicitly considered through regional pole placement constraints in the LMI framework.

Thus efficient control parameters are derived to achieve a good compromise between transient performance, sinusoidal reference tracking, and harmonics rejection. Multiple-resonant controller attenuates the periodic disturbance efficiently resulting in low THD of the UPS output voltage.

2.4.3.3 Slide Mode control

For non-linear load, Slide Mode Control (SMC) (Muthu & Kim, 1998; Rech, Pinheiro, Grundling, Hey, & Pinheiro, 2003) strategy has gained special interest. SMC has been widely implemented in the power inverters because of its effective performance against non-linear system with uncertainties. A major feature of the SMC is its robustness, good dynamic response, stability against non-linear loading conditions, and easy implementation (El Fadil & Giri, 2008).

In order to implement the slide mode control, a proper sliding surface has to be introduced to track the errors and deviation, and reduced it to satisfactory level. However, implementation of the traditional (first-order) SMC method introduces some drawbacks such as chattering effect, limited flexibility for the designer with a sliding function and constant gain as the error variable. The chattering is due to the inclusion of the sign function in the switching term and it can cause the control input to start oscillating around the zero sliding surface, resulting in variable and high frequency switching in the converter. This phenomenon increases power losses and also produces severe electromagnetic compatibility (EMC) noise.

The phenomena of the chattering can be solved by two approaches as suggested in the literature. The first is to smoothen the switching term as the sliding surface gets closer to zero (soft switching) by using the continuous approximations of the discontinuous sign function, and the second is to generate "higher-order sliding modes".

Continuous-time SMC methods have been proposed in (Kukrer, Komurcugil, & Doganalp, 2009). The SMC can be introduced with fixed switching frequency and no load current measurement, but the load current observer increases the complexity of the controller (H Pinheiro, Martins, & Pinheiro, 1994). SMC strategy has been implemented in inverters due to its good dynamic response, strong robustness, and good regulation properties in a wide range of operating conditions.

Table 2.4 shows the comparison of the modern control schemes used in the UPS system. The synchronous reference frame voltage control provides better performance with low THD for both linear and non-linear loads. The response time of this control scheme is very fast. However, the implementation is quite complex. The SPWM control is relatively less complex but it shows average performance for the control scheme non-linear loading condition. Similarly the implementation of the multi-resonant control is quite complex. The SMC shows better overall performance with low THD for both linear and non-linear load, fast transients response, and simple implementation of the system.

Table 2.4: Comparison of modern control schemes

Ref	(Tamyurek, 2013)	(Pereira et al., 2014)	(Monfared, Golestan, & Guerrero, 2014)	(Abrishamifar, Ahmad, & Mohamadian, 2012)	(Lim, Park, Han, & Lee, 2014)
Controller	SPWM Controller	Multiple Resonant Controller	Synchronous Ref. Frame Voltage Control	Fix Switch Frequency Slide Mode Control	Robust Tracking Controller
THD(L)	1.1%	-	0.2%	1.1%	1.3%
THD(NL)	3.8%	2.7%	1.68%	1.7%	5.5%
Transient (ms)	60	16	1.0	0.5	-
Complexity	Medium	Complex	Complex	Simple	Medium

2.4.4 Application of Slide Mode Control

Slide Mode Control (SMC) provides better performance against non-linear system with uncertainties and changing loading conditions. A major feature of the SMC is its robustness, good dynamic response, stability against non-linear loads, and easy implementation.

However, the SMC has the inherit drawback of Chattering phenomena because of the variable switching frequency which cause low control accuracy, high power losses, and complication in the filter design. In order to eliminate chattering, SMC has been implemented with fixed switching frequency variable width hysteresis comparator (Malesani, Rossetto, Spiazzi, & Zuccato, 1996) and quasi-sliding control based on zero-average dynamic (ZAD) (Ramos, Biel, Fossas, & Guinjoan, 2003). Chattering problem can also be eliminated by smoothing the control discontinuous in a thin boundary layer neighbouring the switching surface (Slotine & Li, 1991).

Integral SMC method has been proposed for efficient AC tracking of the system in (Tan, Lai, & Tse, 2008; Wai & Wang, 2008). Though this system has reduced the harmonics contents in output voltage but has limited ability for high order harmonics. Slide mode control with continuous time control method has been implemented in (Carpita & Marchesoni, 1996; Chiang, Tai, & Lee, 1998). But the filter inductor's current has been used as a state variable which requires complex computation for its reference function. Also the SMC operates at variable switching frequency which leads to undesirable chattering phenomena. Hysteresis type switching function has been introduced for each leg of the inverter which increases the hardware complexity (Kukrer et al., 2009). In rotating slide mode control (H. Komurcugil, 2012), time varying slope based on SMC method was proposed which rotate the sliding surface in order to get the faster response for the non-linear conditions. This different value for the slope has been applied during the transient and steady state operation, causing the surface to rotate according to load variation. Slide mode control with PI controller has been implemented in (Gudey & Gupta, 2014). Though PI controller provides an infinite gain with a constant variable and step reference without steady-state error, but is unable to track a sinusoidal reference. Hence its performance for inverter control is not satisfactory.

Proportional-Resonant (PR) controller can achieve tight sinusoidal reference tracking for the voltage source inverter, by providing large gain at the resonance frequency, thus eliminating the steady state error and improve the system performance. Keeping in view the performance of both the SMC, and the PR control, the cascaded control can be implemented for the control of the UPS system. The slide mode control is used to control the current loop, while the PR control can be employed to control the voltage, thus give superior overall performance of the system. The explanation of the cascade control will be explained in chapter 4.

2.5 Summary

This chapter presents the literature on the topology based classification of the UPS system. The transformer-based UPS system are robust, reliable, and with galvanic isolation, but has large volumetric size, bulky, and expensive systems. Transformerless UPS system has small volumetric size and weight, however, the battery bank in these UPS system is very high. Bidirectional DC-DC converter is employed to reduce the battery bank voltage, in order to overcome the problem of series connected battery bank.

Different control schemes such as single-loop, multi-loop control scheme, and non-linear control applied to the UPS system has been explained in this chapter. Since the UPS system undergoes different loading conditions, a robust control scheme should be adopted for the control of the UPS system. Of all the non-linear control schemes, the slide mode control shows better performance, with fast transient response, and low THD for both linear and non-linear loading conditions.

CHAPTER 3: PROPOSED TRANSFORMERLESS ONLINE UPS SYSTEM

3.1 Introduction

This chapter presents the proposed topology of transformerless online UPS system and describes in detail different parts of the UPS system. Modes of operation of the proposed system are described, whereas mathematical modeling and design procedure of each part has been added to validate the feasibility of the implemented system.

3.2 Proposed Transformerless UPS system

The block diagram of the proposed transformerless UPS system is shown in Figure 3.1. The system consists of three parts.

1. Bridgeless Power Factor Correction (PFC) Boost Rectifier
2. Battery Charger/Discharger (Bidirectional Converter)
3. H-Bridge Inverter

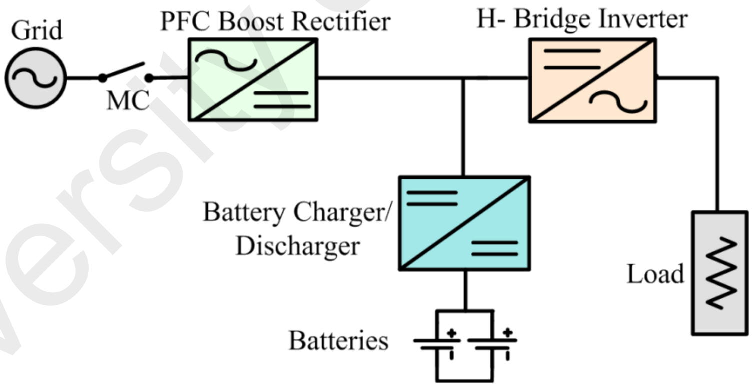

Figure 3.1: Block diagram of proposed online UPS system

Figure 3.2 shows the schematics of the proposed UPS system. The rectifier is introduced at the front end of the proposed UPS system. The boost rectifier provides the power factor correction and regulates the DC-link voltage. The efficiency of the bridgeless rectifier is also high as compared to a conventional rectifier as it eliminates some devices from the power flow path reduces the conduction losses considerable.

A bidirectional DC-DC converter is introduced between the DC-link and the battery bank. Introducing a bidirectional converter for battery charging and discharging with high voltage gain reduces the battery bank significantly, thus making the proposed UPS favorable for low power application.

The H-bridge inverter at the back end provides a continuous supply of power to the connected load. A new robust control scheme for the H-bridge inverter is proposed for controlling the non-linear load and provides a fast transient response during a change of modes.

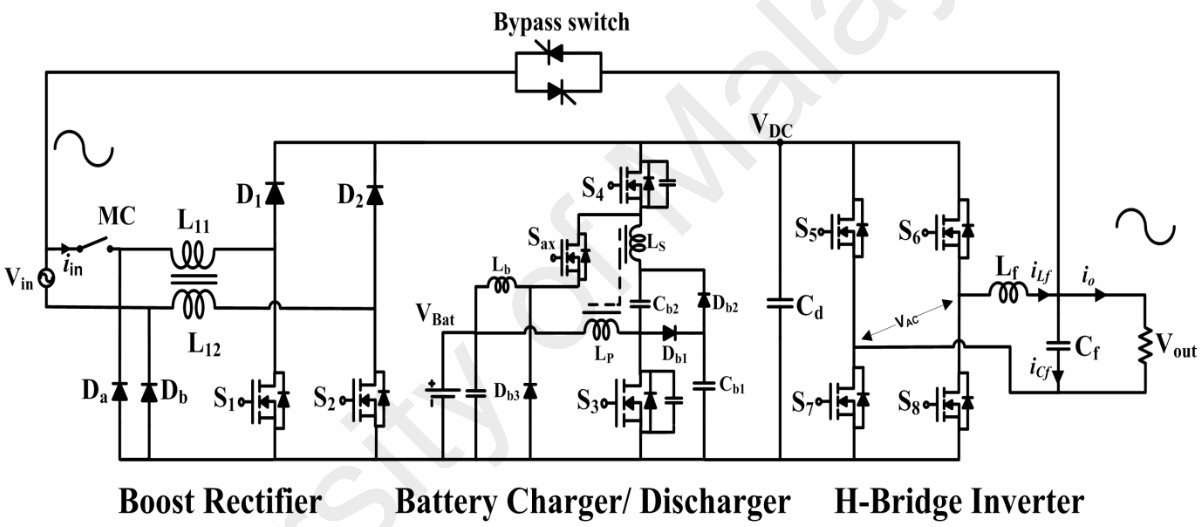

Figure 3.2: Schematic of the proposed UPS system

3.3 Modes of Operation

The operation of the UPS can be divided into two modes of operation. Normal mode and battery mode as shown in the Figure. 3.3.

Grid Mode

When the grid voltage is stable and there is no power failure, the UPS system operates in grid mode. The rectifier provides the regulated DC-link voltage to feed the inverter while the bidirectional converter keeps charging the battery bank. The inverter delivers regulated output voltage to the load connected to the UPS system

Battery Mode

With the loss of the input power or any other voltage sag, the magnetic contactor (MC) is opened and the rectifier is disabled. Now the power required by the load is supplied by the battery through the battery discharger into the inverter connected to the load. The value of the DC-link capacitor is kept high in order to provide sufficient energy to the inverter during the transition between the battery mode and grid mode of operation. Hence the inverter keeps operating and delivers output power irrespective of the changes in the grid

Bypass switch has been added to the system to increase the reliability of the system. During any internal fault in the system, overloading or overheating of the circuit, the bypass switch turns ON and provides a direct path for the power transfer from utility grid to the connected load (Y. Zhang, Yu, Liu, & Kang, 2013).

The sensitivity of the magnetic contactor determines the degree of protection provided by the UPS system. If the load is very sensitive and high protection is required, the selection of the magnetic contactor will be done accordingly.

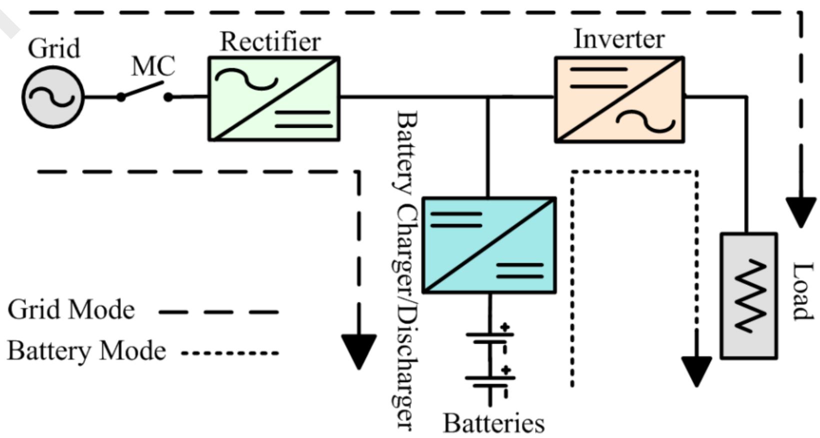

Figure 3.3: Modes of operation of proposed UPS system

3.4 Bidirectional Converter

A new non-isolated bidirectional DC-DC converter with coupled inductor has been proposed which works as battery charger/discharger and operates between the battery bank and the DC-link as shown in Figure 3.4. The low voltage side of the converter is connected to the battery bank while the high voltage side of the converter is connected to the DC-link of the UPS system. Since the main focus of this study is to reduce the battery bank voltage and allows the batteries for parallel operation, hence the bidirectional converter provides flexibility in selecting the battery bank voltage level and making it possible to minimize the battery cost, volume, and weight.

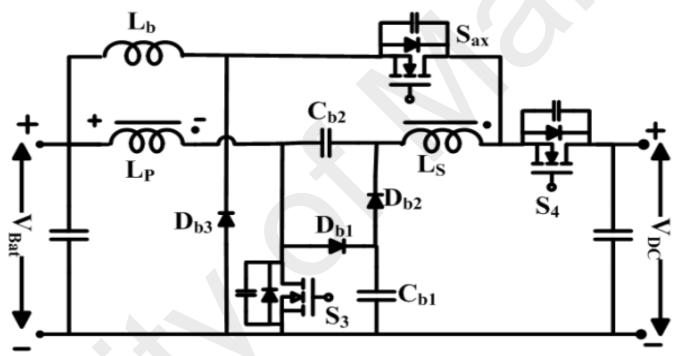

Figure 3.4: Proposed Bidirectional DC-DC Converter

The converter steps down the DC-link voltage into low battery bank voltage, in order to charge the batteries during the normal mode of operation. Similarly, during battery mode, the converter steps up the battery voltage to high DC-link voltage in order to supply the power to the load. The proposed bidirectional converter has the following advantages.

1. High voltage gain in both the buck and boost mode
2. Less number of passive components in the circuit
3. Only three active switches are used to perform the bidirectional operation.
4. Zero Voltage Switching (ZVS), synchronous rectification, and voltage clamping circuit are used that reduces the switching and conduction losses.

Coupled inductor has been used with L_P as primary inductance and L_S as the secondary inductance. Capacitor C_{b2} inserted in the main power across the primary and secondary winding of the transformer give high voltage conversion ratio and reduces the peak current stress allowing continuous current in the primary. Also, the voltage stress of the capacitor C_{b2} is a minimum at this position in the circuit.

3.4.1 Battery Charging/Buck operation

The characteristic waveforms of the converter during battery charging mode are shown in Figure 3.5. D_1 is the duty ratio of S_3 and S_{ax}, where D_3 is the duty ratio of switch S_4. Both D_1 and D_3 are related to each other by a relationship D_1 (= $1 - D_3$). The coupled inductor can be modelled as an ideal transformer with the magnetizing inductor L_m and turns ratio $N = N_2/N_1$, where N_1 and N_2 are the winding numbers in the primary and secondary side of the coupled inductor respectively. The operation of the circuit during battery charging mode during each interval is explained in next section.

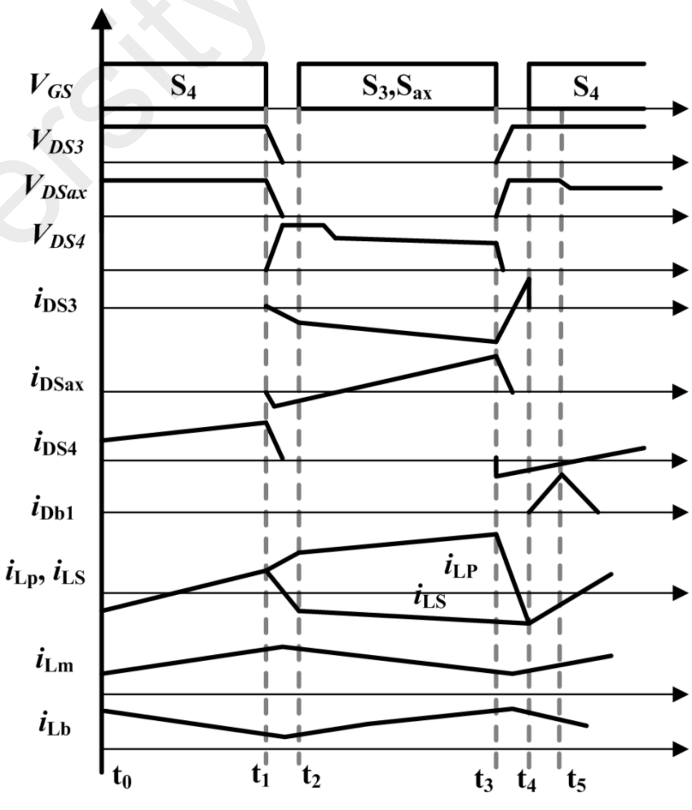

Figure 3.5: Characteristic waveforms of the buck mode of operation

Interval 1 ($t_0 \sim t_1$): The Switch S_4 remains ON while the switches S_3 & S_{ax} are OFF during interval 1. The current i_{LS} flows from DC-link to the battery bank through the capacitor C_{b2} and both the windings of the coupled inductor. Applying KVL, we get equation (3.1).

$$V_{DC} = V_{LS} + V_{Cb2} + V_{LP} + V_{Bat} \tag{3.1}$$

$$V_{DC} = V_{LP}(1 + N) + V_{Cb2} + V_{Bat} \tag{3.2}$$

The diode D_{b3} is also conducting with continuous inductor current i_{Lb} into the battery bank. Hence, V_{Bat} is the voltage across inductor L_b.

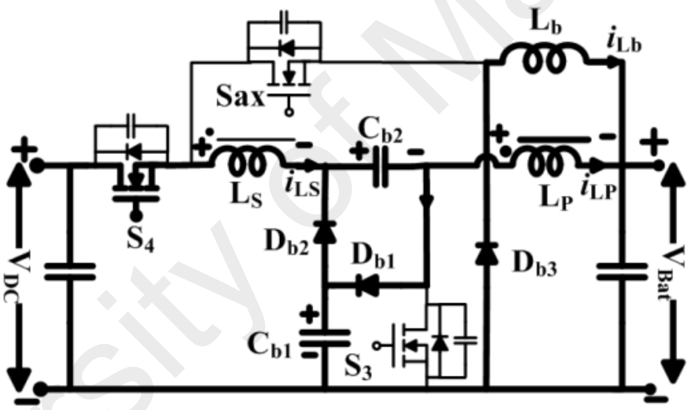

Figure 3.6: Operation in buck mode during interval 1 ($t_0 \sim t_1$)

Interval 2 ($t_1 \sim t_2$): At the start, the switch S_4 turns OFF. Due to the storage energy in the leakage inductor, the polarities are reversed across the primary and secondary windings (L_S & L_P) of the coupled inductor. Switch S_4 is OFF in this mode, but the secondary current i_{LS} is still conducting, so the switch S_{ax} body diode turns ON in order to keep the current i_{LS} flowing. The diode D_{b3} keeps conducting in this mode. The switch S_3 body diode also turns ON because though the secondary current i_{LS} decreases, but the primary current i_{LP} remains the same.

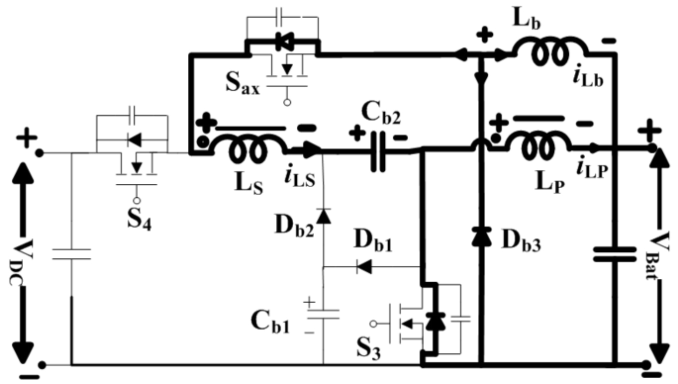

Figure 3.7: Operation in buck mode during interval 2 ($t_1 \sim t_2$)

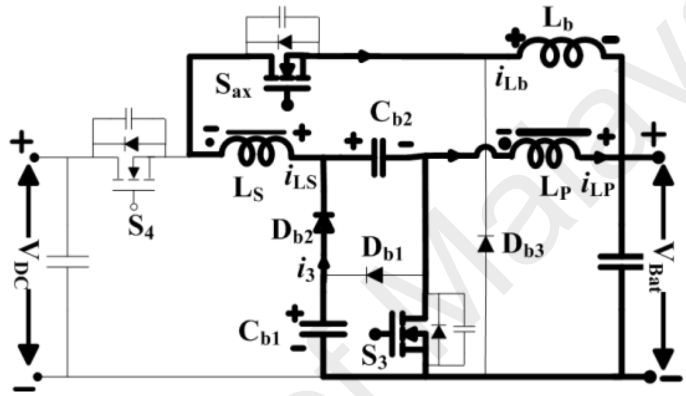

Figure 3.8: Operation in buck mode during interval 3 ($t_2 \sim t_3$)

Interval 3 ($t_2 \sim t_3$): Both the Switches S_3 and S_{ax} turns ON following zero voltage switching (ZVS) condition. The capacitor C_{b2} starts discharging across battery bank through the switch S_{ax} and inductor L_b. Thus, the secondary current is induced in reverse by discharging capacitor C_{b2}. Clamp capacitor C_{b1} also discharge through the diode D_{b2} by adding small current i_3 into the secondary current flowing into the battery bank.

Using the voltage second balance, V_{Cb2} will be,

$$V_{Cb2} = V_{Lb} + V_{Bat} + V_{LS} \tag{3.3}$$

The stored energy in the coupled inductor is released by primary current through the switch S_3 into the battery bank.

Using the voltage-second balance, the V_{Lb} is given by,

$$D_1 V_{Lb} = D_3 V_{Bat} \tag{3.4}$$

Primary winding voltage V_{LP} can be obtained as,

$$D_3 V_{LP} = D_1 V_{Bat} \tag{3.5}$$

Putting equation (3.4) and the values of V_{Lb} and V_{LP} in equation (3.2), the voltage gain during buck mode of operation is given by equation,

$$G_{buck} = V_{Bat}/V_{DC} = [D_3(1 - D_3)]/[2N(1 - D_3)^2 + 1] \tag{3.6}$$

Interval 4 ($t_3 \sim t_4$): Both the switches S_3 and S_{ax} turn OFF at the start of this mode. The primary and secondary winding currents i_{LP} & i_{LS} will continue conduction due to the leakage inductance of the coupled inductor. The secondary current will charge the parasitic capacitance of the switches S_3 & S_{ax}, and discharge the parasitic capacitance of the switch S_4. When the voltage across the switch S_{ax} equals to V_{DC}, the body diode of the switch S_4 turns ON. The primary current i_{LP} starts decreasing unless it equals to the secondary current i_{LS}, then this mode finishes.

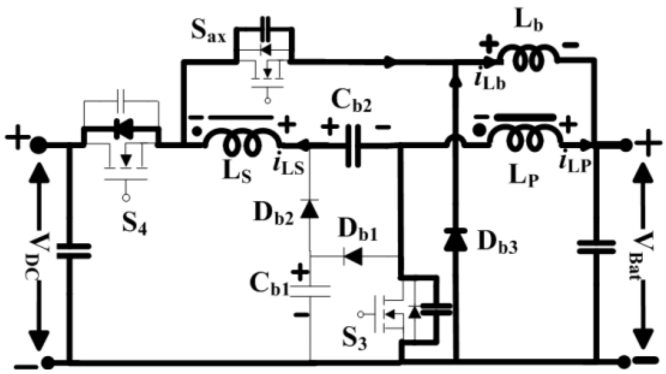

Figure 3.9: Operation in buck mode during interval 4 ($t_3 \sim t_4$)

Interval 5 (t_4 ~ t_5): The switch S_4 turns ON under zero voltage switching (ZVS) condition. The capacitor C_{b1} is charged through the clamped Diode D_{b1}. The primary and secondary current starts increasing. At the end of this mode, the circuit starts repeating interval 1of the next cycle.

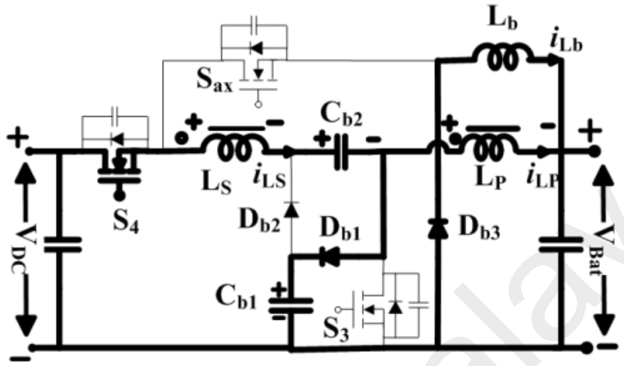

Figure 3.10: Operation in buck mode during interval 5 (t_4 ~ t_5)

Table 3.1: Summary of buck operation mode

Modes	**Switches**			**Diodes**			**Capacitors**		**Comments**
	S_3	**S_4**	**S_{ax}**	**D_{b1}**	**D_{b2}**	**D_{b3}**	**C_{b1}**	**C_{b2}**	
Mode 1	OFF	ON	OFF	ON	ON	ON	-	Ch	Start of switching cycle
Mode 2	OFF	OFF	OFF	OFF	OFF	ON	-	-	Body diode of switch S_{ax} and S_3 turns ON
Mode 3	ON	OFF	ON	OFF	ON	OFF	D.Ch	D.Ch	ZVS for S_3 and S_{ax}
Mode 4	OFF	OFF	OFF	OFF	OFF	ON	-	-	Parasitic capacitance of S_3 and S_4 charges Discharges across S_4,
Mode 5	OFF	ON	OFF	ON	OFF	ON	Ch	-	ZVS condition for S_4
Note: 'Ch' and 'D.Ch' means capacitor charging and discharging respectively									

3.4.2 Battery discharging/ Boost Operation

The characteristic waveform of the bidirectional converter during battery discharge mode is shown in Figure 3.11. The bidirectional converter steps up the low battery bank voltage to high DC-link voltage. The switch S_{ax} remains OFF during battery discharging. The battery discharger operation during each interval is explained in the coming section.

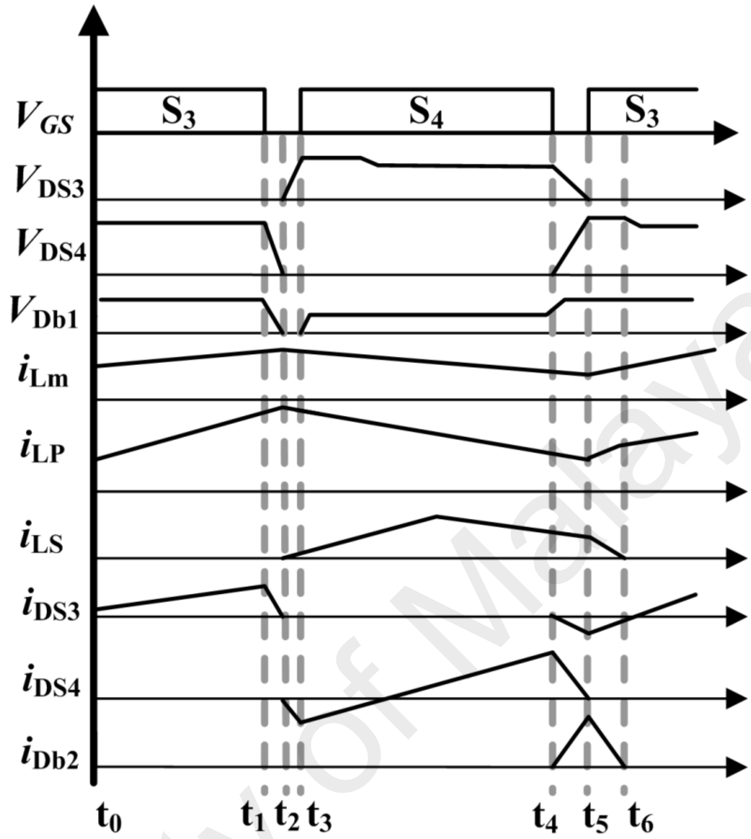

Figure 3.11: Characteristic waveforms of the boost mode

Interval 1 ($t_0 \sim t_1$): During interval 1, the switch S_3 was ON, while the switch S_4 was OFF. Low battery bank voltage is applied at the Low voltage side LVS of the circuit. Capacitor C_{b2} remains charged before interval 1 and the magnetizing current i_{LM} of the coupled inductor increase linearly as shown in the Figure 3.10. Applying KVL, we get,

$$V_{Bat} = V_{Lp} = V_{LS}/N \qquad (3.7)$$

The voltage across the primary winding can be derives using voltage second balance

$$V_{LP}D_3 = V_{Bat}D_1 \qquad (3.8)$$

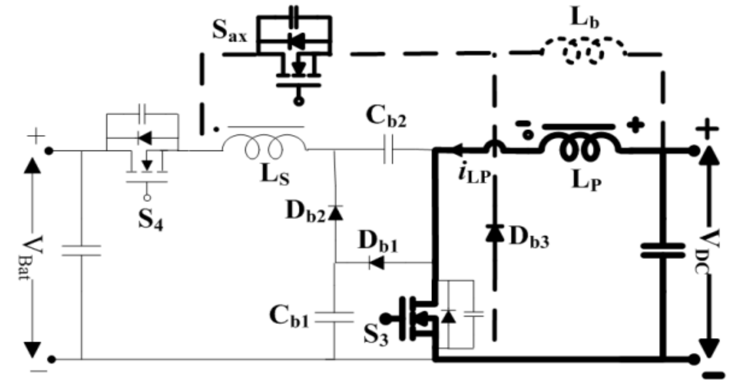

Figure 3.12: Operation in boost mode during interval 1 ($t_0 \sim t_1$)

Interval 2 ($t_1 \sim t_2$): The switch S_3 turns OFF in interval 2. The primary current i_{LP} charges the parasitic capacitance across the switch S_3 and the secondary current i_{LS} discharges the parasitic capacitance across switch S_4. When the voltage across switch S_3 equals to the capacitor voltage V_{Cb1}, this interval finishes.

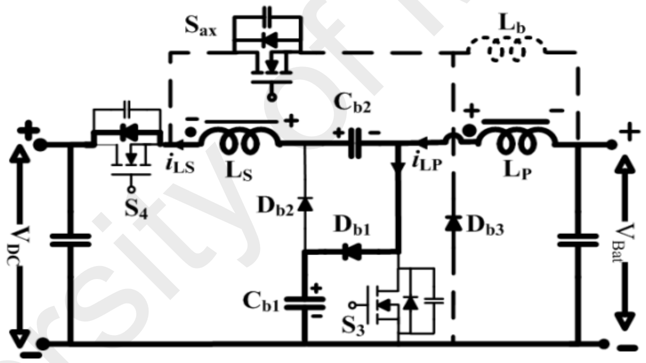

Figure 3.13: Operation in boost mode during interval 2 ($t_1 \sim t_2$)

Interval 3 ($t_2 \sim t_3$): Since the switch S_3 is OFF, leakage inductance causes the primary current i_{LP} to decrease while the secondary current i_{LS} increases. As a result, the body diode of switch S_4 turns ON. Capacitor C_{b1} starts charging through diode D_{b1} because the voltage across the switch S_3 gets higher than capacitor C_{b1}. This limits the voltage stress across the switch S_3. The voltage across the capacitor is given by,

$$V_{C1} = V_{Bat} + V_{LP} \tag{3.9}$$

Using equation (3.7),

$$V_{C1} = V_{Bat}/D_3 \tag{3.10}$$

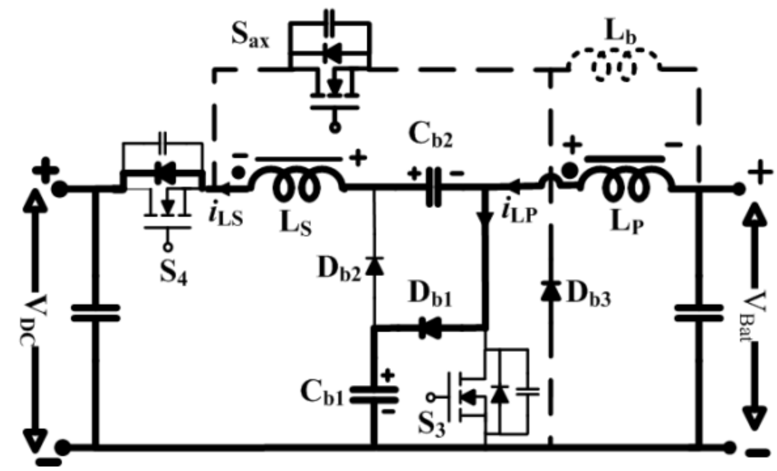

Figure 3.14: Operation in boost mode during interval 3 ($t_2 \sim t_3$)

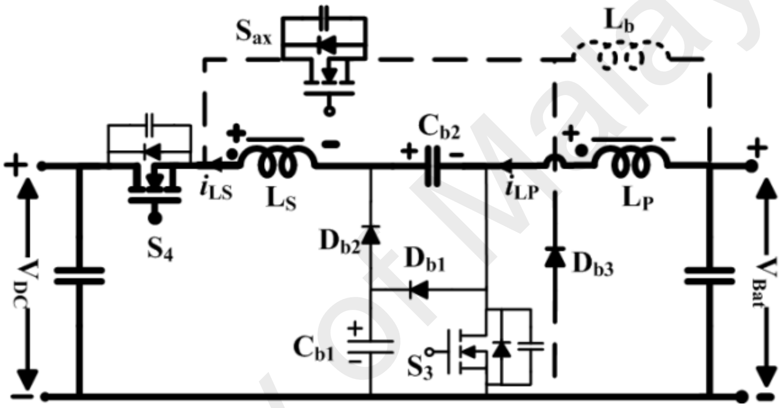

Figure 3.15: Operation in boost mode during interval 4 ($t_3 \sim t_4$)

Interval 4 ($t_3 \sim t_4$): Switch S_4 turns ON under the condition of zero voltage switching (ZVS). The primary and secondary windings of the coupled inductor and the capacitor C_{b2} are all now connected in series to transfer the energy to the DC-link. The i_{LS} starts increasing until it reaches the i_{LP}, then it follows the i_{LP} till the end of the interval 4. Thus, the energy stored in the primary and secondary discharges across the DC-link. Both the diodes D_{b1} and D_{b2} remain OFF during this interval as shown in Figure 3.15. Using voltage second balance, we get equation (3.11)

$$V_{DC} = V_{Bat} + V_{LS} + V_{C2} + V_{Lp} \tag{3.11}$$

$$V_{DC} = V_{Bat} + V_{C2} + (N+1)V_{LP} \tag{3.12}$$

Interval 5 ($t_4 \sim t_5$): During this interval, the switch S_4 turns OFF. The current i_{LS} charges the parasitic capacitance of the switch S_4. The capacitor C_{b1} starts discharging across the capacitor C_{b2}, through the diode D_{b2}.

$$V_{Cb2} = V_{Cb1} = V_{Bat}/D_3 \tag{3.13}$$

By putting equation (3.8) and equation (3.13) in (3.12),

$$V_{Dc} = V_{Bat} + V_{Bat}/D_3 + (N+1)\, D_1/D_3\, V_{Bat} \tag{3.14}$$

$$G_{boost} = V_{DC}/V_{Bat} = (2 + ND_1)/(1 - D_1) \tag{3.15}$$

Equation 3-15 give the voltage gain of the bidirectional converter in boost mode of operation. The body diode of the switch S_3 turns ON because of the polarities of the capacitor C_{b2} and inductor L_P in this interval.

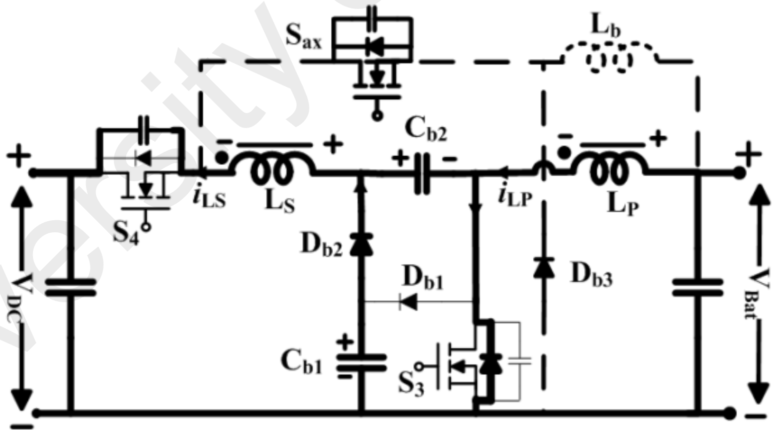

Figure 3.16: Operation in buck mode during interval 5 ($t_4 \sim t_5$)

Interval 6 ($t_5 \sim t_6$): During interval 6, switch S_3 turns ON under the condition of zero voltage switching. Since S_3 is not deriving any current from the clamped circuit, thus the switching losses remain low due to ZVS and the efficiency of the circuit increases. When both the V_{Cb1} and V_{Cb2} get equal, then the next switching cycle starts and repeats the operation in interval 1.

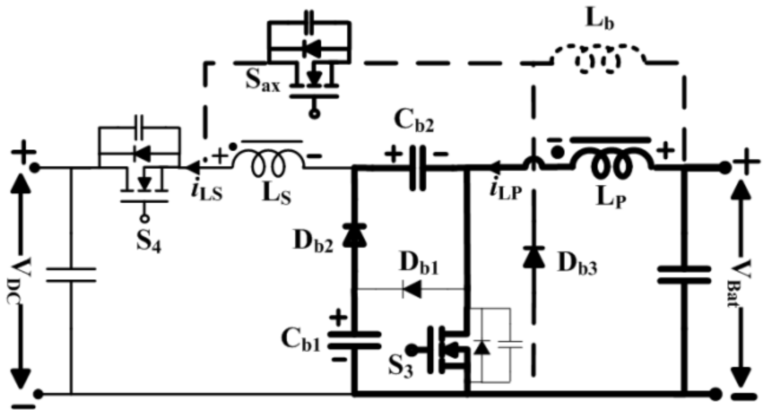

Figure 3.17: Operation in boost mode during interval 6 ($t_5 \sim t_6$)

Table 3.2: Summary of the Boost mode of Operation

Modes	**Switches**		**Diodes**		**Capacitors**		**Comments**
	S_3	**S_4**	**D_{b1}**	**D_{b2}**	**C_{b1}**	**C_{b2}**	
Mode 1	ON	OFF	OFF	OFF	-	-	Start of switching cycle
Mode 2	OFF	OFF	OFF	OFF	-	-	Parasitic capacitance of S_3 charges and S_4 discharges
Mode 3	OFF	OFF	ON	OFF	Ch	-	Body diode of switch S_4 turns ON
Mode 4	OFF	ON	OFF	OFF	-	D.Ch	ZVS condition for S_4
Mode 5	OFF	OFF	OFF	ON	D. Ch	Ch	The parasitic capacitance of S_4 charges and S_3 discharges. Body diode of switch S_3 turns ON
Mode 6	ON	OFF	OFF	ON			ZVS condition for S_3
Note: 'Ch' and 'D.Ch' means capacitor charging and discharging respectively							

3.4.3 Coupled Inductor Design

The inductor needs to be high enough to minimize the ripple and associated losses. In order to design a coupled inductor, analyze the circuit in either buck or boost mode of operation and calculate the magnetizing inductor Lm, and the number of turns N_1 & N_2 of the coupled inductor (Batarseh, 2004). Consider boost mode of operation, the magnetizing current i_{Lm} when the switch S_1 turns ON is given by

$$i_{Lm} = \frac{1}{L_m} V_{Bat} t + I_L(0) \qquad 0 \leq t < DT \tag{3.16}$$

where $I_L(0)$ is the initial current at t = 0. The i_{LM}, when switch S_1 turns OFF and S_3 ON is given by,

$$i_{Lm} = \frac{1}{Lm}\left(\frac{V_{DC} - 2V_{Bat}}{2+N}\right)(t - D_1T) + I_L(D_1T) \quad DT \leq t < T \tag{3.17}$$

Putting $t = D_1T$ in (16) and $t = T$ in (17), we get

$$I_L(D_1T) - I_L(0) = \frac{1}{Lm} V_{DC}(D_1T) \tag{3.18}$$

$$I_L(D_1T) - I_L(0) = -\frac{1}{Lm}\left(\frac{2V_{Bat} - V_{DC}}{2+N}\right)(1 - D_1T)T \tag{3.19}$$

$$\frac{V_{DC}}{V_{Bat}} = \frac{2+ND_1}{1-D_1} \tag{3.20}$$

The inductor ripple current is given by,

$$\Delta I = \frac{1}{Lm} \frac{Vo(1-D_1)D_1T}{2+ND_1} \tag{3.21}$$

Average input current is given by,

$$I_{in} = \frac{I_{Lm(max)} + I_{Lm(min)}}{2} \tag{3.22}$$

Average Output Inductor Current is given by,

$$I_o = \left(\frac{I_{Lm(max)} + I_{Lm(min)}}{2}\right)(1 - D_1) = \frac{V_{DC}}{R} \tag{3.23}$$

$$I_{Lm(max)} = \left(\frac{2+ND_1}{(1-D_1)^2R} + \frac{D_1T}{2Lm}\right) \tag{3.24}$$

To solve for the minimum critical magnetizing inductance value, that keeps the converter into Continuous conduction mode (CCM), we set the $I_{Lm(min)} = 0$,

$$L_{m(crit)} = \frac{D_1(1-D_1)^2RT}{2(2+ND_1)} \tag{3.25}$$

Using equation (3.25), the number of turns can be calculated as (Erickson & Maksimovic, 2001),

$$\frac{N_2}{N} = N_1 = \frac{L_m I_m}{B_{max A_c}} 10^4 \tag{3.26}$$

B_{max} is max flux density; A_C is the core cross-sectional area.

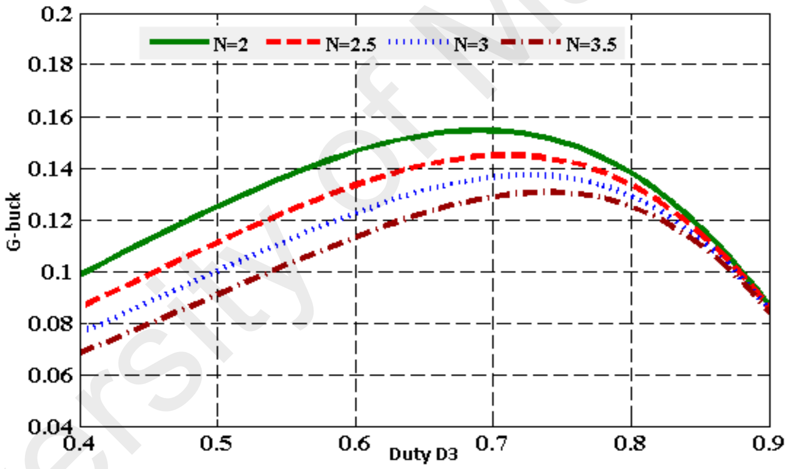

(a) Buck mode of operation

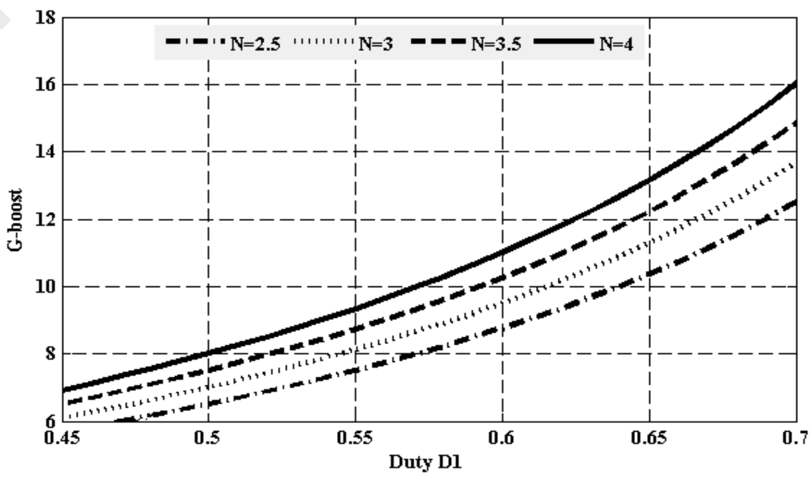

(b) Boost mode of operation

Figure 3.18: Graph of voltage gain vs duty ratio

Table 3.3: Comparison of bidirectional converter

Features	(Wai & Liaw, 2015)	(Hsieh et al., 2014)	(Duan & Lee, 2012)	(Lin et al., 2013)	Proposed Topology
Switches	4	5	4	4	3
Auxiliary Capacitors	2	3	2	2	2
Coupled-Inductor	1	1	1	0	1
Auxiliary Inductor	1	0	0	1	1
M_{BOOST}	$\frac{N}{1-D}$	$\frac{1+N}{(1\text{-}D)}+N$	$\frac{2+N}{D}$	$\frac{2}{1-D}$	$\frac{2+ND}{1-D}$
M_{BUCK}	$\frac{D}{N}$	$\frac{D}{1+N+DN}$	$\frac{D}{N+2}$	$\frac{D}{2}$	$\frac{D(1\text{-}D)}{2N(1\text{-}D)^2+1}$
Efficiency	97%	96%	95%	94%	96%
Size	Large	Large	Medium	Medium	Small
Estimated Cost(US $)	~130	~172	~118	~136	~116

The turn ratio N is selected as such to satisfy the G_{boost} and G_{buck} gains for required DC-link and battery bank voltage. Figure 3.18 shows the voltage gain of buck and boost modes with respect to duty cycle D_3 and D_1 respectively at the different turn ratio. Turn ratio N = 6 satisfies the operation of the bidirectional converter between the required DC-link and battery bank.

Table. 3.3 shows the comparison of different bidirectional converters recently published. The size of the circuit is related to the number of components used in the circuit. The voltage conversion ratio of the proposed converter shows more diversity as compared to (Duan & Lee, 2012) and (Lin et al., 2013), with fewer numbers of switches. In (Hsieh et al., 2014) the authors have shown high gain ratio but with five switches, that increase the size and cost of the circuit. The size of the proposed circuit is considerably small with small heat sink for the given power rating, and only a few passive auxiliary components are used. Since the battery voltage is very low and high current flows from the battery bank into the converter. Thus it increases conduction losses. However, the switching losses are not significant as all the switches of the bidirectional DC-DC converter are following ZVS condition. The high current can increase the size and cost of the system, hence limits the operation of proposed topology for very high power applications where the input current can be very high.

3.5 Rectifier

The rectifier performing the unity power factor consists of bridgeless PFC dual boost rectifier. The bridgeless rectifier consists of two boost converters, each operating in the half-cycle of the AC supply. The bridgeless PFC has the advantage of reducing the conduction loss by 30% (Su & Lu, 2010). By adding two slow diodes $D_a \sim D_b$, the common mode noise (EMI Losses) can be suppressed considerably, and high efficiency can be achieved as compared to the conventional rectifier. Both the switches S_1 and S_2 of the rectifier are driven by the same gate signal, thus makes the control of the circuit quite easy.

The two inductors at the input make the bridgeless rectifier likes two DC-DC boost converters each operation for half cycle of the grid voltage. During the positive half cycle, the first DC-DC converter S_1, L_{11} and D_1 are active through the diode D_b, while during the negative half cycle, the second DC-DC converter S_2, L_{12}, and D_2, are active through the diode D_a . The drawback of the bridgeless boost rectifier is that addition of one extra inductor L_{12} as compare to other bridgeless rectifier, but it should also be noted that two inductors compared to a single inductor have better thermal performance. The inductors L_{11} and L_{12} of the boost rectifier can be wind in the same core in order to increase the utilization of magnetic material (Jang & Jovanovic, 2009).

3.5.1 Circuit Operation

The operation of the rectifier during positive half cycle has been shown in Figure 3.19. When the AC input voltage goes positive, the switch S_1 turns ON. The current flows from the input through the inductors L_{11} and L_{12}, storing the energy in both inductors. The change in the input current is same as the change in the inductor current, given by equation (3.27).

$$\Delta i_{in} = \frac{1}{L_{11}+L_{12}} V_i D T_s \tag{3.27}$$

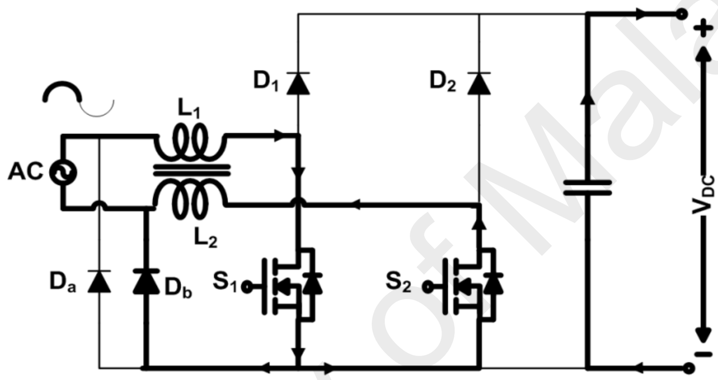

(a). Switches S_1 & S_2 are ON

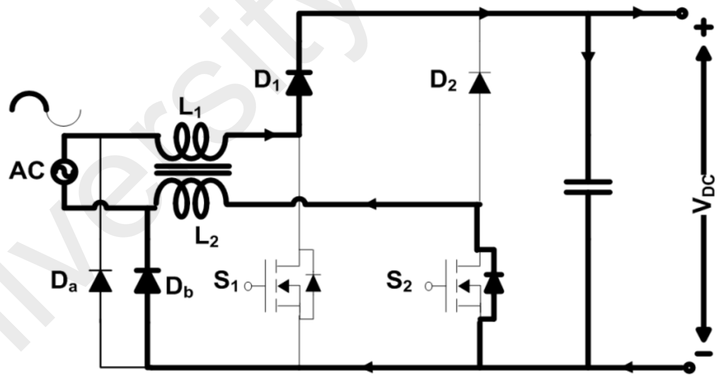

(b). Switches S_1 & S_2 are OFF

Figure 3.19: The operation of the rectifier during positive half cycle

When the switch S_1 turns OFF, the energy is released by the inductors. The current flows through the diode D_1 into DC-link V_{DC}, returning through the body diode of the switch S_2 into the input supply. The input current in D_1 and S_2 is same as the inductor current given by equation (3.28).

$$\Delta i_{in} = \frac{1}{L_{11}+L_{12}}(V_{in} - V_{DC})(1 - D)T_s \qquad (3.28)$$

Depending on the duty ratio D of both the switches S_1 and S_2, the input current variation for one complete switching cycle T_S is given by,

$$(L_{11} + L_{12})\frac{\Delta i_{in}}{T_S} = V_i D T_s + (V_{in} - V_{DC})(1 - D)T_s \qquad (3.29)$$

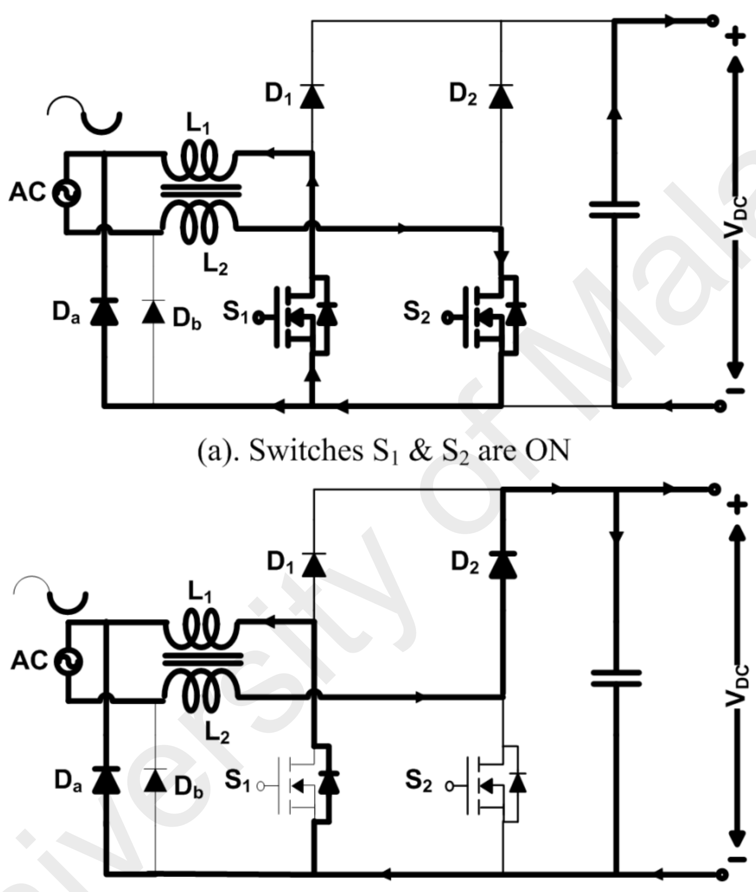

(a). Switches S_1 & S_2 are ON

(b). Switches S_1 & S_2 are OFF

Figure 3.20: The operation of the rectifier during negative half cycle

The operation of the rectifier during the negative half cycle is shown in Figure 3.20. During the negative half cycle, the switch S_2 turns ON. The current flows through the switch into the inductors L_{11} and L_{12} storing energy in the inductors. When S_2 turns OFF, the stored energy in the inductor L_{11} and L_{12} is released through the diode D_1 into the DC-link. The body diode of the switch S_1 turns ON during this interval.

$$(L_{11} + L_{12})\frac{\Delta i_{in}}{T_S} = V_i D T_s + (V_{in} + V_{DC})(1 - D)T_s \tag{3.30}$$

The EMI noise suppression diode D_a remains active during positive cycle and D_b remains active during the negative cycle of the input voltage.

3.5.2 Power factor correction ability

It is desired that the rectifier presents a resistive load to the input utility AC supply. The rectifier input current i_{in} is given by $i_{in} = \frac{v_{in}}{R_e}$, where Re is the emulated resistance of the rectifier (W.-Y. Choi, Kwon, & Kwon, 2008; Erickson & Maksimovic, 2001). The Re is selected by the controller as such that the desire DC output voltage is obtained.

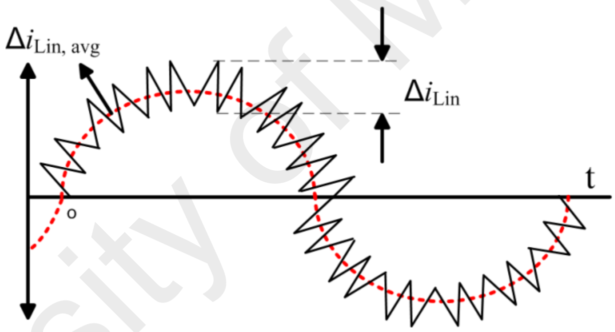

Figure 3.21: Waveform of boost inductor current in CCM mode

Now the average power is represented as

$$P_{av} = \frac{V_{rms}^2}{R_e} \tag{3.31}$$

Rectifier peak current can be expressed as

$$i_{Lin,\ pk} = \frac{v_{in}}{R_e} \tag{3.32}$$

Simplifying the equations, the peak value of the input current is given by,

$$i_{Lin,\ pk} = \frac{P_{av}\, v_{in}}{v_{rms}^2} \tag{3.33}$$

As shown in Figure 3.21, the average inductor current $i_{Lin,\ avg}$ can be shown by equation (3.34)

$$i_i = i_{Lin,\ avg} = i_{Lin,\ peak} - 0.5\Delta i_{Lin} \tag{3.34}$$

The ripple current during one switching cycle is given by

$$\Delta i_{Lin} = \frac{v_{in}}{L_{in}f_s}[1 - \frac{\sqrt{2}v_{in}}{V_d}|\sin wt|] \tag{3.35}$$

$$i_{Lin,\ avg} = \left(\frac{P_{av}}{V_{rms}^2} - \frac{1}{2L_{in}f_s}[1 - \frac{\sqrt{2}v_{in}}{V_d}|\sin wt|]\right) v_{in} \tag{3.36}$$

The root mean square value of the input current

$$i_{in} = \sqrt{\frac{1}{2\pi}\int_0^{2\pi} i_{in,\ avg}^2\, dwt} \tag{3.37}$$

The input real power and the power factor are specified by equation (3.38) and (3.39) respectively.

$$\text{Input real power } P_{in} = \frac{1}{2\pi}\int_0^{2\pi} v_{in} i_{in,\ avg} dwt \tag{3.38}$$

$$\text{Power Factor } = \frac{P_{in}}{v_{in}, i_{in}} = \frac{P_{in}}{v_{in}\sqrt{\frac{1}{2\pi}\int_0^{2\pi} i_{in,\ avg}^2 dwt}} \tag{3.39}$$

3.5.3 Input Inductor in CCM Mode

The input current of the rectifier is continuous in CCM mode of operation. Hence minimum inductance needed to practice the CCM operation and the value can be determined by equation (3.40)

$$L_{22} = L_{11} > \frac{V_{DC}^2 T_s D(1-D)^2}{2P_o} \tag{3.40}$$

The current ripple around the average is

$$\Delta i_{L_{in}} = \frac{|V_m \sin \omega t| D T_s}{2 L_{in}} \tag{3.41}$$

The peak current is given by equation (3.42)

$$i_{L_{in}}\Big|_{peak} = i_{L_{in}(avg)} + \Delta i_{L_{in}} = \frac{|V_m \sin \omega t|}{R_e} + \frac{|V_m \sin \omega t| D T_s}{2 L_{in}} \tag{3.42}$$

As shown in equation 3-42, the peak current of the inductor is not very high due to the large value of the inductor which will maintain the continuous conduction of input current.

3.6 Single Phase H-bridge Inverter

The single-phase full-bridge inverter is the most common topology for the UPS application. By selecting the full bridge configuration, the minimal allowed DC-link voltage can be set to be the peak value of the AC grid voltage (plus margins). Thus, power MOSFET, instead of higher voltage IGBTs can be used as the switching devices which enable use of a high switching frequency (> 20kHz) without introduction of excessive switching loss. AC output voltage is created by switching the full-bridge in an appropriate sequence. The output voltage of the bridge, V_{ac}, can be either $+V_{DC}$, $-V_{DC}$ or 0 depending on how the switches are controlled.

Notice that both switches on one leg cannot be ON at the same time; otherwise, there would be a short circuit across the DC source, which would destroy the switches or the converter itself. Table 3.2 summarizes all the possible switching combinations for the single-phase inverter and their corresponding created full-bridge voltage, V_{ac}.

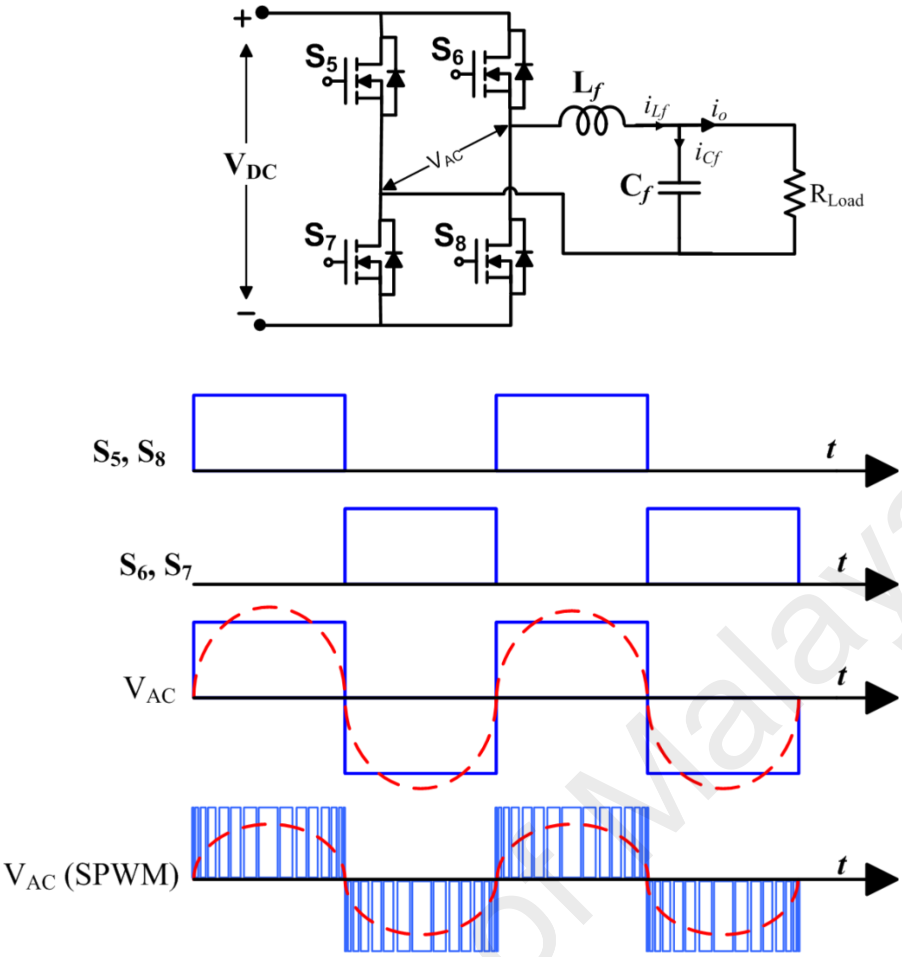

Figure 3.22: Single phase full bridge inverter

Table 3.2: Switching combination of single phase inverter

Mode	S_5	S_6	S_7	S_8	V_{AC}	**Note**
I	ON	OFF	ON	OFF	0	Freewheeling
II	ON	OFF	OFF	ON	$-V_{DC}$	-
III	OFF	ON	ON	OFF	$+V_{DC}$	-
IV	OFF	ON	OFF	ON	0	Freewheeling

The circuit diagram of a single phase inverter for the Uninterruptible Power Supply (UPS) system with LC filter as shown in Figure 3.22, where V_{DC} is applied voltage, V_{out}

the filter capacitor C_f output voltage. i_L is the inductor L_f current, and i_O the output current through the load R, given by $i_O = V_{out}/R_{Load}$. The state equations of the inverter are given as

$$L_f \frac{di_L}{dt} = uV_{DC} - V_{out} \tag{3.43}$$

$$C_f \frac{dV_{out}}{dt} = i_c = i_L - i_o \tag{3.44}$$

The behavior of the system can be represented by the following state space equation

$$\frac{d}{dt}\begin{bmatrix} V_{out} \\ i_{Lf} \end{bmatrix} = \begin{bmatrix} 0 & {}^{1}/_{C_f} \\ -{}^{1}/_{L_f} & 0 \end{bmatrix}\begin{bmatrix} V_{out} \\ i_{Lf} \end{bmatrix} + \begin{bmatrix} 0 \\ {}^{V_{DC}}/_{L_f} \end{bmatrix} u + \begin{bmatrix} -{}^{i_o}/_{C_f} \\ 0 \end{bmatrix} \tag{3.45}$$

Where $u = Control\ input = \{-1, 0, +1\}$

3.6.1 Output Filter Design

The second order low pass LC filter is employed at the output of the inverter of UPS system to get the sinusoidal output voltage. The filter inductance is chosen based on maximum allowable current ripples while filter capacitor C_f is selected considering the output voltage ripple value. The design of the LC filter is performed using following steps.

1. First, the value of the inductor can be calculated as;

$$L_f = \frac{V_{DC}}{8.f_{sw}.\Delta I_1.I_{ref}} \tag{3.46}$$

where V_{DC} is the DC-link voltage, I_{ref} is the rated reference peak current, f_{sw} is the switching frequency, ΔI_1 is the inverter-side current ripple ratio, which generally is lower than 15~20% of the rated current for LC filter (Wu, He, & Blaabjerg, 2012).

2. Decide the resonant circuit. The resonance frequency of the filter is selected between the range of ten times the line frequency and one tenth of the switching frequency

$$f_{sw}/10 > f_r > 10f_o \tag{3.47}$$

3. The value of filter capacitor is determined using the resonance frequency equation of the LC filter;

$$f_r = {}^{1}\!\Big/_{2\pi\sqrt{L_f C_f}} \tag{3.48}$$

3.7 Power loss calculation for the UPS system:

Different parts of the propose UPS contributes in the power loss of the system. The power loss in the rectifier and the inverter is not very prominent. However, the power loss in the battery charger/discharger (Bidirectional converter) is slightly higher because high current flows at the low voltage side of the bidirectional converter. Hence, in grid mode the total power loss is high as all the three parts of the UPS system are active. However, in the battery powered mode, only battery discharger and inverter is active and the power losses is low. In order to analyze the efficiency of the UPS, the power loss of each part is evaluated. The calculation has been done for a 1kVA transformerless online UPS system.

3.7.1 Slow Diodes

The power loss in the slow diodes of rectifier for the conduction time can be calculated as

$$P_{diode} = \frac{1}{\pi}\int_0^{\pi}(V_{FD}I_D + R_D{I_D}^2)\sin\omega\, d\omega \tag{3.49}$$

where V_{FD} is the forward voltage, I_D is the forward diode current, and R_D is the diode on-stage resistance. These values can be obtained from the datasheet.

3.7.2 MOSFET

All the switches used in the rectifier, bidirectional converter, and the inverter are MOSFET. Hence, the power loss in the MOSFET can be estimated for different power stages of the UPS system. The power loss in the switch consists of conduction and switching losses are estimated by,

$$P_{MOSFET} = P_{Cond} + P_{SW} \tag{3.50}$$

$$P_{cond} = D(i_L + \Delta i)^2 R_{DS_{ON}} \tag{3.51}$$

Where i_L is the boost inductor current, and Δi_L is the ripple current which is about 20% of the output current. $R_{DS_{ON}}$ is the on-state resistance of the switch and D is the duty cycle of the PWM. Similarly the switching losses of the MOSFET are given by equation (3.52).

$$P_{SW} = \frac{V_{in} i_L f_{sw} t_{overlap}}{2} \tag{3.52}$$

Where f_{SW} is the switching frequency and $t_{overlap}$ is the time during which the MOSFET is simultaneously sustaining the input voltage V_{in} and conducting current i_L, and can be calculated from the rising and fall time of the MOSFET datasheet and gate driving circuit. If there is zero voltage switching operation of the circuit, the switching loses should reduce while the conduction losses is more promising in the overall power losses of the converter circuit.

3.7.3 Fast Diode

Similarly the losses in the fast recovery diode can be calculated as

$$P_{diode} = \frac{1}{T_{SW}} \int_0^{T_{SW}} (V_{FD} I_D + i_D^2 R_D)\, dt \tag{3.53}$$

3.7.4 Total power loss in the UPS system:

The total power loss in the proposed UPS is mostly from the semiconductor devices used in the system. The power loss in the inductors has not been considered. The power loss in all the three parts for 1kVA UPS system has been calculated as shown in Table 3.4. The power loss by the battery charger is high as high battery current flow at the low voltage side of the circuit. The power loss in the rectifier and the inverter is reasonable low.

Table 3.4: Power loss by each component in UPS system

Circuit	Components	Model	No. of components	Power loss (Watt)	Percentage of power loss
Rectifier	Conduction losses in Switches	SPP11N60C3	2	5.4	0.54
	Switching losses	SPP11N60C3	2	6.1	0.61
	Losses in Fast diode	BYC10-60	2	7.26	0.726
Inverter	Conduction losses in Switches	SPP11N60C3	4	10.8	1.08
	Switching losses	SPP11N60C3	4	4.5	0.45
Battery charger/ discharger	Conduction losses in Switches	IPW60R045	3	41.2	4.1
	Switching losses	IPW60R045	3	0	0
Total Loss				**74.7**	**7.45%**

3.8 Summary

In this chapter, the proposed transformerless online UPS system has been presented. The modes of the operation of the UPS system have been explained. The proposed UPS system consists of bidirectional battery charger/discharger, a rectifier, and an inverter connected to the load. The mathematical modeling of each part of the UPS system has been performed. The bidirectional battery charger operates both as buck and boost circuit depending on the mode of operation of UPS system. The rectifier operates only in the grid mode of operation while the inverter remains active throughout the operation of the UPS system. The design procedure of different components of the UPS system has been explained in detail. Finally, the power loss due to each component has been derived to analyze the overall efficiency of the system.

CHAPTER 4: PROPOSED CONTROL SCHEME

4.1 Introduction

This chapter presents the proposed control scheme for the online transformerless UPS system. The control scheme comprises of the slide mode and proportional-resonant control for the inverter control, constant current/ constant voltage control for the battery charger/discharger, and the average current control scheme of the rectifier of the proposed UPS system. Mathematical modeling and design procedure of each control part has been explained in this chapter.

4.2 Control scheme for the online UPS system

Each power part of the online UPS system is controlled by its dedicated control scheme. The operation of these control schemes changes with the change in modes of operation of the UPS system. The control scheme for inverter keeps operating in both the grid and battery mode since the inverter remains active throughout the operation of the UPS system. For rectifier, the control scheme operates only in grid mode when the utility supply is available. Similarly, the battery charger and discharger also switch in the change of modes. During grid supply, the bidirectional converter acts as a battery charger. When there is grid interruption, the magnetic contactor disconnects the grid from the UPS. The rectifier stops operation and the sensors connected to the rectifier sense the grid interruption, thus switch the bidirectional converter into battery discharging mode. The control schemes for controlling different parts of the UPS, in different modes of operation are shown in Figure 4.1.

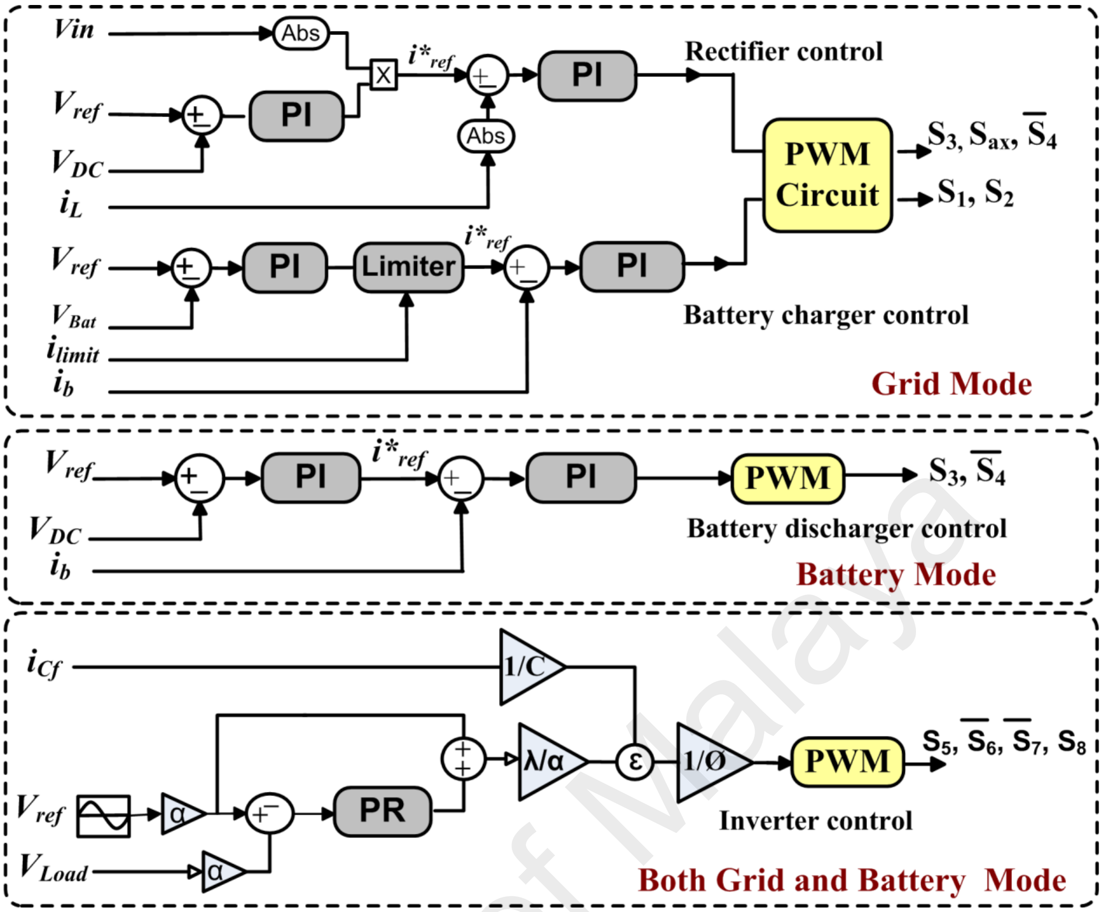

Figure 4.1: Control circuit of proposed UPS system

4.3 Inverter Control

A cascaded control algorithm of SMC and PR control for the inverter of the UPS system has been proposed in this study. It is a new control scheme for the single-phase unipolar voltage source inverter for UPS application. The inner current loop is controlled by the slide mode control because it provides the robust control of the capacitor current which has high harmonics for the nonlinear loading condition. While the outer voltage loop is controlled by the PR control as it tightly tracks the sinusoidal reference voltage resulting in better voltage regulation. Hence PR can be used for implementing selective harmonic compensation without requiring excessive computational resources. The chattering phenomenon in the SMC is eliminated by using smoothed control law in narrow boundary layer. The smoothed control law applied to the pulse width modulator results in the fixed switching frequency of the inverter. Thus the proposed controller adopted the characteristic of both SMC and PR control. The controller shows a good response with low THD and high stability for non-linear loads. The main advantages of the proposed controller are as follows.

1. Very low THD for both linear and non-linear load
2. Very robust in operation
3. Fast transient response
4. Easy implementation

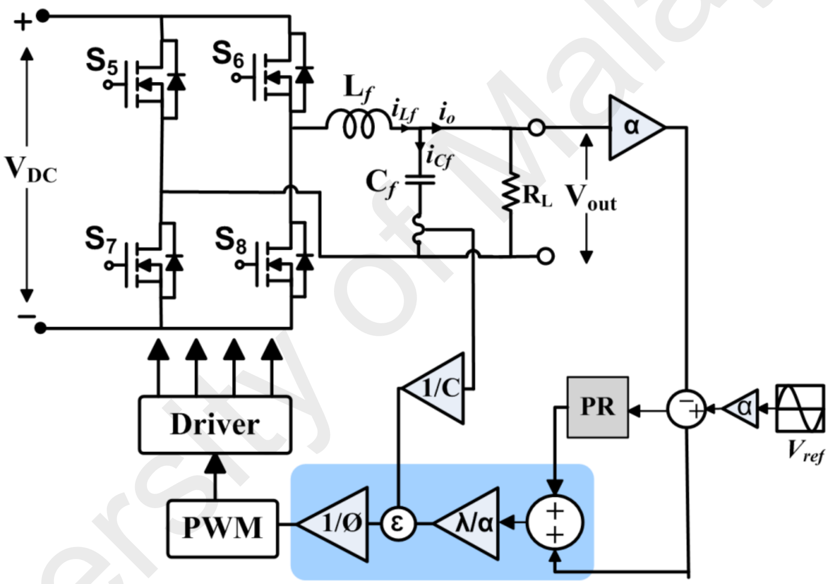

Figure 4.2: Inverter control block diagram

4.1.1. State Space Equation

The circuit diagram of single phase inverter for the Uninterruptible Power Supply (UPS) system with LC filter is shown in Figure 4.2, where V_{DC} is DC-link voltage, V_{out} the filter capacitor C_f output voltage. i_{Lf} is the inductor L_f current, and i_O the output current through the load R_L, given by $i_O = V_{out}/R_L$. The state equations of the inverter are given as

$$L_f \frac{di_L}{dt} = uV_{DC} - V_{out} \tag{4.1}$$

$$C_f \frac{dV_{out}}{dt} = i_c = i_L - i_o \tag{4.2}$$

The behavior of the system can be represented by the following state space equation

$$\frac{d}{dt}\begin{bmatrix} V_{out} \\ i_{Lf} \end{bmatrix} = \begin{bmatrix} 0 & {}^{1}/_{C_f} \\ -{}^{1}/_{L_f} & 0 \end{bmatrix}\begin{bmatrix} V_{out} \\ i_{Lf} \end{bmatrix} + \begin{bmatrix} 0 \\ {}^{V_{DC}}/_{L_f} \end{bmatrix} u + \begin{bmatrix} -{}^{i_o}/_{C_f} \\ 0 \end{bmatrix} \tag{4.3}$$

Where $u = Control\ input = \{-1, 0, +1\}$

In order to implement the sliding mode control, the voltage error x_1, and its derivative $x_2 = \dot{x}_1$ need to be found.

$$x_1 = V_{out} - V_{ref} \tag{4.4}$$

$$x_2 = \dot{x}_1 = \dot{V}_{out} - \dot{V}_{ref} = {}^{i_C}/_{C_f} - \dot{V}_{ref} \tag{4.5}$$

where $V_{ref} = V_m Sin(\omega t)$

$$\begin{bmatrix} \dot{x}_1 \\ \dot{x}_2 \end{bmatrix} = \begin{bmatrix} 0 & 1 \\ -{}^{1}/_{L_f C_f} & -{}^{1}/_{R_L C_f} \end{bmatrix}\begin{bmatrix} x_1 \\ x_2 \end{bmatrix} + \begin{bmatrix} 0 \\ {}^{V_{DC}}/_{L_f C_f} \end{bmatrix} u + \begin{bmatrix} 0 \\ -{}^{V_{ref}}/_{L_f C_f} \end{bmatrix} \tag{4.6}$$

4.1.2. Slide Mode Control

Slide mode control is a non-linear control method which changes the dynamics of the system by employing the discontinuous control signal that forces the system to slide along the system normal behavior. According to the slide mode control theory, a control scheme has to be designed which directs the state trajectory towards the zero sliding surface. The sliding control law is given as,

$$u(t) = \begin{cases} +1 & if\ S(x) > 0 \\ -1 & if\ S(x) < 0 \end{cases} \tag{4.7}$$

where $S(x)$ is called sliding surface and normal system behavior has $S(x) = 0$. The linear sliding surface function can be expressed as equation (4.8)

$$S = \lambda x_1 + x_2 \qquad \lambda > 0 \tag{4.8}$$

where λ is a real constant. For the dynamic behavior equation (4.8) will be

$$S = \lambda x_1 + \dot{x}_1 = 0 \tag{4.9}$$

The objective of the control in equation (4.8) is to drive the trajectory of the system from any initial condition $x(0)$ to the sliding surface $S(x)=0$. This trajectory is maintained at the sliding surface, and consequently directs the system towards the steady state condition. Thus the sliding mode control performs its operation by utilizing the sliding surface as a reference and thus satisfies the inequality condition

$$\lim_{s\to 0^+} \frac{d(s)}{dt} < 0 \qquad \& \qquad \lim_{s\to 0^-} \frac{d(s)}{dt} > 0$$

In order to ensure the stability of the sliding function, the Lyapunov function $V(t) = S^2/2$ has to be satisfied with the minimum condition $\dot{V}(t) < \eta|s|$, keeping the scalar s at zero while η is strictly positive constant (Hasan Komurcugil, 2010; Yan, Hu, Utkin, & Xu, 2008). Hence the condition for stability will be $\dot{V}(t) < 0$.

$$\dot{V}(t) = S\dot{S} \tag{4.10}$$

$$\dot{V}(t) = S[\lambda \dot{x}_1 + \dot{x}_2] \tag{4.11}$$

$$\dot{V}(t) = S[\lambda x_2 - \frac{1}{L_f C_f} x_1 + \frac{V_{DC}}{L_f C_f} u - \frac{Vref}{L_f C_f} - \frac{x_2}{R C_f}] \tag{4.12}$$

Consider the discrete control law as follow;

$$u(t) = sign(s) = \begin{cases} +1 & if\ S(x) > 0 \\ -1 & if\ S(x) < 0 \end{cases} \quad (4.13)$$

In order to satisfy the sliding condition in equation 4-10, despite of the uncertainty on the dynamics of the non-linear function, u is replaced by the '–*sign*(*s*)', where 'sign' is the sign function.

$$V\dot{(t)} = S\left[\lambda x_2 - \frac{1}{L_f C_f} x_1 - \frac{V_{DC}}{L_f C_f} sign(s) - \frac{Vref}{L_f C_f} - \frac{x_2}{RC_f}\right] \quad (4.14)$$

$$V\dot{(t)} = |S|\left[sign(x)\left[\lambda x_2 - \frac{1}{L_f C_f} x_1 - \frac{Vref}{L_f C_f} - \frac{x_2}{RC_f}\right]\right] - \frac{V_{DC}}{L_f C_f} \quad (4.15)$$

$$sign(x)\left[\lambda x_2 - \frac{1}{L_f C_f} x_1 - \frac{Vref}{L_f C_f} - \frac{x_2}{RC_f}\right] < \frac{V_{DC}}{L_f C_f} \quad (4.16)$$

Hence it is clear that the stability condition is fulfilled when equation (4.16) is satisfied. Putting the value of voltage and current error in equation (4.8), provides the sliding control law of the inverter,

$$S = \lambda(V_{out} - V_{ref}) + \frac{i_C}{C_f} - \dot{V}_{ref} \quad (4.17)$$

Since the implementing of slide mode control involves the derivative of the voltage error. But it is well known that the differential operation amplifies high frequency components in a signal. Therefore, capacitor current feedback is used to avoid the derivative operation in creating the sliding function (Kukrer et al., 2009). Hence the state variable x_2 can be obtained as $x_2 = \dot{x}_1 = \frac{1}{C_f}(i_C - i_{ref})$, where $i_{ref} = C_f \dot{V}_{ref}$ is the reference for the capacitor current.

$$S = \lambda(V_{out} - V_{ref}) + \frac{1}{C_f}(i_C - i_{ref}) \quad (4.18)$$

Since the sliding mode controller has the common inherent property of chattering phenomena. It cause low control accuracy and high losses in the circuit. In order to overcome the chattering phenomena, a smoothed slide mode control has been implemented. This can be achieved by smoothing out the control discontinuity in a thin boundary layer neighboring the sliding surface.

$$B(t) = \{x, |S(x;t)| \leq \emptyset\} \qquad \emptyset > 0 \tag{4.19}$$

where $\emptyset$ is the boundary layer thickness and $\varepsilon = \frac{\phi}{\lambda}$ is the boundary layer width. Hence $B(t)$ is choose as such that all the trajectories starting at $B(t=0)$ remain inside the $B(t)$ for all t > 0. Hence we interpolate S inside $B(t)$ for instance, and replace S by an expression S/$\emptyset$. Thus equation 4-18 will be

$$\frac{S(x)}{\emptyset} = \frac{\lambda}{\emptyset}\left[V_{out} - V_{ref}\right] + \frac{1}{C_f \emptyset}\left[i_C - i_{ref}\right] \tag{4.20}$$

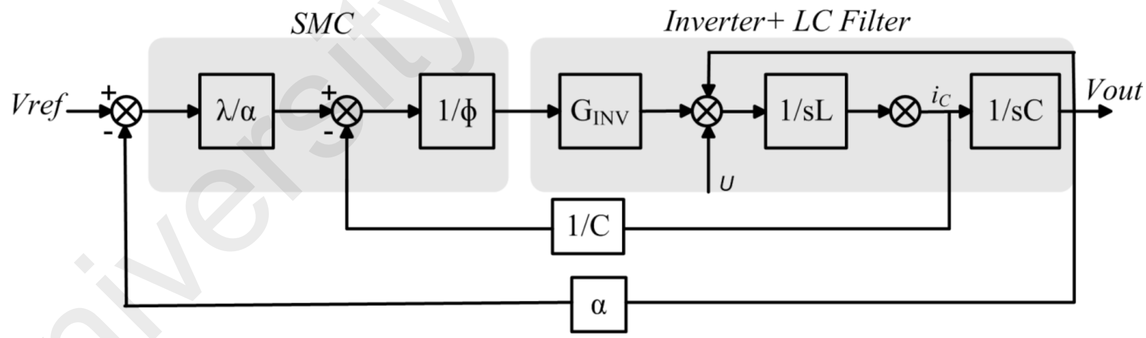

Figure 4.3: Block diagram of the Slide Mode Control with inverter and LC filter

The close loop control of the inverter as shown in Figure 4.3, is obtained from the previous description of the slide mode control. G_{INV} is the model of the inverter with low pass LC filter employed at the output of the inverter. The SMC block represents the implementation of equation (4.20), where V_{ref} is the reference voltage that is compared with the output voltage across the filter capacitor C_d. The voltage error multiplying with λ/α is considered as reference current, and is fed to the inner current loop. The reference current is compared with the feedback capacitor current i_C, and current error multiplied with Ø is provided to the PWM modulator.

The smoothing control discontinuity assign a low pass filter structure to the local dynamics thus eliminates chattering. The control law needs to be tuned very precisely in order to achieve a trade-off between the tracking precision and robustness to the uncontrolled dynamics as shown in Figure 4.4.

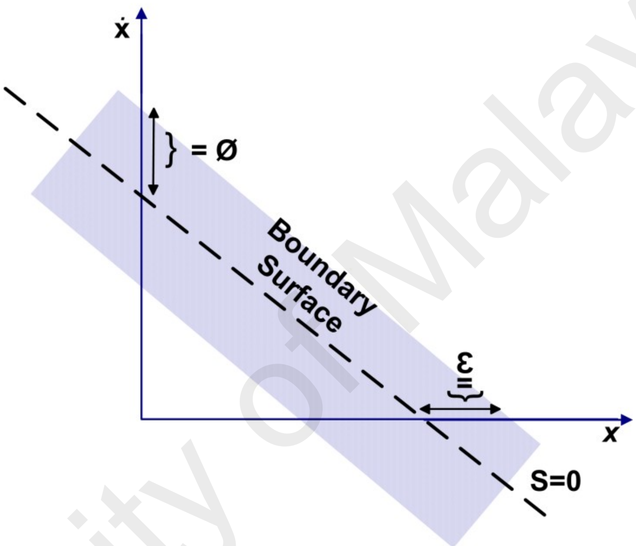

Figure 4.4: Smooth Control Law for Boundary Surface (Slotine & Li, 1991)

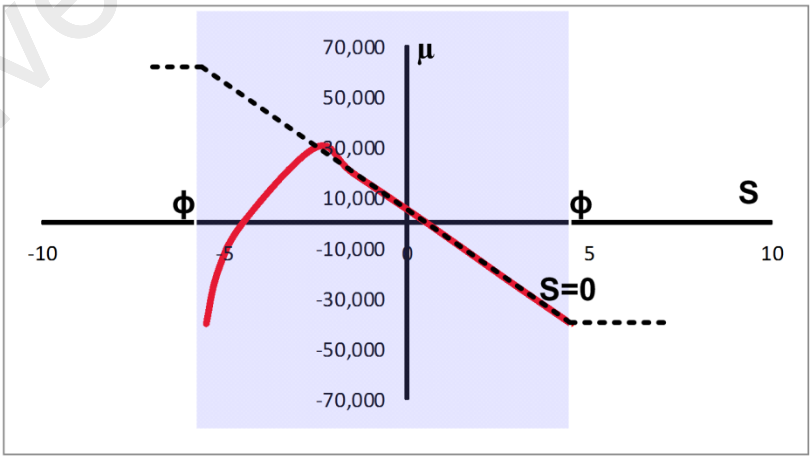

Figure 4.5: Control Interpolation in Boundary Layer

The smoothing control discontinuity assign a low pass filter structure to the local dynamics thus eliminates chattering. The control law needs to be tuned very precisely in order to achieve a trade-off between the tracking precision and robustness to the uncontrolled dynamics as shown in Figure 4.5.

4.1.3. Proportional Resonant Control

Conventionally the PR controller provides a large gain at the fundamental frequency and strictly follows the sinusoidal reference, reducing the steady state error and improving the stability of the system. The transfer function of the ideal PR controller is given by equation (4.21)

$$G_{PR} = K_P + \frac{2K_R s}{s^2 + \omega_o^2} \tag{4.21}$$

where K_P is the proportional gain, ω_0 is the resonant frequency, and K_R is the resonant gain. The ideal PR controller gives infinite gain at the resonant frequency but no gain and phase shift at other frequencies. In order to avoid stability problem associated with infinite gain, more appropriate non-ideal PR controller is used, as shown in equation 4-22

$$G_{PR} = K_P + \frac{2K_R \omega_c s}{s^2 + 2\omega_c s + \omega_o^2} \tag{4.22}$$

Hence selecting a suitable cut-off frequency ω_c can widen the bandwidth, reducing the sensitivity towards the frequency variations. By combining the PR controller with the slide mode control, the performance of the inverter is improved, as the resonance controller provide better regulation of the output voltage and reduce the total harmonic distortion considerable (Hao, Yang, Liu, Huang, & Chen, 2013; Holmes, Lipo, McGrath, & Kong, 2009).

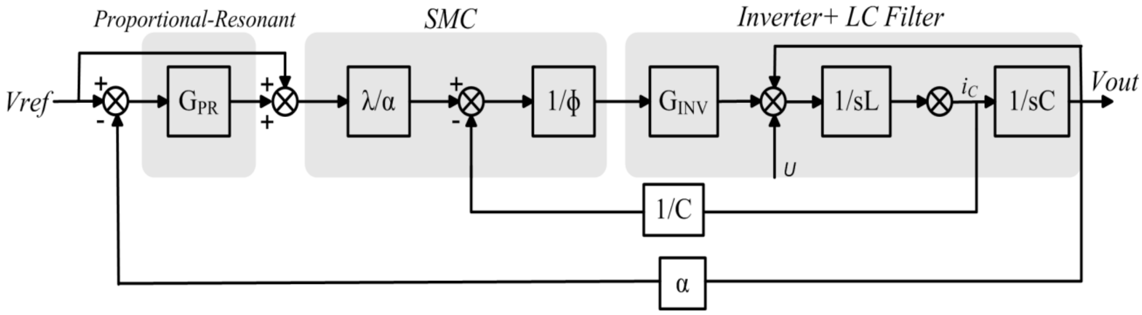

Figure 4.6: Equivalent control diagram with SMC and PR control

The block diagram of slide mode control with PR controller is shown in the Figure 4.6. G_{PR} is the model of the PR controller introduced in the voltage loop of the controller. This increases the performance by precisely tracking the reference AC Voltage. The current loop is control by the previously described SMC (Figure 4.3). In proposed controller, both the PR and SMC work in cascaded to control the inverter of the UPS system. The open loop gain of the voltage control loop with the PR compensator can be obtained by equation (4.23).

$$H(s) = G_{PR}G_{INV} = \left(K_P + \frac{2K_R\omega_c s}{s^2+2\omega_c s+ \omega_0^2}\right)\left(\frac{sC_f r_d+1}{L_f C_f s^2+sC_f r_d+1}\right) \tag{4.23}$$

$$H(s) = \frac{a_3 s^3+a_2 s^2+a_1 s+a_0}{b_4 s^4+b_3 s^3+b_2 s^2+b_1 s+b_0} \tag{4.24}$$

Where

$a_3 = K_p C_f r_d,$

$a_2 = K_p + 2\omega_c C_f r_d(K_r+K_p),$

$a_1 = 2K_p\omega_c + 2K_r\omega_c + K_p C_f r_d\omega_0^2,$

$a_0 = K_p\omega_0^2$

$b_4 = L_f C_f,$

$b_3 = 2\omega_c L_f C_f + C_f r_d,$

$b_2 = L_f C_f \omega_0^2 + 2C_f r_d \omega_c + 1,$

$b_1 = C_f r_d \omega_0^2 + 2\omega_c,$

$b_0 = \omega_0^2$

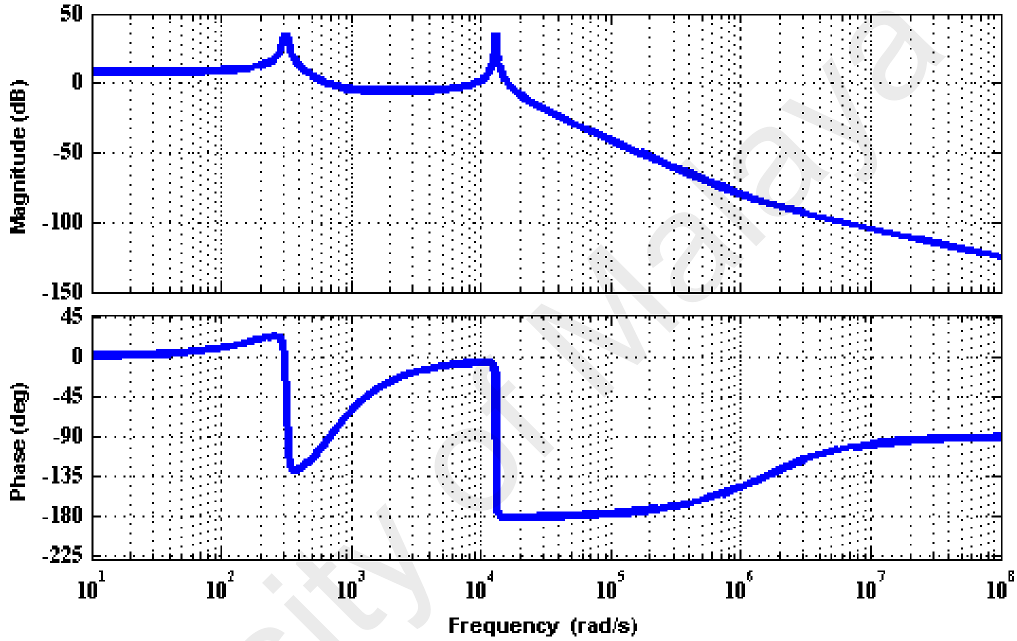

Figure 4.7: Bode plot of voltage loop with PR controller

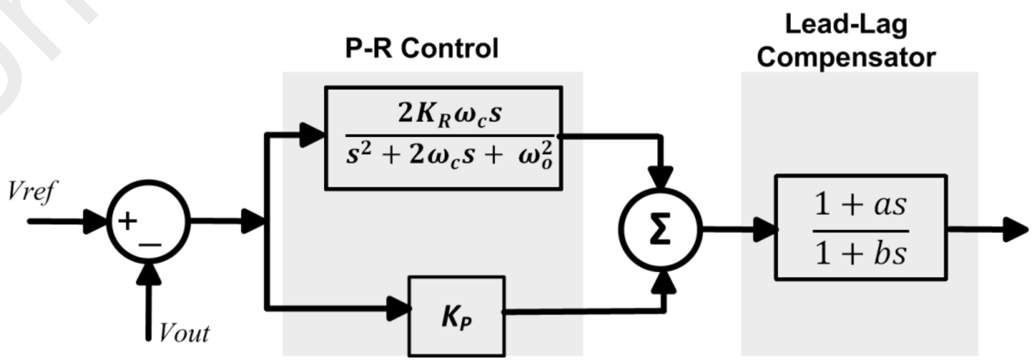

Figure 4.8: PR control with Lead-Lag compensator

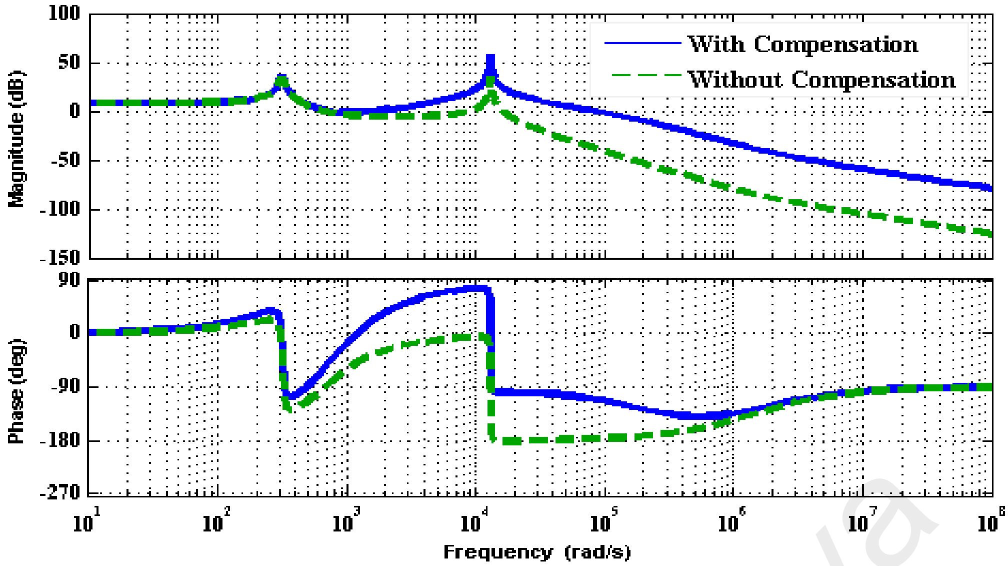

Figure 4.9: Bode plot of voltage loop with lead-lag compensator

The bode plot of the voltage loop is shown in Figure 4.7. It can be seen from the compensated voltage loop gain, the large system bandwidth would give the voltage controller a fast response. Meanwhile, having a phase margin of 2° demonstrates closed loop stability. However, as can be seen from the bode plot in Figure 4.7; the phase margin is very low, which may affect the output voltage by inserting the unwanted oscillations. This can be compensated by adding a suitable lead-lag compensator as shown in the Figure 4.8.

$$G_{lead-lag} = \frac{1+as}{1+bs} \tag{4.25}$$

Where $b = x * a$, and x is the ratio which can be calculated as $(1 - \sin \emptyset)/(1 + sin\emptyset)$, and Ø is the required phase margin. Thus the lead-lag compensator improves the phase margin of the voltage loop by reducing the steady state error to almost zero for harmonic components. Figure 4.9 shows the bode plot of the outer voltage loop with lead lag compensator. The phase margin of the loop is improved to78°, is quite high which lead to oscillating free output of the system.

Hence the slide surface with the PR control can be presented in equation 4-26

$$\frac{S(x)}{\emptyset} = \frac{1}{C\emptyset}\left[i_C - i_{ref}\right] + \frac{\lambda}{\emptyset}\left[K_p\left(V_{out} - V_{ref}\right) + k_i\left(\frac{2s}{s^2+2\omega_c s+\omega_o^2}\right)\left(V_{out} - V_{ref}\right)\right] \quad (4.26)$$

Thus equation 4-26 shows the dynamic behavior of the system with both slide mode control and PR compensator. The error in the voltage loop is compensated by the appropriate PR parameters, thus the output voltage is compelled to follow the reference AC voltage leading to the system stability while the SMC drive the system to the zero sliding surface with maximum stability. Since the capacitor error current contains the ripples from the inductor, the current peak may reach high values. So $\emptyset$ should be carefully assign values in order to compensate the slope from the high current ripple of the capacitor. Hence the PR controller eliminates the steady-state error at resonant frequency or harmonic at that frequency.

Now the condition of stability is modified as

$$|s| \geq \emptyset \qquad => \frac{1}{2}\frac{d}{dt}S^2 \leq \left(\dot{\emptyset} - \eta\right)|s| \qquad (4.27)$$

The $\dot{\emptyset}|s|$ illustrates the fact that the boundary layer attraction condition shows more firmness during boundary layer contraction ($\dot{\emptyset} < 0$) and less firmness during boundary layer expansion($\dot{\emptyset} > 0$).

The response time of the system λ determines the dynamics and robustness of the system. It is clear from equation 4-26, that smaller value of λ leads to slow response time, while higher λ values though increase the response time but takes larger time to reach the sliding surface. Thus the optimal value for λ is equal to the switching frequency of the inverter.

According to (Zargari, Ziogas, & Joos, 1995), in order to maintain proper control over the capacitor current, multiple crossing between the error signal from the current loop and the triangular waveform must be avoided. Hence the maximum slope of the error signal should be less than the slope of the triangular waveform (carrier). This means that the following condition applies in terms of magnitudes

Slope of error signal < Slope of the carrier signal

The slope of the carrier wave is $4V_m \times f_s$, where V_m is the magnitude of the carrier signal, and f_s is the frequency of carrier signal. The slope of the error signal to the modulator is given by $V_{DC}/4L_f C_f \emptyset$. According to the limitation of the pulse width modulator,

$$4V_m \times fs >> {V_{DC}}/{4L_f C_f \emptyset} \tag{4.28}$$

$$\emptyset >> \frac{V_{DC}}{16L_f C_f V_m f_S} \tag{4.29}$$

Considering the limitation of the PWM modulator, the minimum approximate value of $\emptyset$ can be calculated using the equation

$$\emptyset \cong \frac{10V_{DC}}{16L_f C_f V_m f_S} \tag{4.30}$$

Table 4.1 shows the comparison of the proposed control scheme with the slide mode control and other common controllers. The proposed controller shows an improvement in terms of reducing the THD and transient response with robust control of the inverter.

Table 4.1: Comparison of different control methods

Controllers	Model Predictive Control (Cortes et al., 2009)	SPWM Control (Tamyurek, 2013)	Rotating SMC (H. Komurcugil, 2012)	Fix-Freq SMC (Abrishamifar et al., 2012)	Proposed Work
V_{DC}	529	405	300	360	180
V_{RMS}	150	220	200	220	110
C_f (uF)	40	202	100	9.4	6.6
L_f (mH)	2.4	0.03	0.250	0.357	0.84
THD (L)	2.85%	1.11%	-	1.1%	0.45%
THD (NL)	3.8%	3.8%	2.66%	1.7%	1.25%
Ts (ms)	50	60	-	0.5	0.3
Note: L → Linear load, NL → Non-linear load, T_S → Transient response					

4.4 Rectifier Control

The rectifier of the UPS system is controlled by well-known average current mode control as shown in Figure 4.10. In this control scheme, the faster inner current loop regulates the inductor current so that its average value during each period follows the rectified input voltage. The slower outer voltage loop maintains rectified output voltage close to reference voltage and generates the control signal v_c for the current loop. The steady state analysis of the rectifier shows stable performance during grid mode. The state space equations of the rectifier are derived as,

$$\frac{di_L}{dt} = \frac{V_{in}}{L_{11}+L_{12}} D + \frac{(V_{in}-V_{DC})}{L_{11}+L_{12}} (1-D) \qquad (4.31)$$

$$\frac{dv_{DC}}{dt} = -\frac{V_{DC}}{RC_d} D + \left(\frac{i_L}{C_d} - \frac{V_{DC}}{RC_d}\right) (1-D) \qquad (4.32)$$

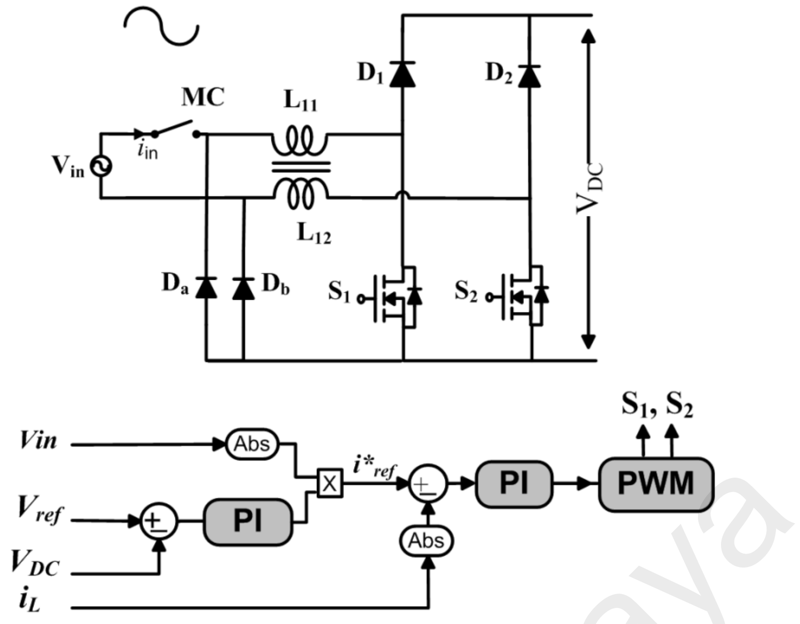

Figure 4.10: Close loop control of the rectifier

Assuming the current loop has high bandwidth as compared to voltage loop, and output capacitor C_d is large enough to give approximately constant output voltage i.e. $dv_{DC}/dt = 0$. With $\hat{V}_{in} = 0$, the small signal control $\hat{d}$ to input current $\hat{\imath}_L$ transfer function $G_{i_L d}(s)$ of the inner current loop is give as,

$$G_{i_L d}(s) = \frac{\hat{\imath}_L}{\hat{d}} = \frac{V_{DC}}{s(L_{11}+L_{12})} \qquad (4.33)$$

The stability of the current loop depends on the current loop gain, hence suitable proportional-integral (PI) controller $G_i(s) = k_{pi} + \frac{k_{ii}}{s}$, is used for compensating the current loop. The bode plot of the current loop gain $T_i = G_{i_L d}(s).G_i(s)$ is obtained considering the circuit parameters as shown in Table 5.5. The value of proportional gain K_{pi} and integral gain K_{ii} is selected as 2.3 and 1200 respectively for the stable operation of the current loop. The value of proportional and integral gain can be calculate using Ziegler-Nichols tuning formula (Hang, Astrom, & Ho, 1991). Figure 4.11 presents the bode plot of the current loop gain with phase margin of 89° and stable operation of the rectifier. Same approach is used to compensate the voltage loop of the average current control scheme. $\hat{v}_c$ is the reference current for the current loop. Assuming constant input voltage, the small signal control $\hat{v}_c$ to output transfer function $G_{V_dV_c}(s)$ of the voltage loop is derived as.

$$G_{V_dV_c}(s) = \frac{\hat{v}_{DC}}{\hat{v}_c} = \frac{V_{in}R}{2V_d(sCR+2)} \tag{4.34}$$

In order to force the output voltage to follow the reference voltage V_{ref}, a proportional-integral (PI) compensator has been employed. Combining the power stage with the PI controller $G_v(s) = k_{pv} + \frac{k_{iv}}{s}$ provides the overall loop gain

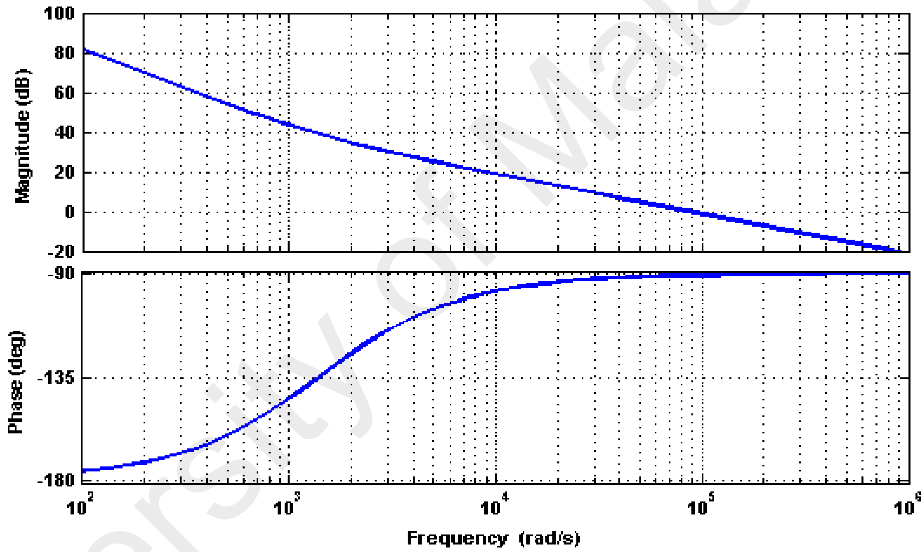

Figure 4.11: Bode response of the current loop gain of the rectifier

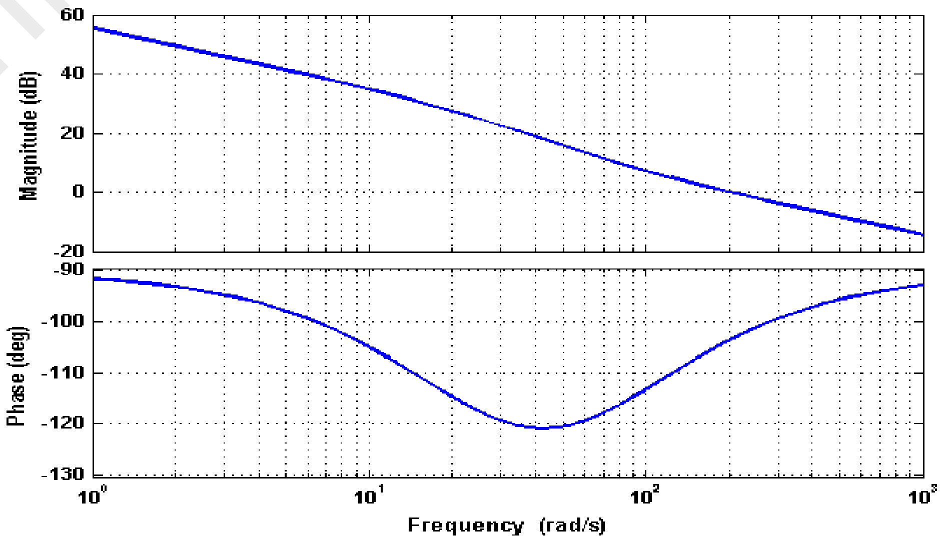

Figure 4.12: Bode response of the voltage loop gain of the rectifier

$T_v = G_v . G_{V_d V_c}(s)$ of the voltage loop. The value of K_{pv} and K_{iv} in voltage loop is selected as 1.2 and 13 respectively. The value of proportional and integral gain can be calculate using Ziegler-Nichols tuning formula (Hang et al., 1991). The stability of the voltage loop can be analyzed using the bode plot obtained by consider the parameters from Table 4.2, shown in Figure 4.12. The system shows good stability with positive phase margin.

Table 4.2: Specifications of the rectifier

Parameters	Symbol	Value
Input Inductor	L_{11}, L_{12}	800 uH, Coupled Torid
DC-link capacitor	C_d	1940 uF
Switching frequency	$f$sw	30 kHz

4.5 Battery Charger and Discharger Control

The controller for the battery charger/discharger during both grid mode and battery mode is shown in Figure 4.13. During battery charging, the controller operates as constant current mode (CC) or constant voltage mode (CV) depending on battery voltage while, in battery discharging, the controller regulates the DC-link voltage as well as the primary inductor current. It is assumed that the primary inductor current i_{LP} flows continuously. The steady-state analysis of the battery charger/discharger is performed using average state variable method (Erickson & Maksimovic, 2001).

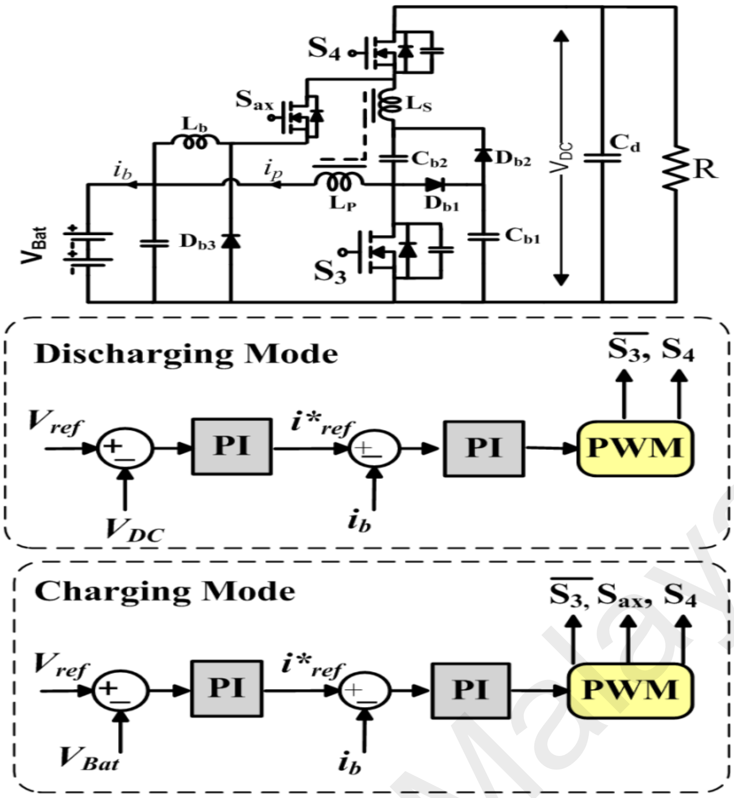

Figure 4.13: Circuit diagram and control of battery charger/discharger

When the switch S_3 is ON and switches S_4 is OFF, the inductor current i_p and the capacitor voltage V_o is given as;

$$\frac{di_p}{dt} = \frac{V_{Bat}}{L_p} \tag{4.35.a}$$

$$\frac{dV_o}{dt} = -\frac{V_o}{RC_d} \tag{4.35.b}$$

When the switch S_3 is OFF and switches S_4 is ON;

$$\frac{di_s}{dt} = \frac{V_{Bat}-V_{DC}}{L_{eq}} \tag{4.36}$$

$$\frac{dV_o}{dt} = \frac{i_s}{C_d} - \frac{V_o}{RC_d} \tag{4.37}$$

where equivalent inductance of the coupled inductor L_p and L_s is given by

$$L_{eq} = (N+1)^2 L_m \tag{4.38}$$

$$i_p = i_s(N+1) \tag{4.39}$$

The state space equations for the charger with coupled inductor are given in equation (4.40) and (4.41)

$$\frac{di_P}{dt} = \frac{V_{Bat}}{dt}D + \frac{(V_{Bat}-V_{DC})(1-D)}{L_m(N+1)} \tag{4.40}$$

$$\frac{dV_o}{dt} = \frac{i_p}{C_d(N+1)}(1-D) - \frac{V_o}{RC_d} \tag{4.41}$$

Now perturb the system

$$d = D + \hat{d}$$

$$V_{Bat} = \mathrm{V_{Bat}} + \hat{v}_{Bat}$$

$$V_o = \mathrm{V_o} + \hat{v}_o$$

$$I_P = \mathrm{I_P} + \hat{\imath}_P$$

Consider only the dynamic terms and eliminate the product of the AC terms because of very small value.

$$\frac{di_p}{dt} = \hat{v}_{Bat}\left(\frac{D}{L_m} + \frac{(1-D)}{L_m(N+1)}\right) - \hat{v}_o\left(\frac{1-D}{L_m(N+1)}\right) + \hat{d}\left(\frac{\mathrm{V_{Bat}}}{L_m} - \frac{\mathrm{V_{Bat}}+V_{DC}}{L_m(N+1)}\right) \tag{4.42}$$

$$\frac{d\mathrm{V_o}}{dt} = \frac{\hat{\imath}_P(1-D)}{C_d(N+1)} - \frac{\mathrm{I_P}\hat{d}}{C_d(N+1)} - \frac{\hat{V}_o}{RC_d} \tag{4.43}$$

Taking Laplace transform, the equations will be

$$\mathrm{s}\hat{\mathrm{v}}_\mathrm{o} = \hat{\mathrm{i}}_\mathrm{P}\left(\frac{1-\mathrm{D}}{C_d(\mathrm{N}+1)}\right) - \frac{\hat{\mathrm{v}}_\mathrm{DC}}{\mathrm{R}C_d} - \frac{\mathrm{I_P}}{C_d(\mathrm{N}+1)}\hat{\mathrm{d}} \tag{4.44}$$

$$\mathrm{s}\hat{\mathrm{i}}_\mathrm{P} = \hat{\mathrm{v}}_\mathrm{Bat}\left(\frac{\mathrm{D}}{\mathrm{L_m}} + \frac{1-\mathrm{D}}{\mathrm{L_m}(\mathrm{N}+1)}\right) - \hat{\mathrm{v}}_\mathrm{DC}\left(\frac{1-\mathrm{D}}{\mathrm{L_m}(\mathrm{N}+1)}\right) + \hat{\mathrm{d}}\left(\frac{\mathrm{V_{Bat}}}{\mathrm{L_m}} - \frac{\mathrm{V_{Bat}}+\mathrm{V_{DC}}}{\mathrm{L_m}(\mathrm{N}+1)}\right) \quad 4.45)$$

Solving state space equations gives the primary inductor to control transfer function $G_{i_{Lp}d}(s)$ and output to control transfer function $G_{v_od}(s)$ of the battery charger/discharger is given in equations (4.46) and (4.47) respectively;

$$G_{i_{Lp}d}(s) = \frac{\hat{i}_{Lp}}{\hat{d}} = \frac{NV_{Bat}+V_{DC}}{(N+1)RC_dL_m}\frac{\left(s+\frac{1}{RC_d}\right)}{\left(s^2+s\frac{1}{RC_d}+\frac{(1-D)^2}{(1+N)^2L_mC_d}\right)} \tag{4.46}$$

$$G_{v_od}(s) = \frac{\hat{v}_o}{\hat{d}} = \frac{s\left(-\frac{I_P}{C_d(N+1)}\right)+\frac{(1-D)}{C_d(N+1)}\left(\frac{NV_{Bat}-V_{DC}}{L_m(N+1)}\right)}{s^2+s\frac{1}{RC_d}+\frac{(1-D)^2}{(1+N)^2L_mC_d}} \tag{4.47}$$

Considering the gain due to clamp capacitor C_{b2}, the transfer equation is given by,

$$G_{v_od}(s) = \frac{\hat{v}_o}{\hat{d}} = \frac{s\left(-\frac{I_P}{C_d(N+1)}\right)+\frac{(1-D)}{C_d(N+1)}\left(\frac{NV_{Bat}-(V_{DC}-V_{Bat}/(1-D))}{L_m(N+1)}\right)}{s^2+s\frac{1}{RC_d}+\frac{(1-D)^2}{(1+N)^2L_mC_d}} \tag{4.48}$$

The right half plane zero in the control to output transfer function has been placed properly with suitable selecting the design components. Using current mode control and selecting an optimum value of L_M, load current, and duty cycle D of the converter, keeps the circuit operation in stable condition (Kapat, Patra, & Banerjee, 2009; Restrepo, Calvente, Romero, Vidal-Idiarte, & Giral, 2012).

In battery discharging control, the voltage loop with PI compensator $G_v = k_p + \frac{k_i}{s}$ regulates the DC-link voltage V_{DC} and provides reference current i_{*ref} for the current loop. Similarly PI compensator is added in the current loop to force the primary inductor current i_P to follow the reference current i_{*ref} from the voltage loop. The bode plot of the current loop gain and voltage loop gain has been generated considering the battery charger/discharger circuit parameters from Table 5.4. The value of k_p and k_i is 1.7 and 9 respectively for voltage loop, while 2.3 and 2300 respectively for current loop.

The value of proportional and integral gain can be calculate using Ziegler-Nichols tuning formula (Hang et al., 1991). The system shows good stability with positive phase margin and has no right half plane poles as shown in Figure 4.15. It is easy to achieve higher cross over frequencies by adjusting a suitable gain of the compensators as the phase never reaches to -180°.

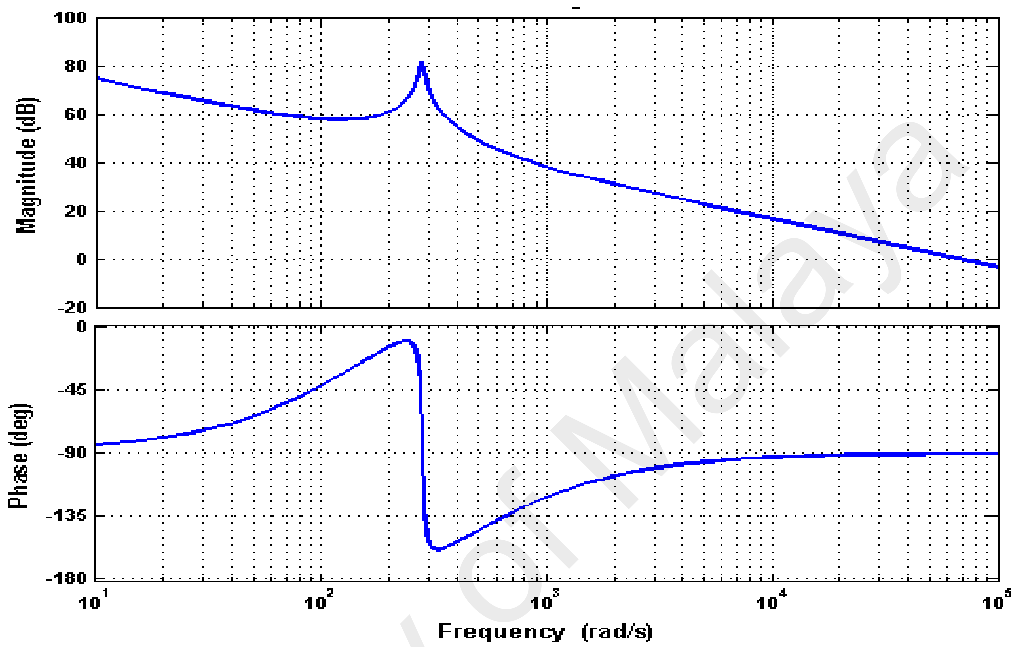

Figure 4.14: Bode response of the current loop gain of the battery charger/discharger

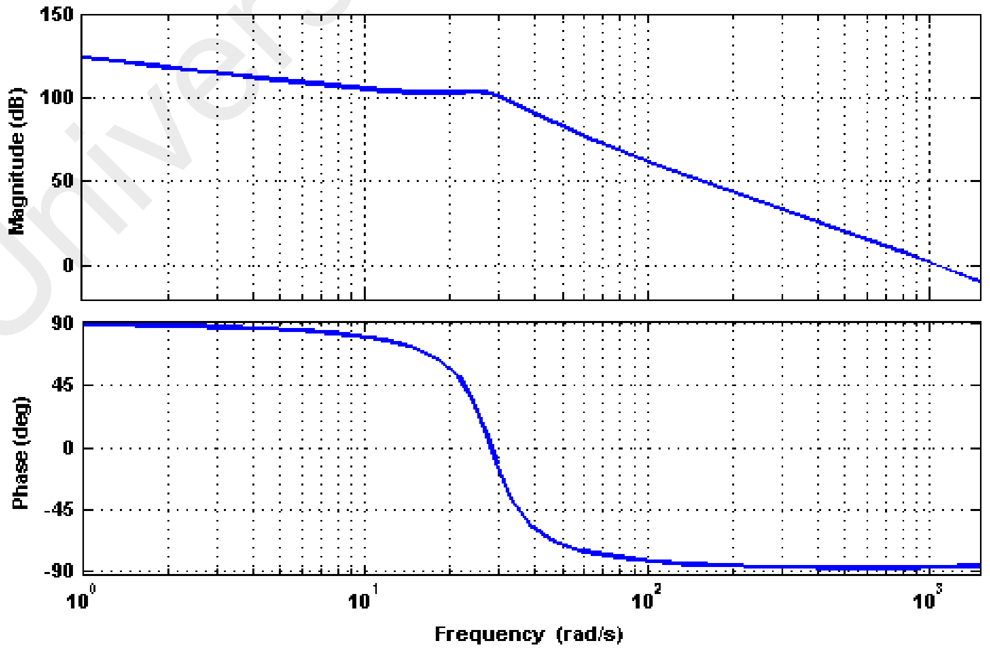

Figure 4.15: Bode response of the voltage loop gain of battery charger/discharger

For designing the battery charging controller, the equivalent electric circuit of the battery is presented in Figure 4.16. The Thevenin battery model is most commonly used model (Hegazy et al., 2013), which consists of an ideal battery voltage E_O, internal resistance R_i, polarization capacitor C_P, and polarization resistance R_P. All the elements used in the model are a function of battery state of charge (SoC). N_S and N_P are the number of cells in series and parallel respectively. The battery terminal voltage V_{Bat} can be presented in equation (4.49).

$$V_{Bat} = N_s(E_0 - I_{Bat}R_i - V_{cp}) \tag{4.49}$$

where V_{CP} is the polarization voltage and $I_{Bat} = \frac{I_{Load}}{N_p}$ is the battery current. Model parameters have been identified for the battery as shown in Table 4.3.

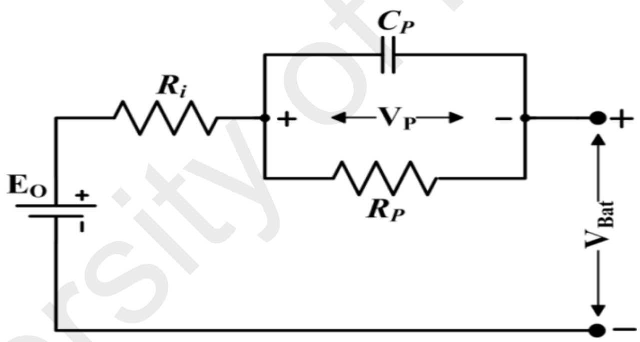

Figure 4.16: Thevenin battery model

Table 4.3 Battery Specifications

Parameters	Value
Rated Capacity	35Ah
Nominal Voltage	24V
Min. Voltage	16V
Max. Charging Current limit	9.9A
Max. Discharge Current	105A
Initial SoC	70%
Internal Resistance	8mΩ

Table 4.4 Specification of the battery charger

Parameters	Symbol	Value
DC-link voltage	V_{DC}	360V
Battery bank voltage	V_{Bat}	24V
Switching frequency	$f$sw	30 kHz
Coupled inductor	L_P,L_S	Turns ratio N = 6; Magnetizing inductor L_m = 107uH; PQ-5050 core;
Inductor	L_b	300uH
Capacitor	C_{b1}, C_{b2}	C_{b1}, C_{b2} = 2×2.2uF (ceramic), C_b = 1000uF, C_d = 1900uF

In charging mode, the controller operates as constant current mode CC or constant voltage mode CV depending on the battery voltage. In current loop, the battery input current i_{Bat} is forced to follow the reference current i_{Ref} using PI compensator in equation (4.50).

$$i^* = K_p(i_{Ref} - i_{Bat}) + K_i \int (i_{Ref} - i_{Bat})dt \qquad (4.50)$$

Similarly the battery voltage is regulated by voltage loop using PI compensator that forces the output battery voltage V_{Bat} to follow the reference voltage V_{ref}. The current limiter is introduced to limit the maximum charging current of the battery as specified in Table 4.4. If the i_{ref} is greater than i_{limit}, the battery is charged at constant current (CC Mode), in contrast if the i_{ref} is less than i_{limit}, the battery is charged at constant voltage (CV mode).

4.6 Summary

This chapter presents the control techniques used for regulating parts of the UPS system such as inverter, rectifier, and battery charger/discharger. The new cascaded PR and SMC have been used to control the inverter of the UPS system. The proposed control scheme shows good performance against linear, non-linear, and step change in the loading condition. Similarly, the average current control scheme has been used to control the rectifier, regulate the DC-link, and maintain unity power factor. The constant voltage (CV) and constant current (CC) control technique have been implemented to control bidirectional charger/discharger. The stability analysis of each control scheme has been performed where all the control schemes show stable operation of the rectifier, inverter, and the battery charger/discharger.

CHAPTER 5: RESULTS AND DISCUSSION

5.1 Introduction

In this chapter, the simulation and experimental results from different parts of the UPS system are presented. Since the UPS system consists of front end rectifier, bidirectional battery charger/discharger, and the inverter connected to the load. The simulation and experimental results of all the three parts are added in this study. This chapter is organized as follows; firstly, the simulation and experimental results of each part are explained separately. And then the experimental results of the combined UPS system are presented. These results depict the performance of the UPS system by displaying the input power factor, battery charging, zero voltage switching, and inverter output for different loading condition. Similarly, experimental results of the changing of operation modes of the UPS system are shown in this chapter. At the end, comparison of the proposed UPS system is performed with other state of the art works.

5.2 System Specifications

To verify the performance of the proposed UPS system, computer simulation as well as the hardware implementation of the circuit is performed. Table 5.1 shows the specification of the UPS system. Each sub-part has been developed keeping in view the overall rating of the system. The control scheme for inverter, rectifier, and battery charger/discharger are implemented using DSP TMS320F28335. The backup storage system consists of two batteries (each battery is 24V/35 Ah), or parallel batteries depending upon the backup time for the connected load.

Table 5.1 Specification of the proposed UPS system

Parameters	Symbol	Value
Input Voltage	V_{in}	220V
Output Voltage	V_{out}	220V
Grid Frequency	fr	50Hz
Output Frequency	fo	50Hz
Number of Batteries	V_b	2 Parallel connected (24V/35Ah)
Maximum Output Power	Po, max	1kVA
DC-link Voltage	V_{DC}	360V

5.3 Single Phase AC-DC Inverter

The performance of the proposed control for the inverter is verified by simulation using MATLAB/Simulink as well as in hardware prototyping. The circuit specifications are given in Table 5.2, and control parameters are listed in Table 5.3. The value of α is selected considering the circuit parameters. The steady-state load tests have been performed using linear and non-linear single phase uncontrolled diode rectifier. The reference non-linear load are designed according to the standard of IEC62040-3, with input series resistance of 0.3Ω, parallel load resistance of 40Ω, and filter capacitor C = 4700uF. The results are evaluated using the transient response, steady-state error, and THD for both linear and non-linear load. Considering the controller parameter, the THD measured for the linear and non-linear load is 0.45% and 1.25% respectively as shown in Figure 5.1. Figure 5.2 shows the output voltage during a step change in load from 0 to 100%, and back from 100% to 0. The controller shows satisfactory performance with only 0.3ms of settling time

Table 5.2 Specifications of the single-phase inverter

Parameters	**Symbol**	**Value**
Switching Frequency	f_{sw}	20 kHz
Switches	S_5~S_8	SPP11N60C3
Output Filter Inductor	L_f	840µH
Output Filter Capacitor	C_f	6.6µF
Cutoff Frequency	f_{cut}	17,00Hz
Load resistance	R_L	40Ω
Power Rating	Po	1kVA

Table 5.3: Controller parameters of inverter

Parameter	**Value**
K_P	0.07
K_I	1570
λ	20,000
Φ	126830
V_m	8V
α	0.045454
V_{ref}	110V_{AC}

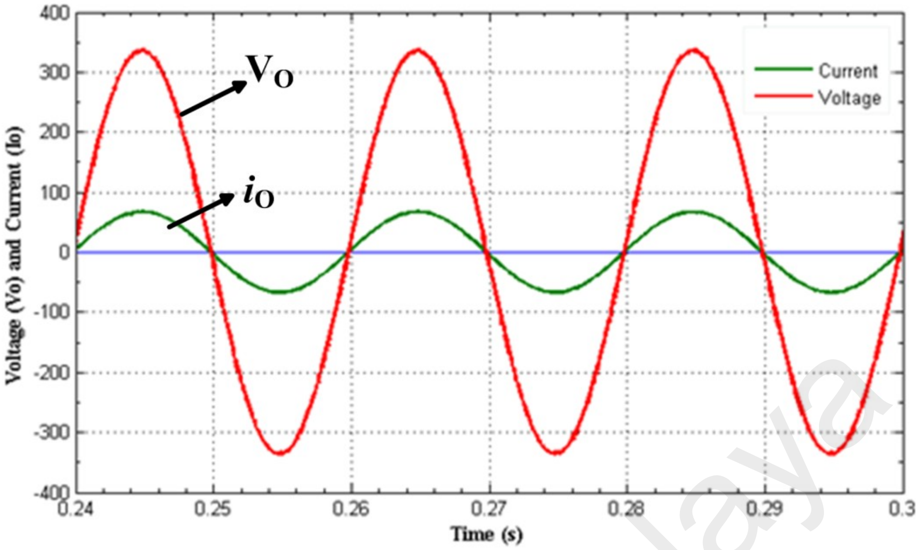

(a). Linear Load (V_O : 100V/div; i_O : 10A/div; Time : 0.01s/div)

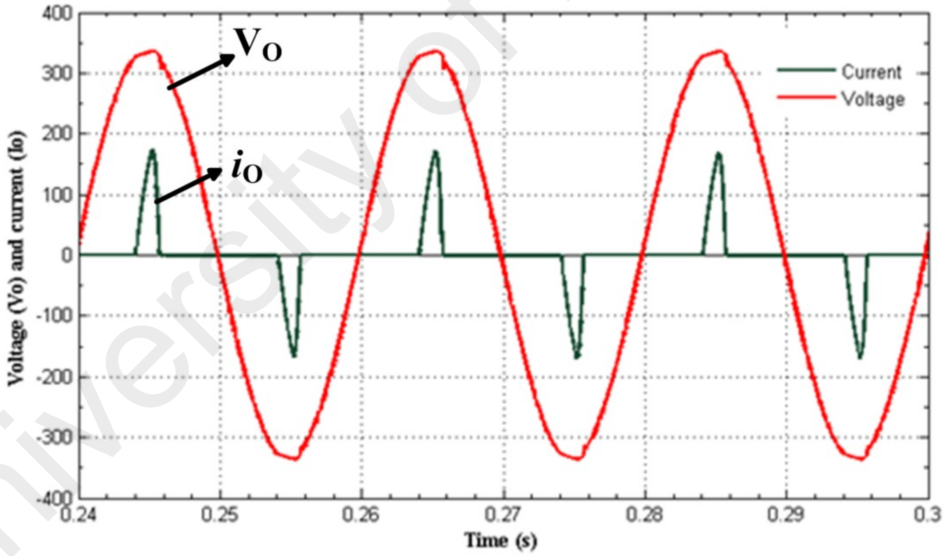

(b). Non-linear load (V_O : 100V/div; i_O : 10A/div; Time : 0.01s/div)

Figure 5.1 Simulation waveform of output voltage and output current for linear and non-linear load

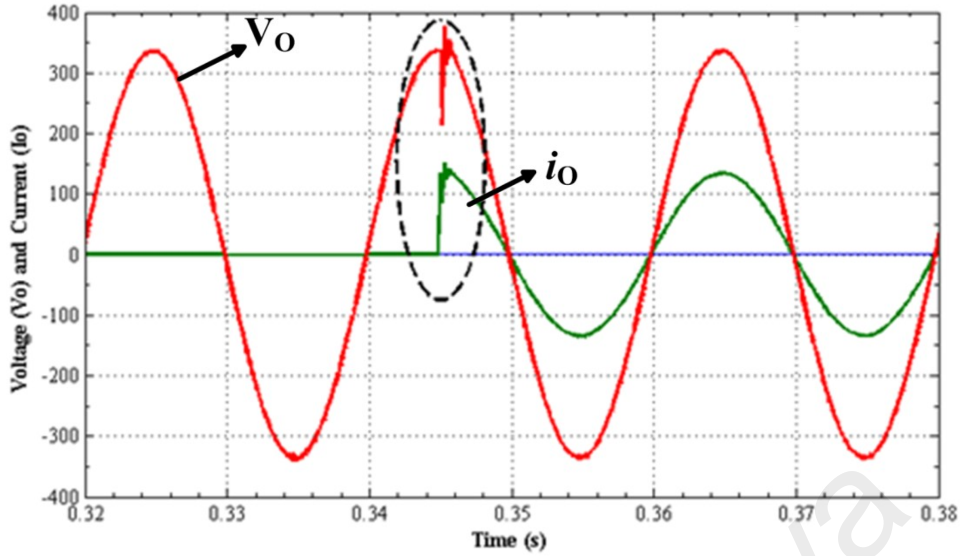

(a). Step response from 0 to 100% (V_O : 100V/div; i_O : 5A/div; Time : 0.01s/div)

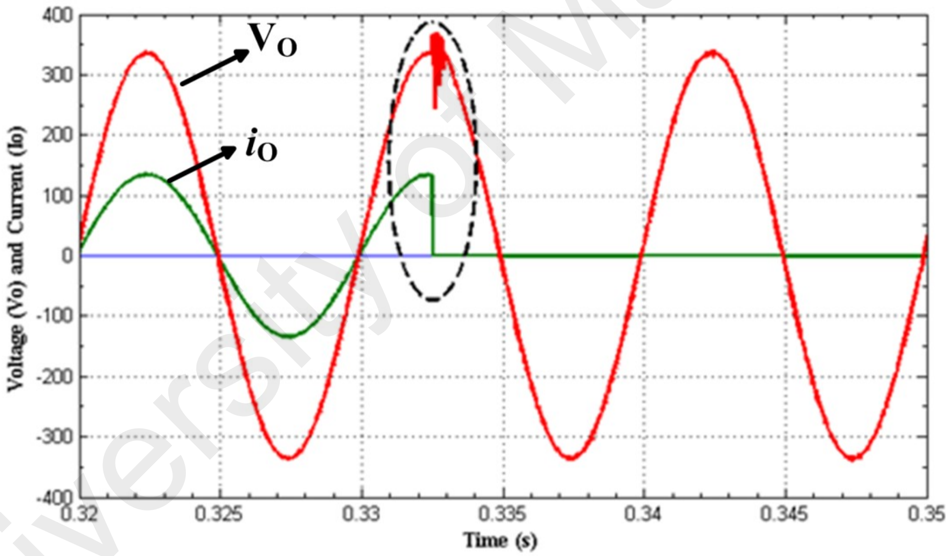

(b). Step response from 100 to 0% (V_O : 100V/div; i_O : 5A/div; Time : 0.01s/div)

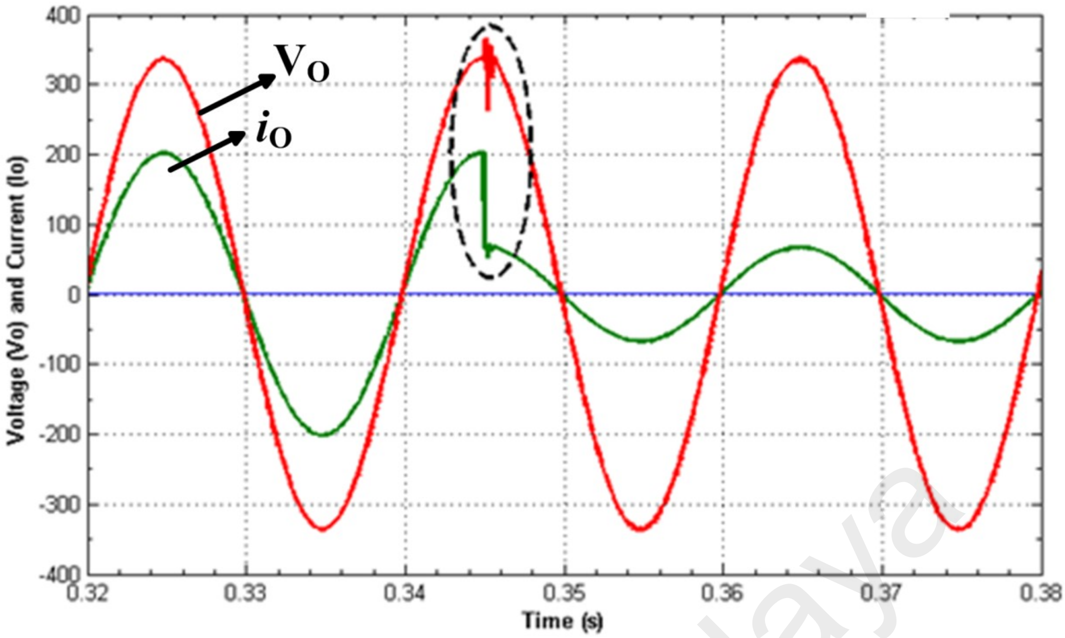

(c). Step response from100 to 30% (V_O : 100V/div; i_O : 5A/div; Time : 0.01s/div)

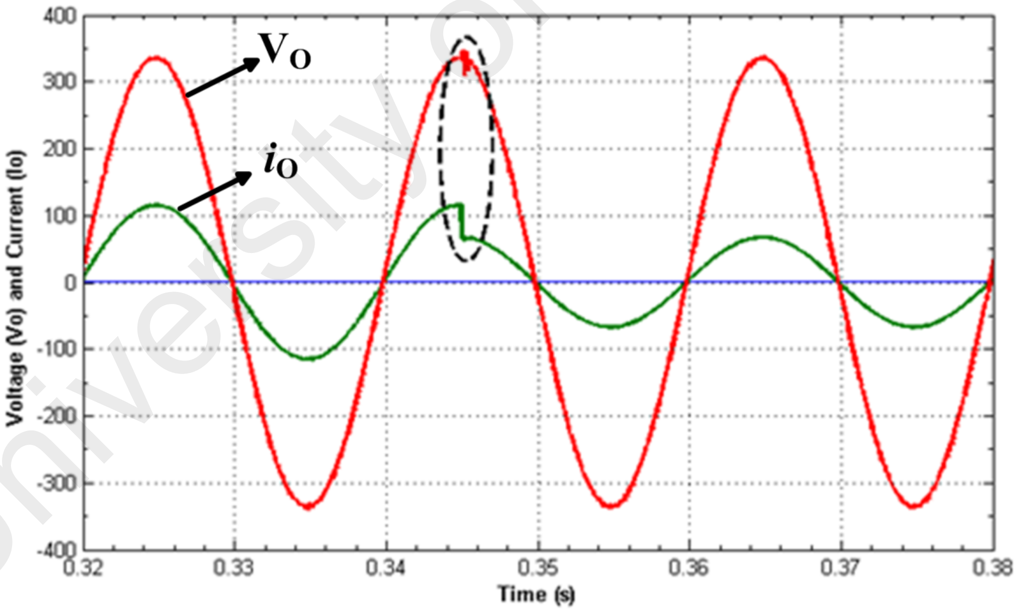

(d). Step response from 100 to 60%(V_O : 100V/div; i_O : 5A/div; Time : 0.01s/div)

Figure 5.2: Simulation waveform of step response of the inverter

A 1kVA prototype has been built to validate the performance of the proposed control scheme for single phase inverter. The output voltage and current waveform for both linear and non-linear load is shown in Figure 5.3 and Figure 5.4 respectively. The THD of the output voltage is about 0.45%, similar with the results obtained in simulation. Similarly, the THD of the output voltage is only 1.25% for non-linear load. It can be seen from these results that the THD of the output voltage is very low even for severe operating condition. The crest factor of the output voltage for the non-linear load is 1.7. The THD of the UPS output voltages shown in Figure 5.5 and Figure 5.6 are well below the limits of IEC 62040-3. Hence, the simulation as well as the experimental results validates the performance of the cascaded combination of slide mode and proportional resonant control schemes. The THD measurements are taken by Yokogawa WT1800 Precision Power Analyzer. Figure 5.7 shows the comparison of the THD between Slide Mode Control (SMC) and cascaded Proportional-Resonant (PR) Slide Mode Control. There is significant improvement in the THD for the cascaded PR and SMS controller, with the reduction of the THD to about 0.8% for linear load and 0.6% for non-linear loads.

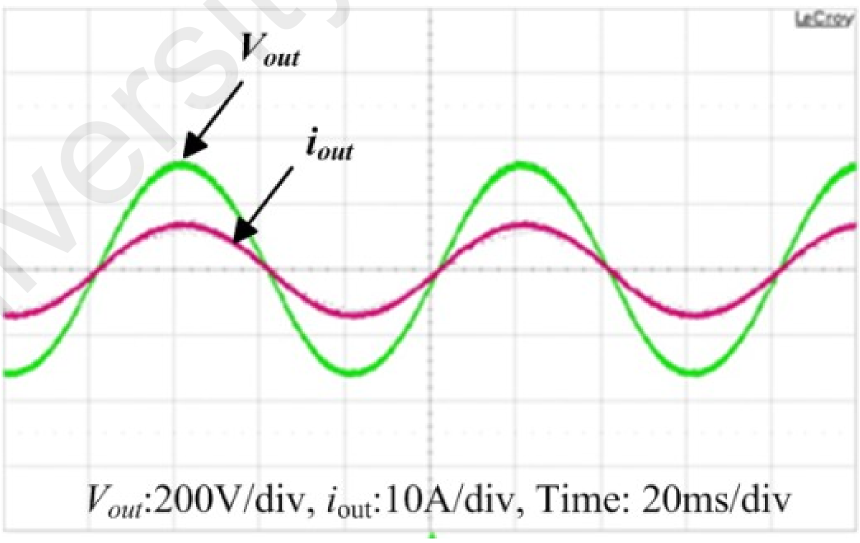

Figure 5.3: Output Voltage and Current for linear load

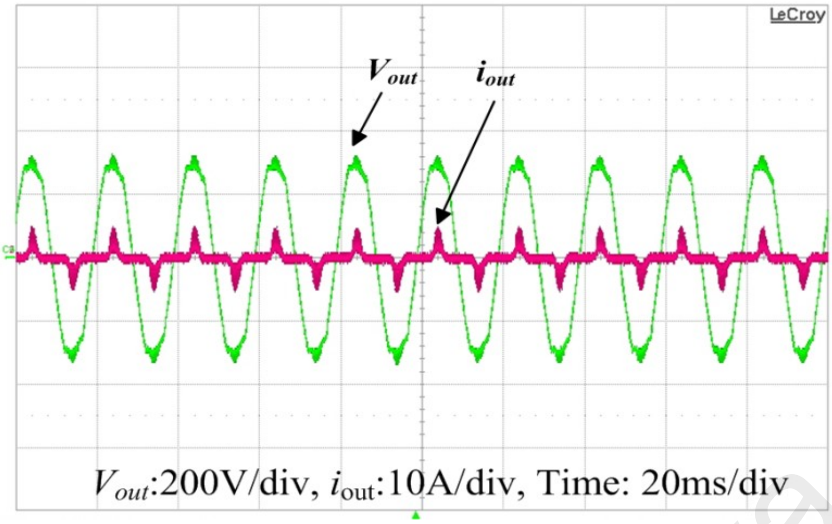

Figure 5.4: Output Voltage and Current for Non-linear Load,

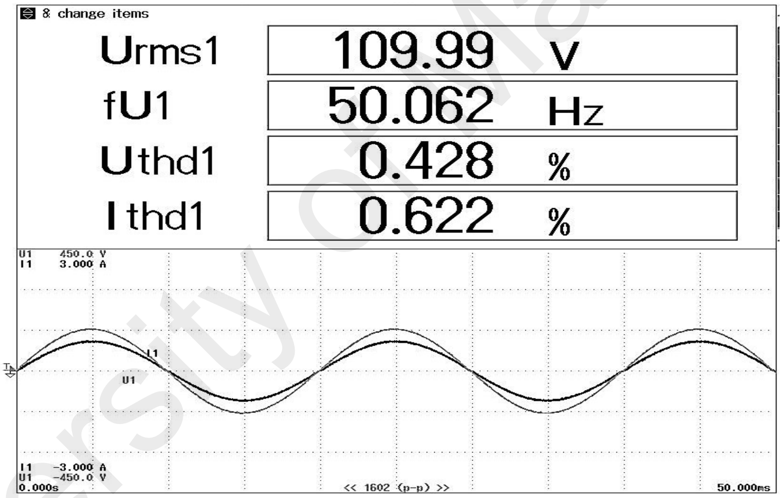

Figure 5.5: Experimental waveform of Output voltage and Current for resistive load

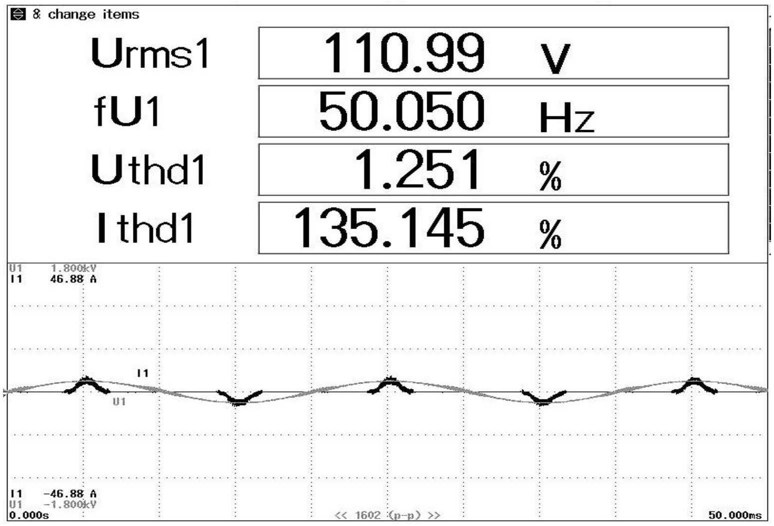

Figure 5.6: Experimental waveform of output voltage and current for the non-linear load

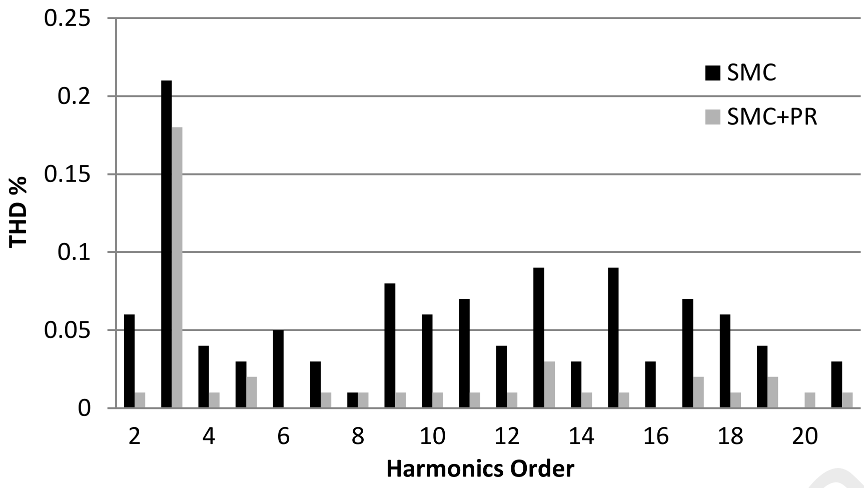

(a) Linear Load, (For SMC THD=1.1%), (SMC+PR THD=0.5%)

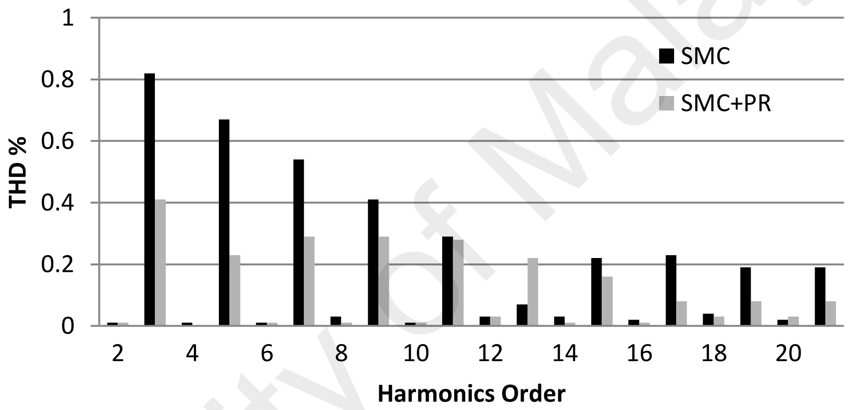

(b) Non-linear Load (For SMC THD=2.1%), (SMC+PR THD=1.25%)

Figure 5.7 Comparison of THD between SMC and SMC+PR

Transient Performance

In order to verify the transient performance of the inverter, the standard tests are carried out. Figure 5.8 shows the experimental waveform of the step change in load from 100 to 0% while Figure 5.9 shows the experimental waveform of step change from 0% to 100%. The settling time in both the case is less than 0.3ms. The experimental results are similar to the simulation results for different loading condition. Hence the simulation as well as the experimental results validates the performance of the proposed inverter control during changing transient conditions. The experimental results show that the dynamic behavior of the controller is satisfactory and is not exceeding the classification 1 of IEC62040-3 standard.

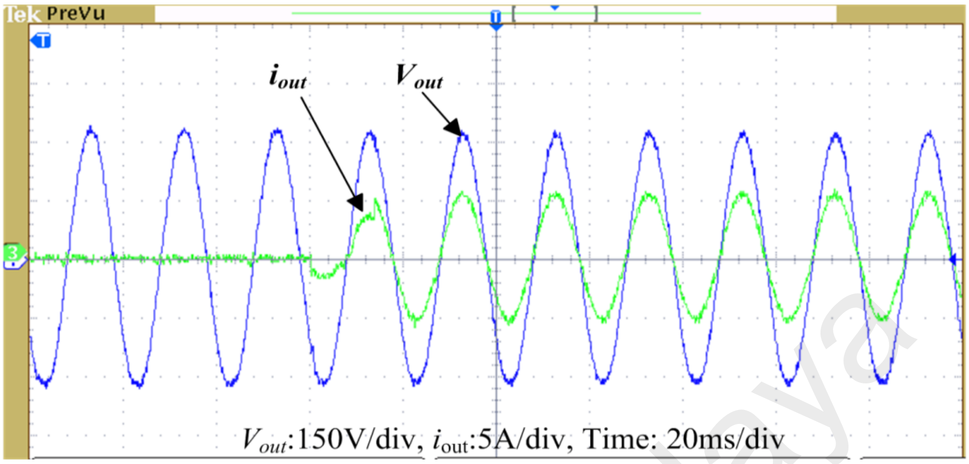

Figure 5.8 Experimental waveform of step change from 0% to 100%

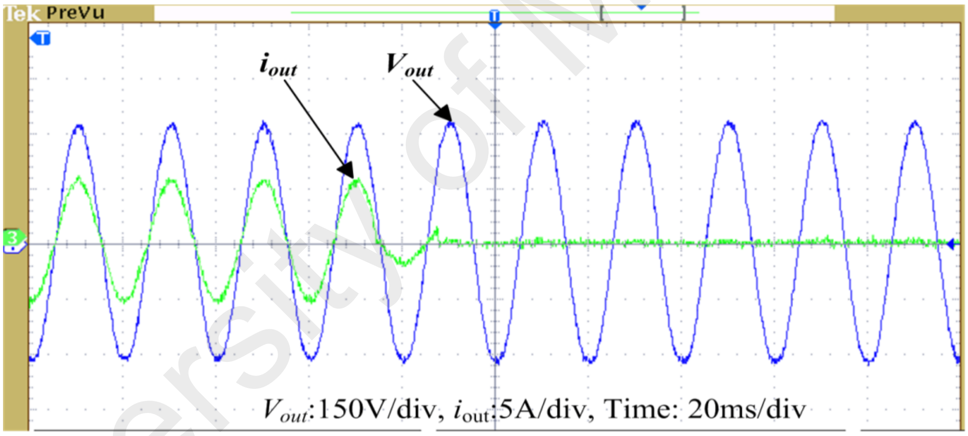

Figure 5.9 Experimental waveform of step change from 100% to 0

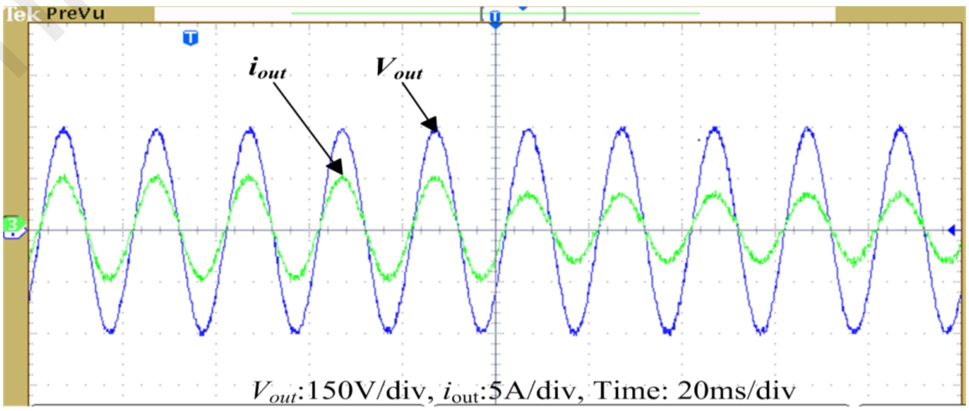

Figure 5.10 Experimental waveform of step change from 100% to 60%

5.4 Bidirectional battery charger/discharger

The specifications of the bidirectional DC-DC converter have been shown in Table 5.4 The prototype has been built to confirm the feasibility of the proposed battery charger/discharger. The circuit operated between DC-link V_{DC} = 360V and battery voltage V_{Bat} =24V. The switching frequency is 30 kHz. Coupled inductor is designed using PQ50-50 with magnetizing inductance of 107uH, and turns ratio N = 6 according to the design procedure explain in section 3.4.3. An inductor L_b has 300uH inductance, so the size is very small. Besides C_{b1} and C_{b2} consists of 4.4uF ceramic capacitors. The diodes D_{b1}, D_{b2}, and D_{bx} used are ultrafast recovery diodes UF5408. Thus all the axillary components are not adding considerable in the size of the circuit. The dead time between the switching PWM is 3us which helps in ZVS of the circuit.

Figure 5.11 shows the experimental waveforms of the battery charger/discharger during charging mode of operation of the proposed circuit. The voltage stress across both the switches S_3 is about 50V, which is quite small as compared to HVS (350V). Similarly, the voltage across the switch S_4 is less than 350V, which is the DC-link voltage of the circuit. The conduction current in the coupled inductor is smoothened. There is a voltage spike at the point of turn ON of the switches S_3 and S_4, however, this spike can easily be overcome by using passive snubber circuit. The snubber circuit can trim the voltage spikes, but the energy is wasted in the form of i^2R losses in the snubber circuit, reducing the efficiency of the circuit. Hence if the spikes are in the range of the selected switch ratings, the snubber circuit can be ignored.

Table 5.4 Specification of the Battery Charger/Discharger

Parameters	Symbol	Value
DC-link Voltage	V_{DC}	360V
Battery Bank Voltage	V_{Bat}	24V
Switching Frequency	f_{sw}	30 kHz
Coupled Inductor	L_P,L_S	Turns ratio N = 6; Magnetizing Inductor L_m = 107uH; PQ-5050 core;
Inductor	L_b	300uH
Capacitor	C_{b1}, C_{b2}	C_{b1}, C_{b2} = 2×2.2uF (ceramic), C_d = 1900uF
Switches	S_3 ,S_4, S_{ax}	IPW60R045CP MOSFET
Diodes	D_{b1} , D_{b2}, D_{b3}	Ultrafast Recovery diode UF5408
Power rating	Po	1.2 kW

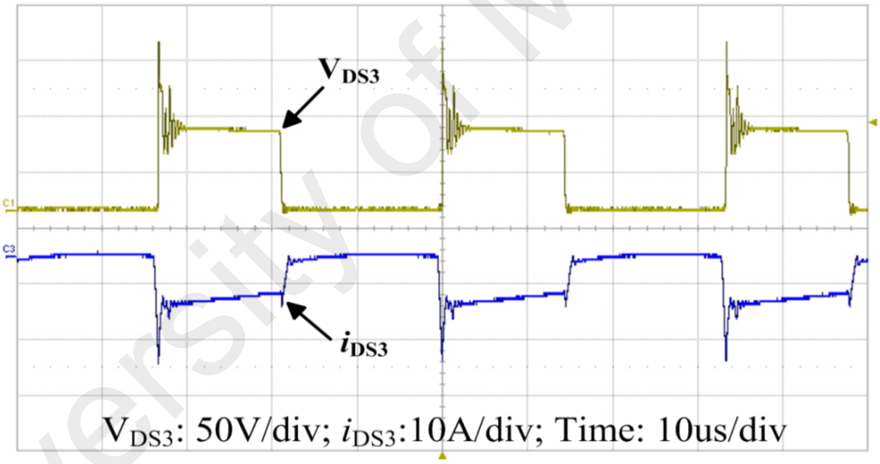

(a). Drain to Source voltage and current of Switch S_3

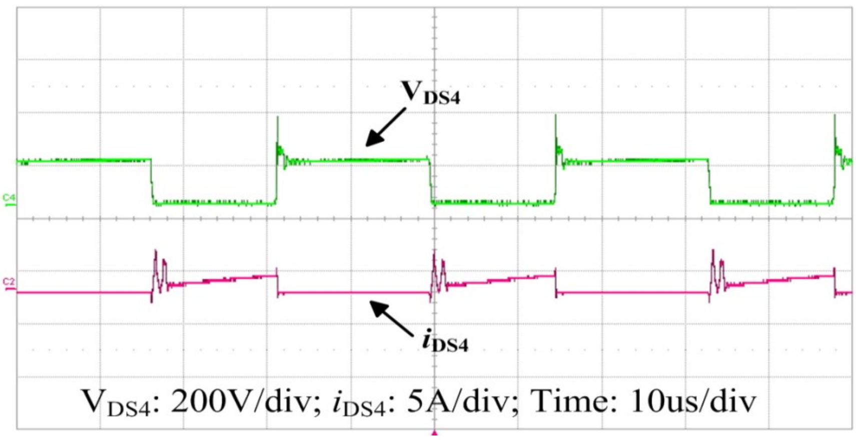

(b). Drain to Source voltage and current of Switch S_4

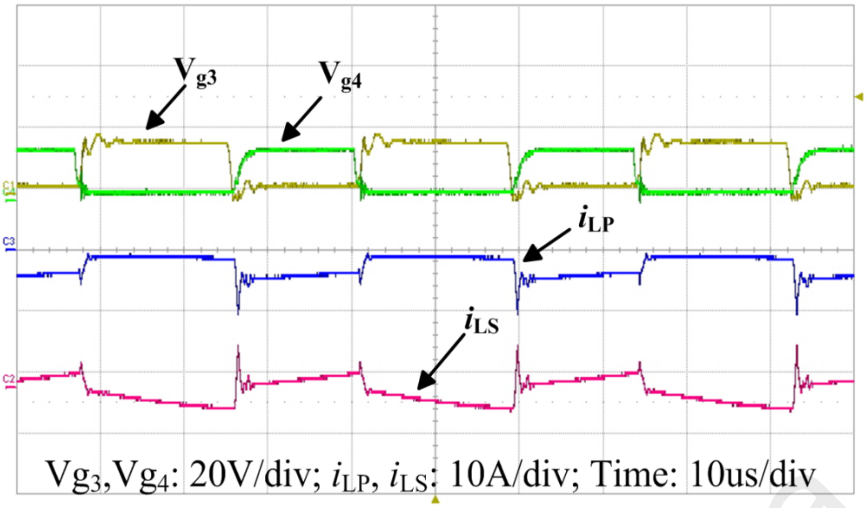

(c). Gate voltage of switch S_3 and S_4, primary and seconday inductor current

Figure 5.11: Experimental waveform of bidirectional converter during buck mode

Similarly, the battery charger/discharger operation during discharging mode (or boost mode) is shown in Figure 5.12. All the switches are operating under zero voltage switching condition. The voltage stress across the switches is less than the DC-link voltage of the system.

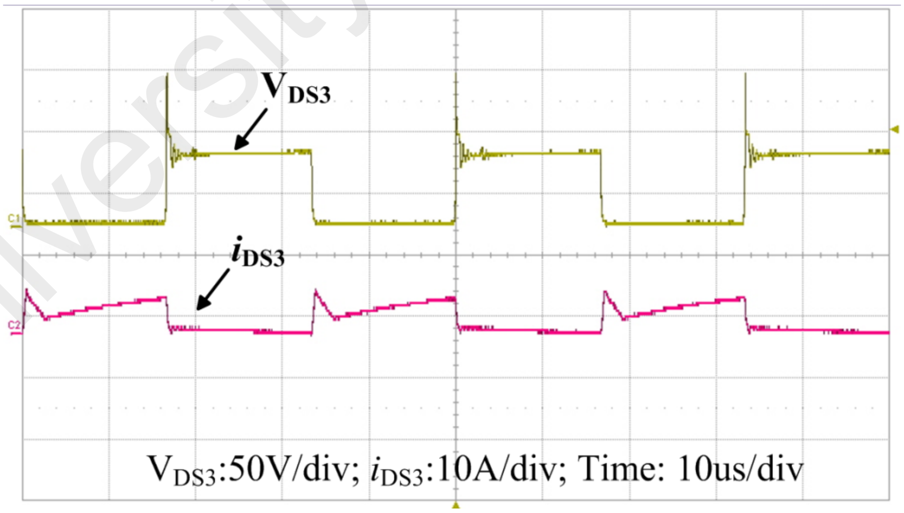

(a). Drain to source voltage and current of switch S_3

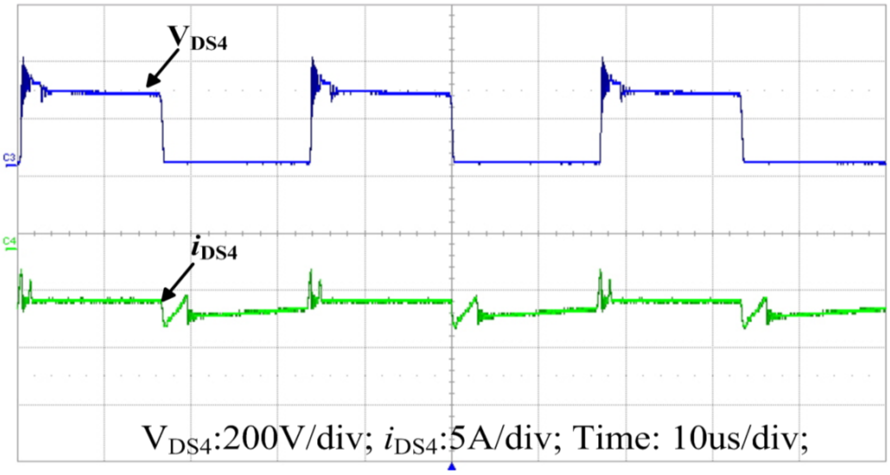

(b). Drain to source voltage and current of switch S_4

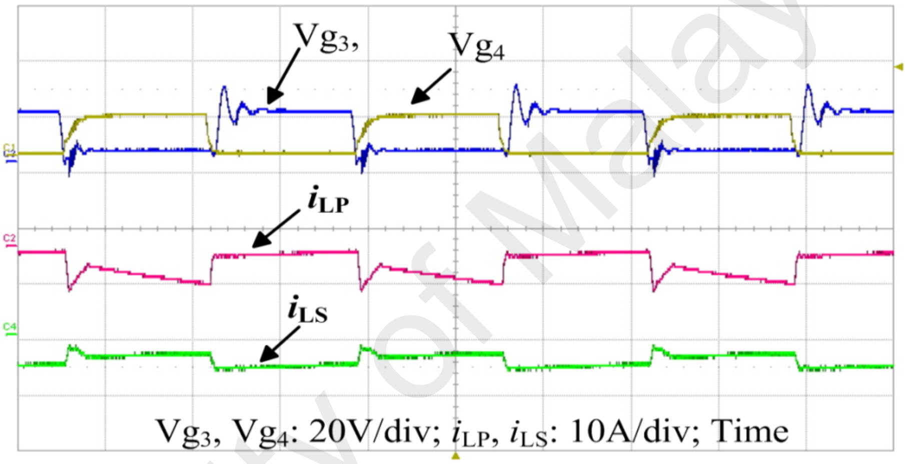

(c). Gate voltage of switch S_3 and S_4, primary and seconday inductor current

Figure 5.12 Experimental waveform of bidirectional converter during boost mode

Figure 5.13 shows the zero voltage switching condition in switch S_3 during buck mode of operation. The ZVS helps in reducing the switching losses and increases the efficieency of the system.

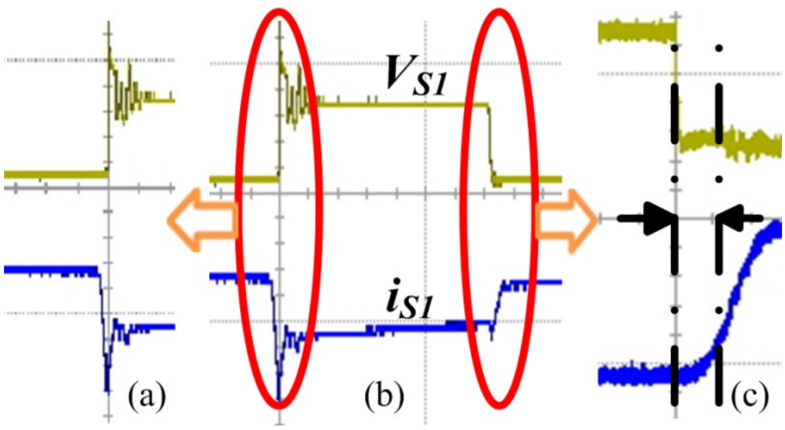

Figure 5.13 ZVS of the switch S_3 during buck mode

5.5 Power Factor Correction (PFC) Rectifier

The specifications of the rectifier is shown in Table 5.5. The utility input voltage and current waveform in Normal mode of operation are shown in the Figure 5.14. The Input current waveform is very close to the sinusoidal and has almost unity power factor.

Table 5.5: Specifications of the Rectifier

Parameters	Symbol	Value
Input Inductor	L_{11}, L_{12}	800 uH, Coupled Torid
Diodes	D_1, D_2	BYC10-600
Switches	S_1, S_2	SPP11N60C3
Slow Diodes	D_a, D_b	GBJ1508
Switching frequency	f_{sw}	30 kHz
Power rating	Po	1.2kVA

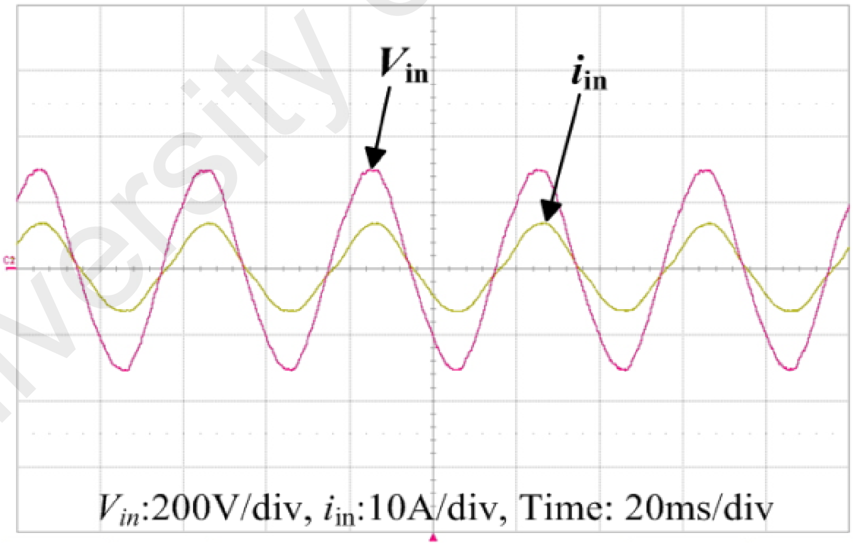

Figure 5.14 Experimental waveforms of input voltage and current

5.6 Transformerless UPS system

When the grid power is interrupted, and the system switches from normal mode to battery mode. The rectifier is no more in operation, and the battery charger/discharger operates in discharging mode giving regulated DC-link voltage. The transient effect in the output voltage is very small, and the UPS system provides uninterruptible power to the load as shown in Figure 5.15. Similarly, the transition from battery mode back to normal mode upon the restoration of the grid power is shown in Figure 5.16. Simple RC snubber has been used to discharge the inductors L_{11} and L_{12}, preventing the overvoltage spike when the MC opens. The THD and the power factor remains the same during both the grid and battery powered mode, which is the important feature of the online UPS system.

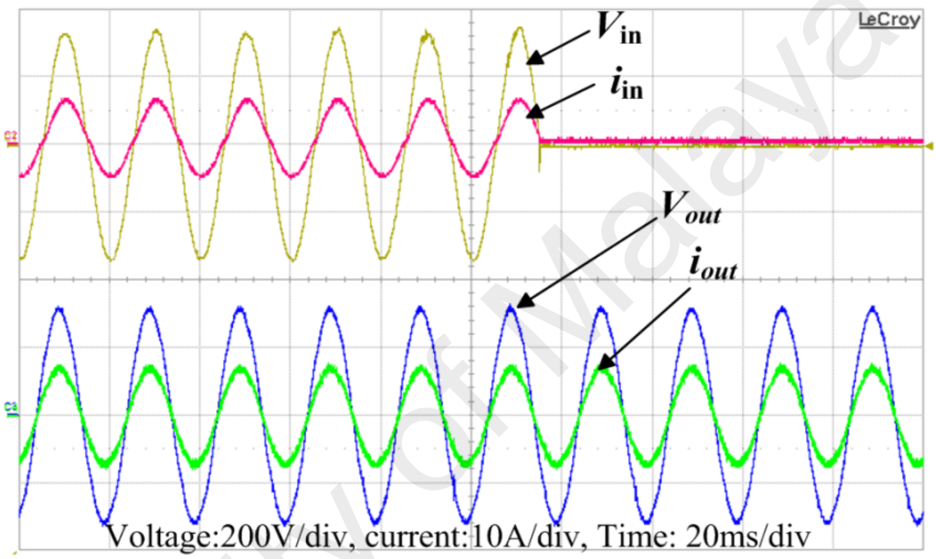

Figure 5.15 Transition from Normal to Battery Powered Mode. Input Voltage V_{in} and Current I_{in}, Output Voltage Vout and Current I_{out}

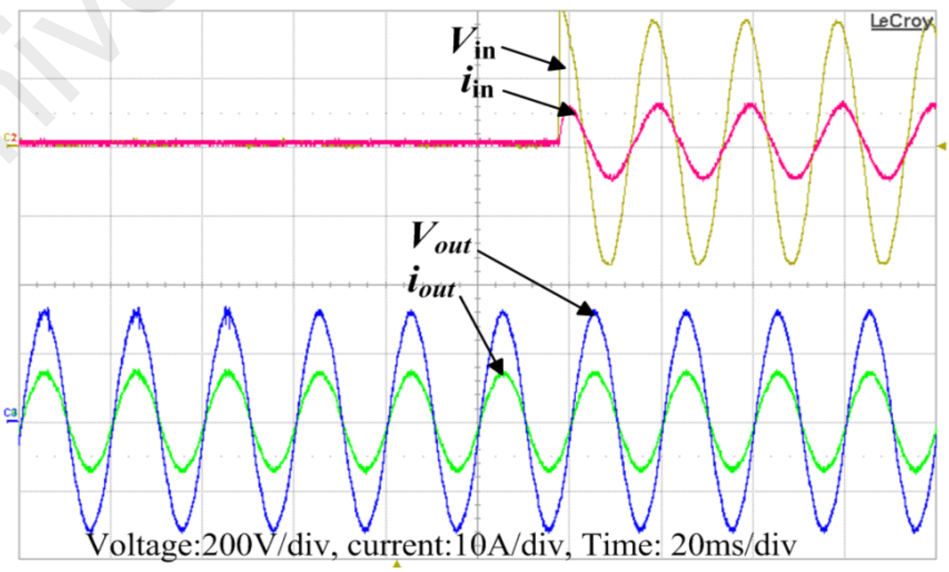

Figure 5.16 Transition from Battery power mode to Normal mode, Input Voltage V_{in} and Current I_{in}, Output Voltage V_{out} and Current I_{out}

Figure 5.17 shows the image of prototype and the experimental setup. Figure 5.18 shows the efficiency graph with maximum efficiency of 94% during battery mode and 92% during the normal mode of operation. Thus utilizing soft switching in bidirectional converter reduces the switch losses and increases the efficiency of the system. The efficiency in battery mode is high as compared to normal mode because less number of power stages are operation during this mode. The efficiency is marginally less for the transformerless system, due to high battery charging current.

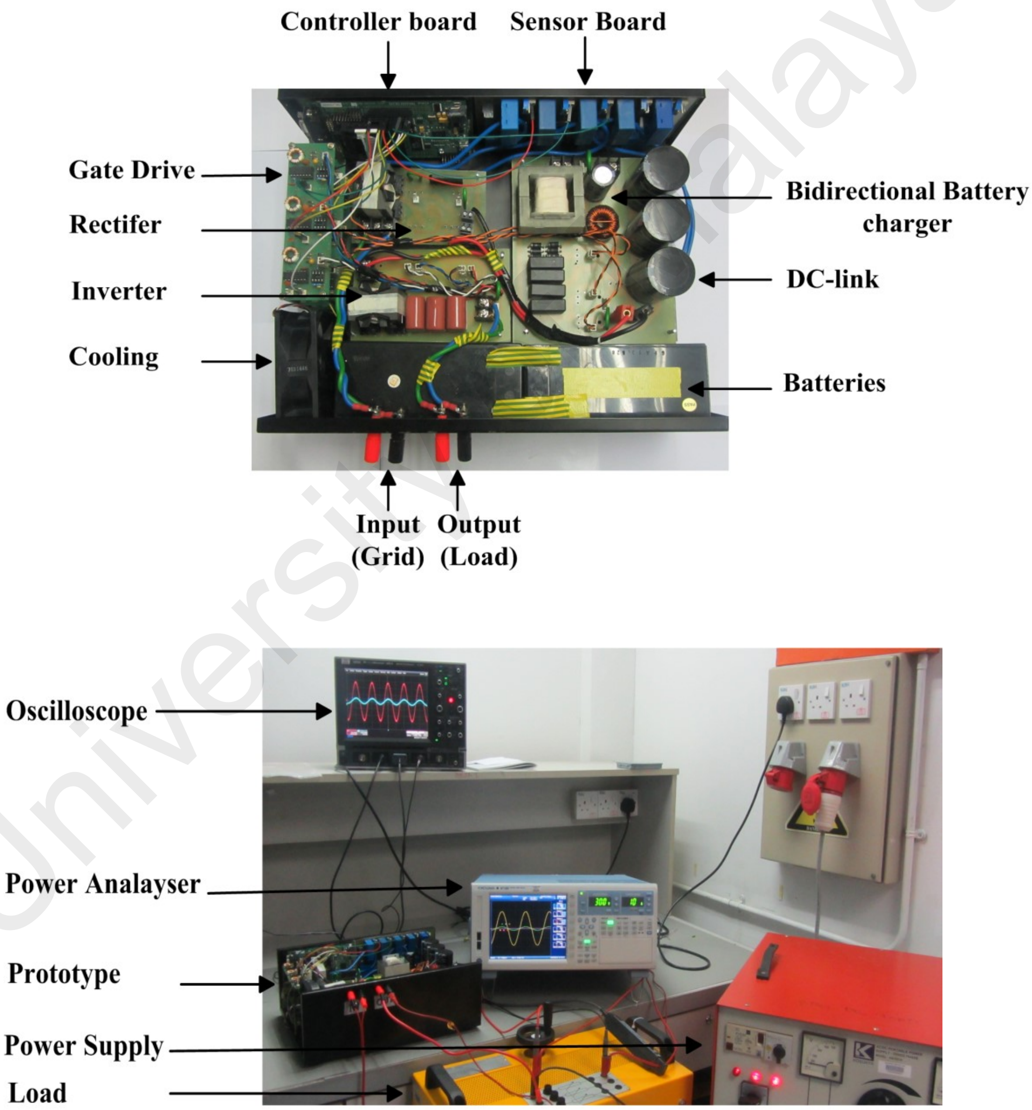

Figure 5.17 Prototype image and experimental setup

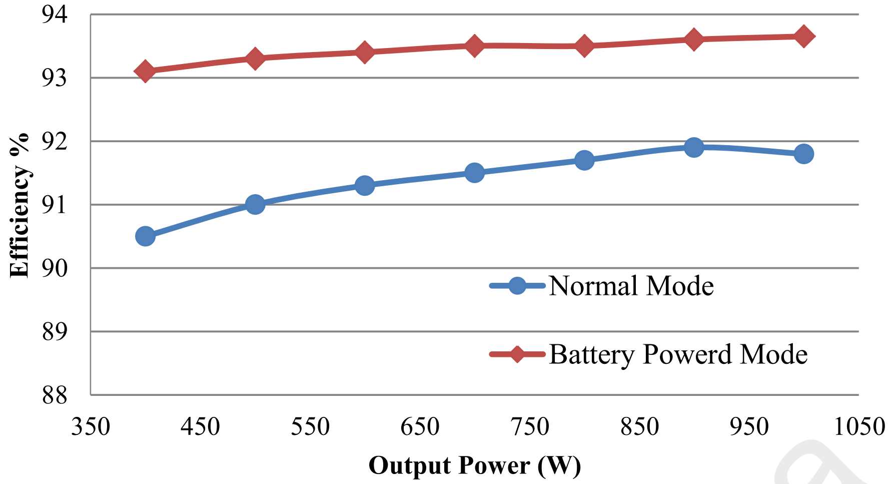

Figure 5.18 Efficiency graph in normal and battery powered mode

Table 5.6 shows the comparison of the proposed UPS system with other transformerless UPS system. The size and weight of the system has been determined by the number of components used in the system for example switches, diodes, capacitors, inductor, coupled inductor, and battery bank. The overall efficiency of the transformerless UPS is higher compared to the transformer based. The UPS proposed by (J. K. Park et al., 2008) claims very high efficiency of 96%. However, this high efficiency is achieved because a conventional battery charger/discharger is used in this circuit. The voltage gain of conventional battery charger/discharger is very low. Hence a huge battery bank is required in this system. This increases the size, weight, and reduces the reliability of the system. The (C. G. C. Branco et al., 2008) proposed system, which has reasonable small battery bank voltage requirement. However, an autotransformer is introduced into the system to get two different output voltages (110/220), which cost the efficiency reduction of the system. The proposed UPS shows the distinct improvement in system efficiency, battery bank requirement, and volumetric size of the system. The battery bank voltage is reduced to only 24 V. Hence, the UPS backup time is only dependent on the parallel connection of the batteries, which increase the reliability and reduce the volumetric size and weight of the system. The efficiency of the system is reasonably good and is about 92% during grid mode of operation. In grid mode of operation, all the three power parts i.e. Rectifier, Battery charger/discharger, and Inverter are active. However, the efficiency increase to about 94% during battery mode, as the rectifier is no more in operation in battery mode of the system.

Table 5.6 Comparison of Transformerless UPS

Properties / UPS Topology	Efficiency	Power Ratings	System Specification	Battery bank	Size & Weight
Transformer-less offline UPS system (Marei et al., 2011)	High	1kVA	220V	144V	Medium
A reconfigurable UPS for Multiple Power Quality(Yeh & Manjrekar, 2007)	High	1kVA	110V	300V	-
Transformer-less Online UPS System(J. K. Park et al., 2008)	96%	3kVA	220V	192V	Smaller
Non-isolated UPS with 110/220 V input –output voltage (C. G. C. Branco et al., 2008)	86%	2.6kVA	Both 110V & 220V	108V	Medium
Z Source Inverter Based UPS System(K. L. Zhou et al., 2009)	>90%	3kVA	220V	360V	Smaller
Proposed UPS system	**92%**	**1kVA**	**220V**	**24V**	**Smallest**

5.7 Summary

This chapter explains the hardware realization of the proposed transformerless UPS system. Experimental results of each power stage of the UPS system have been explained. The cascaded Proportional-Resonant and Slide Mode Control for the UPS inverter show excellent performance by reducing the THD to 0.5% and 1.25 for linear and non- linear load respectively. All the switches of the battery charger/discharger operate under zero voltage switching condition increasing the efficiency of the system. The overall UPS system performance has been analyzed specially during change of modes from grid to battery and vice versa. The transition between the UPS operation modes is very smooth without any transients or spikes in the system. Comparison of the proposed system with the other transformerless UPS system shows considerable improvement in terms of efficiency, reliability, and size and weight of the system.

CHAPTER 6: CONCLUSION AND FUTURE WORK

6.1 Conclusion

A single-phase transformerless online uninterruptible power supply (UPS) has been proposed in this study. The proposed UPS system consists of three major parts; a bridgeless Power factor correction (PFC) rectifier, bidirectional battery charger/discharger, and an inverter. All the three parts have been designed, developed, and analyzed. Experimentally performance of each power part as well as the complete UPS has been investigated. The UPS operates very well in grid and battery mode of operations.

A bridgeless boost rectifier has been used at the front end of the UPS that increases the efficiency of the system and provides efficient PFC regulation. The average current control scheme is employed to regulate the DC-link voltage and performs PFC. A new bidirectional converter for battery charging/discharging has been implemented, which ensures transformerless operation of the UPS. The high voltage gain for both boost and buck operation allows the UPS to reduce the battery bank significantly. The most promising features of the bidirectional converter are high voltage conversion ratio in both modes of operation, fewer numbers of active switches, and low voltage & current stress across the switches. All the switches operating under zero voltage switching condition. This helps in reducing the switching losses and improves the efficiency of the system.

A new control technique for the inverter has been implemented by cascading the slide mode control (SMC) and proportional-resonant control (PR), which provides a regulated sinusoidal output voltage with low THD for both linear and non-linear load. The proposed controller has fast transient response and shows excellent performance against step change in the load condition.

The overall UPS system has been designed, and the performance has been analyzed. The volumetric size of the UPS is minimized by removing the bulky transformer and reducing the voltage of the battery bank. The experimental results show good dynamic and steady-state performance of the system. The efficiency of the proposed UPS system is 94% during battery mode and 92% during the normal mode of operation. The proposed UPS is suitable of low power applications like single computer server, medical equipment, communication devices, etc. It may be recommended to extend this proposed UPS system to three-phase transformerless online UPS system.

6.2 Future Work

Evaluating the observations and findings from this study, the future research can be concentrated on the following points.

1. The proposed idea of single phase transformerless online UPS system can be implemented in three-phase network and the features of the proposed topology can be analyzed for high power applications. This includes the development of three-phase rectifier and three-phase inverter with advance non-linear control of the inverter.
2. The DC-transformerless online UPS can be implemented for the DC grid system. Removing the rectifier stage and optimizing the design for battery charging and discharging stage and the AC/DC inverter constitute the DC-UPS system.
3. Addition of the parallel renewable-energy resources and fuel cell with the battery bank to increase the reliability and add the renewable energy into the system.

REFERENCES

Abdel-Rahim, N. M., & Quaicoe, J. E. (1996). Analysis and design of a multiple feedback loop control strategy for single-phase voltage-source UPS inverters. *IEEE transactions on power electronics, 11*(4), 532-541.

Abrishamifar, A., Ahmad, A. A., & Mohamadian, M. (2012). Fixed Switching Frequency Sliding Mode Control for Single-Phase Unipolar Inverters. *IEEE transactions on power electronics, 27*(5), 2507-2514.

Batarseh, I. (2004). *Power electronic circuits*: John Wiley.

Bekiarov, S. B., & Emadi, A. (2002). *Uninterruptible power supplies: classification, operation, dynamics, and control.* Paper presented at the Seventeenth Annual IEEE Applied Power Electronics Conference and Exposition, APEC 2002. .

Bode, G. H., Loh, P. C., Newman, M. J., & Holmes, D. G. (2005). An improved robust predictive current regulation algorithm. *IEEE Transactions on Industry Applications, 41*(6), 1720-1733.

Botteron, F., & Pinheiro, H. (2007). A three-phase UPS that complies with the standard IEC 62040-3. *IEEE Transactions on Industrial Electronics, 54*(4), 2120-2136.

Branco, C. G., Cruz, C. M., Torrico-Bascopé, R. P., Antunes, F. L., & Barreto, L. H. (2006). *A transformerless single phase on-line UPS with 110 V/220 V input output voltage.* Paper presented at the Twenty-First Annual IEEE Applied Power Electronics Conference and Exposition, APEC'06.

Branco, C. G. C., Cruz, C. M. T., Torrico-Bascope, R. P., & Antunes, F. L. M. (2008). A nonisolated single-phase UPS topology with 110-V/220-V input-output voltage ratings. *IEEE Transactions on Industrial Electronics, 55*(8), 2974-2983.

Business Case for PQ Investment by Commercial Buildings. (2014). Retrieved from http://apqi.org/beta/business-case-for-pq-investment-by-commercial-buildings/

Buso, S., Fasolo, S., & Mattavelli, P. (2001). Uninterruptible power supply multiloop control employing digital predictive voltage and current regulators. *IEEE Transactions on Industry Applications, 37*(6), 1846-1854.

Carpita, M., & Marchesoni, M. (1996). Experimental study of a power conditioning system using sliding mode control. *IEEE transactions on power electronics, 11*(5), 731-742.

Chen, D., Zhang, J. M., & Qian, Z. M. (2013). An Improved Repetitive Control Scheme for Grid-Connected Inverter With Frequency-Adaptive Capability. *IEEE Transactions on Industrial Electronics, 60*(2), 814-823.

Chen, S., Lai, Y., Tan, S.-C., & Tse, C. K. (2008). Analysis and design of repetitive controller for harmonic elimination in PWM voltage source inverter systems. *IET Power Electronics, 1*(4), 497-506.

Chiang, S., Lee, T.-S., & Chang, J. (2000). *Design and implementation of a single phase three-arms rectifier inverter.* Paper presented at the IEE Proceedings Electric Power Applications,.

Chiang, S., Tai, T., & Lee, T.-S. (1998). *Variable structure control of UPS inverters.* Paper presented at the IEE Proceedings Electric Power Applications, .

China Uninterruptible Power System UPS Industry. (2014). from http://www.prnewswire.com/news-releases/china-uninterruptible-power-system-ups-industry-report-2014-2017-300077021.html

Choi, J.-H., Kwon, J.-M., Jung, J.-H., & Kwon, B.-H. (2005). High-performance online UPS using three-leg-type converter. *IEEE Transactions on Industrial Electronics, 52*(3), 889-897.

Choi, W.-Y., Kwon, J.-M., & Kwon, B.-H. (2008). Bridgeless dual-boost rectifier with reduced diode reverse-recovery problems for power-factor correction. *IET Power Electronics,, 1*(2), 194-202.

Cortes, P., Kazmierkowski, M. P., Kennel, R. M., Quevedo, D. E., & Rodriguez, J. (2008). Predictive Control in Power Electronics and Drives. *IEEE Transactions on Industrial Electronics, 55*(12), 4312-4324.

Cortes, P., Ortiz, G., Yuz, J. I., Rodriguez, J., Vazquez, S., & Franquelo, L. G. (2009). Model Predictive Control of an Inverter With Output LC Filter for UPS Applications. *IEEE Transactions on Industrial Electronics, 56*(6), 1875-1883.

Das, P., Laan, B., Mousavi, S. A., & Moschopoulos, G. (2009). A Nonisolated Bidirectional ZVS-PWM Active Clamped DC-DC Converter. *IEEE transactions on power electronics, 24*(1-2), 553-558.

Daud, M. Z., Mohamed, A., & Hannan, M. (2013). An improved control method of battery energy storage system for hourly dispatch of photovoltaic power sources. *Energy Conversion and Management, 73*, 256-270.

De, D., & Ramanarayanan, V. (2010). A Proportional plus Multiresonant Controller for Three-Phase Four-Wire High-Frequency Link Inverter. *IEEE transactions on power electronics, 25*(4), 899-906.

Deng, H., Oruganti, R., & Srinivasan, D. (2005). *Modeling and control of single-phase UPS inverters: a survey.* Paper presented at the International Conference on Power Electronics and Drives Systems, PEDS.

Deng, H., Oruganti, R., & Srinivasan, D. (2007). Analysis and design of iterative learning control strategies for UPS inverters. *IEEE Transactions on Industrial Electronics, 54*(3), 1739-1751.

Deng, H., Oruganti, R., & Srinivasan, D. (2008). Neural controller for UPS inverters based on B-spline network. *IEEE Transactions on Industrial Electronics, 55*(2), 899-909.

Divan, D. (1989). *A new topology for single phase UPS systems.* Paper presented at the Conference Record of the 1989 IEEE Industry Applications Society Annual Meeting.

Do, T. D., Leu, V. Q., Choi, Y. S., Choi, H. H., & Jung, J. W. (2013). An Adaptive Voltage Control Strategy of Three-Phase Inverter for Stand-Alone Distributed Generation Systems. *IEEE Transactions on Industrial Electronics, 60*(12), 5660-5672.

Duan, R. Y., & Lee, J. D. (2012). High-efficiency bidirectional DC-DC converter with coupled inductor. *IET Power Electronics, 5*(1), 115-123.

El Fadil, H., & Giri, F. (2008). *Reducing chattering phenomenon in sliding mode control of Buck-Boost power converters.* Paper presented at the IEEE International Symposium on Industrial Electronics, ISIE.

Emadi, A., Nasiri, A., & Bekiarov, S. B. (2004). *Uninterruptible power supplies and active filters*: CRC press.

Erickson, R. W., & Maksimovic, D. (2001). *Fundamentals of power electronics*: Springer Science & Business Media.

Escobar, G., Mattavelli, P., Stankovic, A. M., Valdez, A. A., & Leyva-Ramos, J. (2007). An adaptive control for UPS to compensate unbalance and harmonic distortion using a combined capacitor/load current sensing. *IEEE Transactions on Industrial Electronics, 54*(2), 839-847.

Fu-Sheng, P., & Shyh-Jier, H. (2006). A novel design of line-interactive uninterruptible power supplies without load current sensors. *IEEE transactions on power electronics, 21*(1), 202-210.

Fukuda, S., & Imamura, R. (2005). Application of a sinusoidal internal model to current control of three-phase utility-interface converters. *IEEE Transactions on Industrial Electronics, 52*(2), 420-426.

Gudey, S. K., & Gupta, R. (2014). Sliding-mode control in voltage source inverter-based higher-order circuits. *International Journal of Electronics*(ahead-of-print), 1-22.

Gurrero, J., De Vicuna, L. G., & Uceda, J. (2007). Uninterruptible power supply systems provide protection. *IEEE Industrial Electronics Magazine, 1*(1), 28-38.

Han, S., & Divan, D. (2008). *Bi-directional DC/DC converters for plug-in hybrid electric vehicle (PHEV) applications.* Paper presented at the Twenty-Third Annual IEEE Applied Power Electronics Conference and Exposition, APEC.

Haneyoshi, T., Kawamura, A., & Hoft, R. G. (1988). Waveform Compensation of Pwm Inverter with Cyclic Fluctuating Loads. *IEEE Transactions on Industry Applications, 24*(4), 582-589.

Hang, C. C., Astrom, K. J., & Ho, W. K. (1991). Refinements of the Ziegler-Nichols tuning formula. *IEE Proceedings D - Control Theory and Applications, 138*(2), 111-118.

Hao, X., Yang, X., Liu, T., Huang, L., & Chen, W. J. (2013). A Sliding-Mode Controller With Multiresonant Sliding Surface for Single-Phase Grid-Connected VSI With an LCL Filter. *IEEE transactions on power electronics, 28*(5), 2259-2268.

Hegazy, O., Barrero, R., Van Mierlo, J., Lataire, P., Omar, N., & Coosemans, T. (2013). An Advanced Power Electronics Interface for Electric Vehicles Applications. *IEEE transactions on power electronics, 28*(12), 5508-5521.

Hirachi, K., Sakane, M., Niwa, S., & Matsui, T. (1994). *Development of UPS using new type of circuits.* Paper presented at the 16th International.Telecommunications Energy Conference, 1994. INTELEC'94.

Hirachi, K., Yoshitsugu, J., Nishimura, K., Chibani, A., & Nakaoka, M. (1997). *Switched-mode PFC rectifier with high-frequency transformer link for high-power density single phase UPS.* Paper presented at the 28th Annual IEEE Power Electronics Specialists Conference, 1997. PESC'97 Record.

Holmes, D. G., Lipo, T. A., McGrath, B. P., & Kong, W. Y. (2009). Optimized Design of Stationary Frame Three Phase AC Current Regulators. *IEEE transactions on power electronics, 24*(11), 2417-2426.

Holtz, J., Lotzkat, W., & Werner, K.-H. (1988). A high-power multitransistor-inverter uninterruptable power supply system. *Power Electronics, IEEE Transactions on, 3*(3), 278-285.

Hsieh, Y.-P., Chen, J.-F., Yang, L.-S., Wu, C.-Y., & Liu, W.-S. (2014). High-conversion-ratio bidirectional dc–dc converter with coupled inductor. *IEEE Transactions on Industrial Electronics*(61), 210-222.

Jacobina, C. B., Oliveira, T. M., & da Silva, E. R. C. (2006). Control of the single-phase three-leg AC/AC converter. *IEEE Transactions on Industrial Electronics, 53*(2), 467-476.

Jain, P. K., Espinoza, J. R., & Jin, H. (1998). Performance of a single-stage UPS system for single-phase trapezoidal-shaped ac-voltage supplies. *IEEE transactions on power electronics, 13*(5), 912-923.

Jang, Y., & Jovanovic, M. M. (2009). A bridgeless PFC boost rectifier with optimized magnetic utilization. *IEEE Transactions on Power Electronics, 24*(1), 85-93.

Jung, S.-L., & Ying-Yu Tzou. (1997, Jun). *Multiloop control of an 1-phase PWM inverter for ac power source,.* Paper presented at the IEEE PESC Conf. Rec.

Kapat, S., Patra, A., & Banerjee, S. (2009). A Current-Controlled Tristate Boost Converter With Improved Performance Through RHP Zero Elimination. *IEEE transactions on power electronics, 24*(3-4), 776-786.

Karshenas, H., & Niroomand, M. (2005). *Design and implementation of a single phase inverter with sine wave tracking method for emergency power supply with high performance reference.* Paper presented at the Proceedings of the Eighth International Conference onElectrical Machines and Systems, ICEMS.

Karve, S. (2000). Three of a kind [UPS topologies, IEC standard]. *IEE Review, 46*(2), 27-31.

Kiehne, H. A. (2003). *Battery technology handbook* (Vol. 118): CRC Press.

Kim, E. H., Kwon, J. M., Park, J. K., & Kwon, B. H. (2008). Practical Control Implementation of a Three- to Single-Phase Online UPS. *IEEE Transactions on Industrial Electronics, 55*(8), 2933-2942.

Kim, I.-D., Paeng, S.-H., Ahn, J.-W., Nho, E.-C., & Ko, J.-S. (2007). *New bidirectional ZVS PWM sepic/zeta DC-DC converter.* Paper presented at the IEEE International Symposium on.Industrial Electronics, 2007. ISIE.

Kim, S.-K., Park, C. R., Yoon, T.-W., & Lee, Y. I. (2015). Disturbance-observer-based model predictive control for output voltage regulation of three-phase inverter for uninterruptible-power-supply applications. *European Journal of Control, 23*, 71-83.

King, A., & Knight, W. (2003). Uninterruptible Power Supplies and Standby Power Systems. *McGraw-Hill*.

Kley, J., Papafotiou, G., Papadopoulos, K., Bohren, P., & Morari, M. (2008). *Performance evaluation of model predictive direct torque control.* Paper presented at the IEEE Power Electronics Specialists Conference, PESC.

Koffler, R. (2003). Transformer or transformerless UPS? *Power Engineer, 17*(3), 34-36.

Komurcugil, H. (2010). *A new sliding mode control for single-phase UPS inverters based on rotating sliding surface.* Paper presented at the IEEE International Symposium on Industrial Electronics (ISIE),.

Komurcugil, H. (2012). Rotating-Sliding-Line-Based Sliding-Mode Control for Single-Phase UPS Inverters. *IEEE Transactions on Industrial Electronics, 59*(10), 3719-3726.

Kukrer, O., Komurcugil, H., & Doganalp, A. (2009). A Three-Level Hysteresis Function Approach to the Sliding-Mode Control of Single-Phase UPS Inverters. *IEEE Transactions on Industrial Electronics, 56*(9), 3477-3486.

Kwon, B. H., Choi, J. H., & Kim, T. W. (2001). Improved single-phase line-interactive UPS. *IEEE Transactions on Industrial Electronics, 48*(4), 804-811.

Kwon, M., Oh, S., & Choi, S. (2014). High Gain Soft-Switching Bidirectional DC–DC Converter for Eco-Friendly Vehicles. *Power Electronics, IEEE Transactions on, 29*(4), 1659-1666.

Le-Huy, H., Slimani, K., & Viarouge, P. (1994). Analysis and implementation of a real-time predictive current controller for permanent-magnet synchronous servo drives. *IEEE Transactions on Industrial Electronics, 41*(1), 110-117.

Lee, Y. S., & Cheng, G. T. (2006). Quasi-resonant zero-current-switching bidirectional converter for battery equalization applications. *IEEE transactions on power electronics, 21*(5), 1213-1224.

Lee, Y. S., & Cheng, M. W. (2005). Intelligent control battery equalization for series connected lithium-ion battery strings. *IEEE Transactions on Industrial Electronics, 52*(5), 1297-1307.

Li, X. D., & Bhat, A. K. S. (2010). Analysis and Design of High-Frequency Isolated Dual-Bridge Series Resonant DC/DC Converter. *IEEE transactions on power electronics, 25*(4), 850-862.

Liang, T. J., Liang, H. H., Chen, S. M., Chen, J. F., & Yang, L. S. (2014). Analysis, Design, and Implementation of a Bidirectional Double-Boost DC-DC Converter. *IEEE Transactions on Industry Applications, 50*(6), 3955-3962.

Lim, J. S., Park, C., Han, J., & Lee, Y. (2014). Robust Tracking Control of a Three-Phase DC-AC Inverter for UPS Applications. *IEEE Transaction on Industrial Electronics, 61*(8), 4142 - 4151.

Lin, C.-C., Yang, L.-S., & Wu, G. (2013). Study of a non-isolated bidirectional DC–DC converter. *IET Power Electronics, 6*(1), 30-37.

Liserre, M., Teodorescu, R., & Blaabjerg, F. (2006). Multiple harmonics control for three-phase grid converter systems with the use of PI-RES current controller in a rotating frame. *IEEE transactions on power electronics, 21*(3), 836-841.

Malesani, L., Rossetto, L., Spiazzi, G., & Zuccato, A. (1996). An AC power supply with sliding-mode control. *IEEE Industry Applications Magazine, 2*(5), 32-38.

Marei, M. I., Abdallah, I., & Ashour, H. (2011). Transformerless Uninterruptible Power Supply with Reduced Power Device Count. *Electric Power Components and Systems, 39*(11), 1097-1116.

Martinez, S., Castro, M., Antoranz, R., & Aldana, F. (1989). Off-line uninterruptible power supply with zero transfer time using integrated magnetics. *IEEE Transactions on Industrial Electronics, 36*(3), 441-445.

Mattavelli, P. (2005). An improved deadbeat control for UPS using disturbance observers. *IEEE Transactions on Industrial Electronics, 52*(1), 206-212.

Monfared, M., Golestan, S., & Guerrero, J. M. (2014). Analysis, Design, and Experimental Verification of a Synchronous Reference Frame Voltage Control for Single-Phase Inverters. *IEEE Transactions on Industrial Electronics, 61*(1), 258-269.

Montagner, V. F., & Peres, P. L. (2003). *Robust state feedback control applied to a UPS system.* Paper presented at the The 29th Annual Conference of the IEEE Industrial Electronics Society, IECON'03.

Muthu, S., & Kim, J. (1998). *Discrete-time sliding mode control for output voltage regulation of three-phase voltage source inverters.* Paper presented at the Conference Proceedings Thirteenth Annual Applied Power Electronics Conference and Exposition, APEC'98.

Nakajima, K., Sato, S., & Kawakami, K. (1990). *Three phase IGBT inverter with improved voltage waveform.* Paper presented at the IPEC-Tokyo.

Nasiri, A. (2007). Digital control of three-phase series-parallel uninterruptible power supply systems. *IEEE transactions on power electronics, 22*(4), 1116-1127.

Nasiri, A., Nie, Z., Bekiarov, S. B., & Emadi, A. (2008). An on-line UPS system with power factor correction and electric isolation using BIFRED converter. *IEEE Transactions on Industrial Electronics, 55*(2), 722-730.

Nian, H., & Zeng, R. (2011). Improved control strategy for stand-alone distributed generation system under unbalanced and non-linear loads. *IET renewable power generation, 5*(5), 323-331.

Niroomand, M., & Karshenas, H. (2010). *Review and comparison of control methods for uninterruptible power supplies.* Paper presented at the 1st Power Electronic & Drive Systems & Technologies Conference (PEDSTC).

Park, H. S., Kim, C. H., Park, K. B., Moon, G. W., & Lee, J. H. (2009). Design of a Charge Equalizer Based on Battery Modularization. *IEEE Transactions on Vehicular Technology, 58*(7), 3216-3223.

Park, J. K., Kwon, J. M., Kim, E. H., & Kwon, B. H. (2008). High-performance transformerless online UPS. *IEEE Transactions on Industrial Electronics, 55*(8), 2943-2953.

Park, S.-H., Park, S.-R., Yu, J.-S., Jung, Y.-C., & Won, C.-Y. (2010). Analysis and design of a soft-switching boost converter with an HI-Bridge auxiliary resonant circuit. *Power Electronics, IEEE Transactions on, 25*(8), 2142-2149.

Per Grandjean-Thomsen. (1992). UPS System Design Handbook. *Merlin Gerin (Aust) Pty Limited*.

Pereira, L. F. A., Flores, J. V., Bonan, G., Coutinho, D. F., & da Silva, J. M. G. (2014). Multiple Resonant Controllers for Uninterruptible Power Supplies-A Systematic Robust Control Design Approach. *IEEE Transactions on Industrial Electronics, 61*(3), 1528-1538.

Pinheiro, H., & Jain, P. K. (2002). Series-parallel resonant UPS with capacitive output DC bus filter for powering HFC networks. *IEEE transactions on power electronics, 17*(6), 971-979.

Pinheiro, H., Martins, A., & Pinheiro, J. (1994). *A sliding mode controller in single phase voltage source inverters.* Paper presented at the 20th International Conference on Industrial Electronics, Control and Instrumentation, IECON'94.

Racine, M. S., Parham, J. D., & Rashid, M. (2005). *An overview of uninterruptible power supplies.* Paper presented at the Power Symposium, 2005. Proceedings of the 37th Annual North American.

Ramos, R. R., Biel, D., Fossas, E., & Guinjoan, F. (2003). A fixed-frequency quasi-sliding control algorithm: Application to power inverters design by means of FPGA implementation. *IEEE transactions on power electronics, 18*(1), 344-355.

Rech, C., Pinheiro, H., Grundling, H. A., Hey, H. L., & Pinheiro, J. R. (2003). A modified discrete control law for UPS applications. *IEEE transactions on power electronics, 18*(5), 1138-1145.

Restrepo, C., Calvente, J., Romero, A., Vidal-Idiarte, E., & Giral, R. (2012). Current-Mode Control of a Coupled-Inductor Buck-Boost DC-DC Switching Converter. *IEEE transactions on power electronics, 27*(5), 2536-2549.

Rodriguez, J., Kazmierkowski, M. P., Espinoza, J. R., Zanchetta, P., Abu-Rub, H., Young, H. A., & Rojas, C. A. (2013). State of the Art of Finite Control Set Model Predictive Control in Power Electronics. *IEEE Transactions on Industrial Informatics, 9*(2), 1003-1016.

Rodriguez, J., Pontt, J., Silva, C. A., Correa, P., Lezana, P., Cortes, P., & Ammann, U. (2007). Predictive current control of a voltage source inverter. *IEEE Transactions on Industrial Electronics, 54*(1), 495-503.

Schuch, L., Rech, C., Hey, H. L., Grundling, H. A., Pinheiro, H., & Pinheiro, J. R. (2006). Analysis and design of a new high-efficiency bidirectional integrated ZVT PWM converter for dc-bus and battery-bank interface. *IEEE Transactions on Industry Applications, 42*(5), 1321-1332.

Shen, J. M., Jou, H. L., & Wu, J. C. (2012). Transformerless single-phase three-wire line-interactive uninterruptible power supply. *IET Power Electronics, 5*(9), 1847-1855.

Shiji, H., Harada, K., Ishihara, Y., Todaka, T., & ALZAMORA, G. (2004). A zero-voltage-switching bidirectional converter for PV systems. *IEICE transactions on communications, 87*(12), 3554-3560.

Slotine, J.-J. E., & Li, W. (1991). *Applied nonlinear control* (Vol. 199): Prentice-Hall Englewood Cliffs, NJ.

Solter, W. (2002). *A new international UPS classification by IEC 62040-3.* Paper presented at the 24th Annual International Telecommunications Energy Conference, INTELEC .

Su, B., & Lu, Z. (2010). An interleaved totem-pole boost bridgeless rectifier with reduced reverse-recovery problems for power factor correction. *Power Electronics, IEEE Transactions on, 25*(6), 1406-1415.

Tamyurek, B. (2013). A High-Performance SPWM Controller for Three-Phase UPS Systems Operating Under Highly Nonlinear Loads. *IEEE transactions on power electronics, 28*(8), 3689-3701.

Tan, S. C., Lai, Y. M., & Tse, C. K. (2008). Indirect sliding mode control of power converters via double integral sliding surface. *IEEE transactions on power electronics, 23*(2), 600-611.

Tao, H. M., Duarte, J. L., & Hendrix, M. A. M. (2008). Line-interactive UPS using a fuel cell as the primary source. *IEEE Transactions on Industrial Electronics, 55*(8), 3012-3021.

Torrico-Bascopé, R., Oliveira, D., Branco, C., & Antunes, F. (2005). *A PFC pre-regulator with 110 V/220 V input voltage and high frequency isolation for UPS applications.* Paper presented at the 31st Annual Conference of IEEE Industrial Electronics Society, IECON 2005.

Torrico-Bascopé, R. P., Oliveira, D., Branco, C. G., Antunes, F. L., & Cruz, C. M. (2006). *A high frequency transformer isolation 110V/220V input voltage UPS system.* Paper presented at the Twenty-First Annual IEEE Applied Power Electronics Conference and Exposition, APEC'06, 2006. .

Torrico-Bascope, R. P., Oliveira, D. S., Branco, C. G. C., & Antunes, F. L. M. (2008). A UPS with 110-V/220-V input voltage and high-frequency transformer isolation. *IEEE Transactions on Industrial Electronics, 55*(8), 2984-2996.

Tzou, Y. Y., & Lin, S. Y. (1998). Fuzzy-tuning current-vector control of a three-phase PWM inverter for high-performance AC drives. *IEEE Transactions on Industrial Electronics, 45*(5), 782-791.

Tzou, Y. Y., Ou, R. S., Jung, S. L., & Chang, M. Y. (1997). High-performance programmable AC power source with low harmonic distortion using DSP-based repetitive control technique. *IEEE transactions on power electronics, 12*(4), 715-725.

Vazquez, N., Aguilar, C., Arau, J., Caceres, R. O., Barbi, N., & Gallegos, J. A. (2002). A novel uninterruptible power supply system with active power factor correction. *IEEE transactions on power electronics, 17*(3), 405-412.

Veenstra, M., & Rufer, A. (2005). Control of a hybrid asymmetric multilevel inverter for competitive medium-voltage industrial drives. *IEEE Transactions on Industry Applications, 41*(2), 655-664.

Wai, R. J., Duan, R. Y., & Jheng, K. H. (2012). High-efficiency bidirectional dc-dc converter with high-voltage gain. *IET Power Electronics, 5*(2), 173-184. 4

Wai, R. J., & Liaw, J. L. (2015). High-Efficiency-Isolated Single-Input Multiple-Output Bidirectional Converter. *IEEE transactions on power electronics, 30*(9), 4914-4930.

Wai, R. J., & Wang, W. H. (2008). Grid-connected photovoltaic generation system. *IEEE Transactions on Circuits and Systems I-Regular Papers, 55*(3), 953-964.

Windhorn, A. (1992). A Hybrid Static Rotary Ups System. *IEEE Transactions on Industry Applications, 28*(3), 541-545.

Wu, W. M., He, Y. B., & Blaabjerg, F. (2012). An LLCL Power Filter for Single-Phase Grid-Tied Inverter. *IEEE transactions on power electronics, 27*(2), 782-789.

Xiao, S., Chow, M. H. L., Leung, F. H. F., Dehong, X., Yousheng, W., & Yim-Shu, L. (2002). Analogue implementation of a neural network controller for UPS inverter applications. *IEEE transactions on power electronics, 17*(3), 305-313.

Xu, D., Li, H., Zhu, Y., Shi, K., & Hu, C. (2015). High-surety Microgrid: Super Uninterruptable Power Supply with Multiple Renewable Energy Sources. *Electric Power Components and Systems, 43*(8-10), 839-853.

Xuewei, P., & Rathore, A. K. (2014). Novel bidirectional snubberless naturally commutated soft-switching current-fed full-bridge isolated DC/DC converter for fuel cell vehicles. *IEEE Transactions on Industrial Electronics, 61*(5), 2307-2315.

Yamada, R., Kuroki, K., Shinohara, J., & Kagotani, T. (1993). *High-frequency isolation UPS with novel SMR.* Paper presented at the Proceedings of the International Conference on Industrial Electronics, Control, and Instrumentation, IECON'93,1993.

Yan, W. G., Hu, H. G., Utkin, V., & Xu, L. Y. (2008). Sliding mode pulsewidth modulation. *IEEE transactions on power electronics, 23*(2), 619-626.

Yeh, C. C., & Manjrekar, M. D. (2007). A reconfigurable uninterruptible power supply system for multiple power quality applications. *IEEE transactions on power electronics, 22*(4), 1361-1372.

Zargari, N. R., Ziogas, P. D., & Joos, G. (1995). A two-switch high-performance current regulated DC/AC converter module. *IEEE Transactions on Industry Applications, 31*(3), 583-589.

Zhang, J. H., Lai, J. S., Kim, R. Y., & Yu, W. S. (2007). High-power density design of a soft-switching high-power bidirectional dc-dc converter. *IEEE transactions on power electronics, 22*(4), 1145-1153.

Zhang, K., Kang, Y., Xiong, J., & Chen, J. (2003). Direct repetitive control of SPWM inverter for UPS purpose. *IEEE transactions on power electronics, 18*(3), 784-792.

Zhang, Y., Xie, W., & Zhang, Y. (2014). Deadbeat direct power control of three-phase pulse-width modulation rectifiers. *IET Power Electronics, 7*(6), 1340-1346.

Zhang, Y., Yu, M., Liu, F. R., & Kang, Y. (2013). Instantaneous Current-Sharing Control Strategy for Parallel Operation of UPS Modules Using Virtual Impedance. *IEEE transactions on power electronics, 28*(1), 432-440.

Zhou, K. L., & Wang, D. W. (2003). Digital repetitive controlled three-phase PWM rectifier. *IEEE transactions on power electronics, 18*(1), 309-316.

Zhou, K. L., Wang, D. W., Zhang, B., & Wang, Y. G. (2009). Plug-In Dual-Mode-Structure Repetitive Controller for CVCF PWM Inverters. *IEEE Transactions on Industrial Electronics, 56*(3), 784-791.

Zhou, Z. J., Zhang, X., Xu, P., & Shen, W. X. (2008). Single-phase uninterruptible power supply based on Z-source inverter. *IEEE Transactions on Industrial Electronics, 55*(8), 2997-3004.

Zhu, L. (2006). A novel soft-commutating isolated boost full-bridge ZVS-PWM DC–DC converter for bidirectional high power applications. *Power Electronics, IEEE Transactions on, 21*(2), 422-429.

LIST OF PUBLICATIONS AND PAPERS PRESENTED

1. Aamir, M; Mekhilef, S; Jun K. H, "High-Gain Zero-Voltage Switching Bidirectional Converter With a Reduced Number of Switches," *IEEE Transactions on Circuits and Systems II: Express Briefs,* vol. 62, no. 8, pp. 816-820, 2015.

2. Aamir, M; Mekhilef, S; Ahmed.K, "Review: Uninterruptible Power Supply (UPS) System" *Renewable and sustainable energy: Reviews,* 58, 1395–1410, 2016.

3. Aamir, M; Mekhilef, S; "Online Transformer-less Uninterruptible Power Supply (UPS) system with reduced battery bank for low power applications" *IEEE Transaction on Power Electronics* vol. 32, no. 1, pp. 233-247, Jan. 2017

4. Aamir, M; Mekhilef, S; Ahmed. K, "Proportional-Resonant and Slide Mode Control for Single Phase UPS Inverter," *Electric Power Components and Systems* **Accepted**